POLITECNICO DI TORINO

Collegio di Ingegneria Chimica e dei Materiali

Corso di Laurea
in Ingegneria dei Materiali

Processing and characterization of recycled polymers containing rPET

Tutori

prof. Alberto Frache
prof.ssa Maria Lluisa Maspoch

Candidato

Brunella Bitto

Ottobre 2019

TABLE OF CONTENTS

RIASSUNTO

Uno dei temi, nel panorama mondiale, di maggiore rilevanza negli anni più recenti riguarda la sempre più elevata produzione di rifiuti e di conseguenza la loro corretta gestione. Secondo la *"International Solid Waste Association"* oggi nel mondo vengono prodotte circa 4 tonnellate all'anno di rifiuti e se ne prevede una continua crescita nel corso degli anni.

Tale problema ha radici ben profonde e, se durante quasi tutto il XX secolo non ci si è preoccupati della gestione e dello smaltimento dei rifiuti, dagli anni '90 in poi è stato necessario adoperare delle strategie che fossero il più possibile efficaci. La crescita dell'urbanizzazione, infatti, ha portato contemporaneamente all'incremento dei consumi, quindi all'aumento della produzione di rifiuti, e alla riduzione delle zone disabitate che venivano utilizzate come discariche.

Aspetto da non sottovalutare è che il '900 è da considerarsi il secolo del vero e proprio avvento della plastica. Nel 1910 viene brevettata la Bakelite e appena due anni dopo si scopre il processo produttivo del PVC che negli anni successivi troverà applicazione vastissima a livello industriale. Nel 1913 viene inventato il Cellophane, che può considerarsi il padre dei materiali destinati al packaging, fu infatti il primo materiale flessibile, trasparente e impermeabile. Dagli anni '20 in poi inizia il vero e proprio studio della chimica dei polimeri e quindi si susseguono le scoperte di nuovi materiali plastici e si procede ad adattare le tecniche di lavorazione ad un materiale così innovativo e versatile. Durante gli anni '60 la plastica viene vista come un materiale insostituibile nella vita quotidiana e le sue applicazioni si estendono sempre più fino ad abbracciare tutti i settori, tanto da modificare in modo irreversibile la società rivoluzionando abitudini consolidate da secoli e rendendo una vasta gamma di prodotti, prima considerati di nicchia, accessibili alla massa. Successivamente, arrivando fino all'età moderna, lo sviluppo dei tecnopolimeri, materiali con caratteristiche tali da essere in grado di sostituire metalli speciali e materiali ceramici in diverse applicazioni.

In figura è possibile notare come la produzione europea e mondiale della plastica dal 2005 al 2016 abbia seguito un trend via via sempre crescente

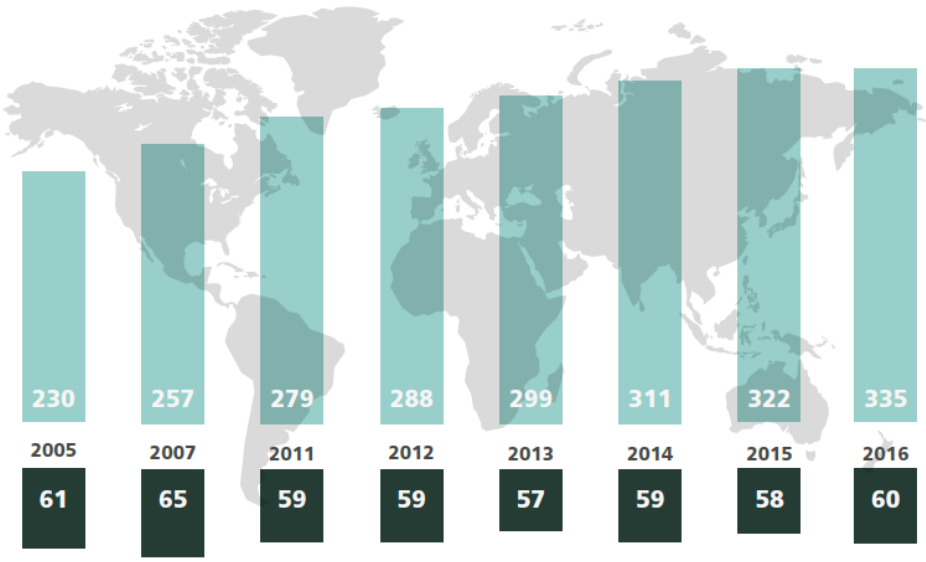

I settori applicativi in cui vi è la maggiore richiesta di plastica, sono osservabili in figura.

La plastica è dunque una risorsa ingegneristica fondamentale, ma si porta dietro delle problematiche importantissime a livello ambientale dovute non al materiale in sé, bensì alla cattiva amministrazione post-consumo causate dalla poca cultura riguardo a come i consumatori gestiscono i rifiuti.

Basti pensare che in passato le uniche soluzioni adottate furono discariche e inceneritori che, oltre ad alimentare il traffico e lo smaltimento illegale dei rifiuti, comportavano gravi conseguenze sull'ambiente a causa dell'elevata concentrazione di rifiuti in un unico territorio e a causa delle emissioni tossico-nocive dovute ai processi di combustione cui venivano sottoposti i rifiuti plastici.

Le possibilità per tutelare l'ambiente sono diverse, in figura si osserva l'ordine gerarchico decrescente di desiderabilità nella gestione delle risorse e dei rifiuti.

La ricerca scientifica oggi va nella direzione delle bioplastiche (biodegradabili e bio-based) e nel riciclo delle materie plastiche, per molti polimeri si riescono a ottenere buone proprietà meccaniche anche dopo aver sottoposto il materiale a diverse rilavorazioni. Nel 2016, infatti, per la prima volta il riciclo e il recupero energetico hanno superato la quantità di materiale immesso in discarica.

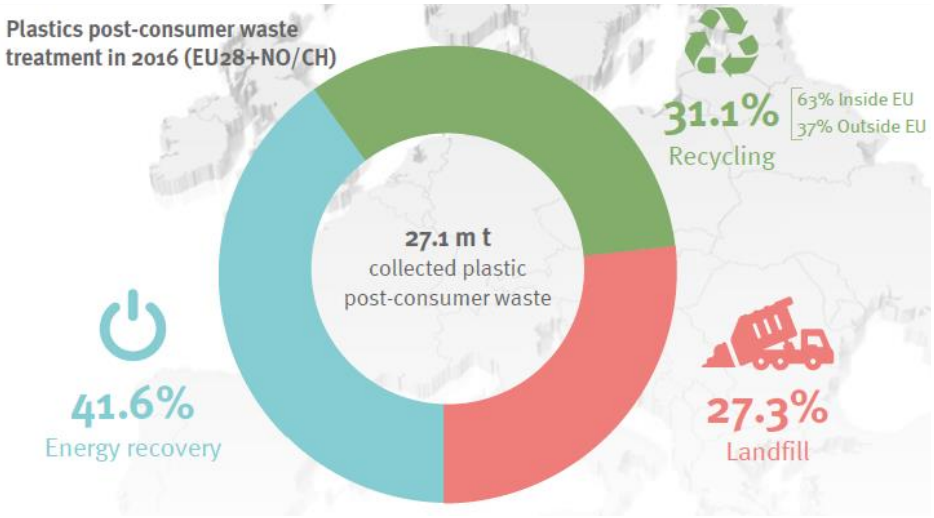

Nonostante le strade intraprese da numerosi gruppi di ricerca siano plurime, non si è ancora trovata una soluzione definitiva al problema dei rifiuti plastici.

Il progetto "RevalPET" si pone come obiettivo sia la ricerca della corretta strategia per poter riciclare un materiale che attualmente risulta non riciclabile, sia quello della valorizzazione del materiale riciclato, ricercando delle applicazioni come materiale innovativo.

Questo lavoro di ricerca è stato svolto al "Centre Català del Plastic" (Terrassa, Spagna) nell'ambito delle azioni previste dal progetto "RevalPET", finanziato dal FESR attraverso il programma INTERREG VA, attuando una collaborazione tra il Politecnico di Torino e l'Università Politecnica della Catalunya. L'obiettivo principale è stato quello di analizzare e confrontare il comportamento meccanico, termico e di frattura di due materiali polimerici riciclati, il Polipropilene (rPP) e il polietilene tereftalato opaco (rPET-O), nonché di studiare il rapporto morfologia-proprietà di un sistema bifasico costituito da una matrice di rPP e una seconda fase di rPET-O e di un altro sistema che aggiunge il 5% di TiO_2 al compound rPP/rPET-O.

I materiali utilizzati al fine della sperimentazione sono stati:

- Fiocchi di PET riciclato fornito dalla FLORAL costituito dal 10-12% di PET opaco e dall'88-90% di PET colorato al fine di diluire la quantità di TiO_2 presente nel PET opaco;
- Pellets di Polipropilene riciclato *"rPP QCP™ EXPP 152A"*;
- Diossido di Titanio (TiO_2) idrofobico.

Durante la prima fase della sperimentazione si è proceduto con la realizzazione dei compound d'interesse. Inizialmente si è effettuata l'omogeneizzazione dei fiocchi di rPET-O per poter ottenere i pellets. A tal fine il materiale è stato preventivamente sottoposto a essiccamento e successivamente lavorato in estrusore bivite alla temperatura necessaria.

I compound realizzati sono stati due: il primo costituito dall'80% in peso di rPP e dal 20% in peso di rPET-O (20/80); nel secondo invece si è aggiunto al compound precedente il 5% di TiO_2 (20/80+5%TiO_2). Le procedure per realizzare i due compound sono state differenti: per il 20/80 si è utilizzato il medesimo estrusore bivite con il quale si era effettuata l'omogeneizzazione del PET-O; per il compound 20/80+5%TiO_2 è stato necessario per prima cosa lavorare rPP e TiO_2 in estrusore monovite e, dopo aver formato i pellets, questi sono stati processati con il rPET-O in estrusore bivite.

Successivamente, utilizzando in estrusore la testa piana, si sono realizzate le lamine dei compounds d'interesse.

La prima caratterizzazione effettuata, sia sulle materie prima che sui due compound, è stata quella reologica. Per quanto riguarda rPET-O si è valutata la viscosità mediante viscosimetria capillare, mentre per ciò che concerne rPP, 20/80 e 20/80+5%TiO_2 si è proceduto con la valutazione del *Melt Flow Index*.

Dal punto di vista termico, si è effettuata la calorimetria differenziale a scansione (DSC).

In tal caso, si è ritenuto opportuno confrontare i materiali di partenza (rPP e rPET-O) sotto forma di pellets e sotto forma di film, al fine di visualizzare eventuali differenze dovute al processo di calandratura.

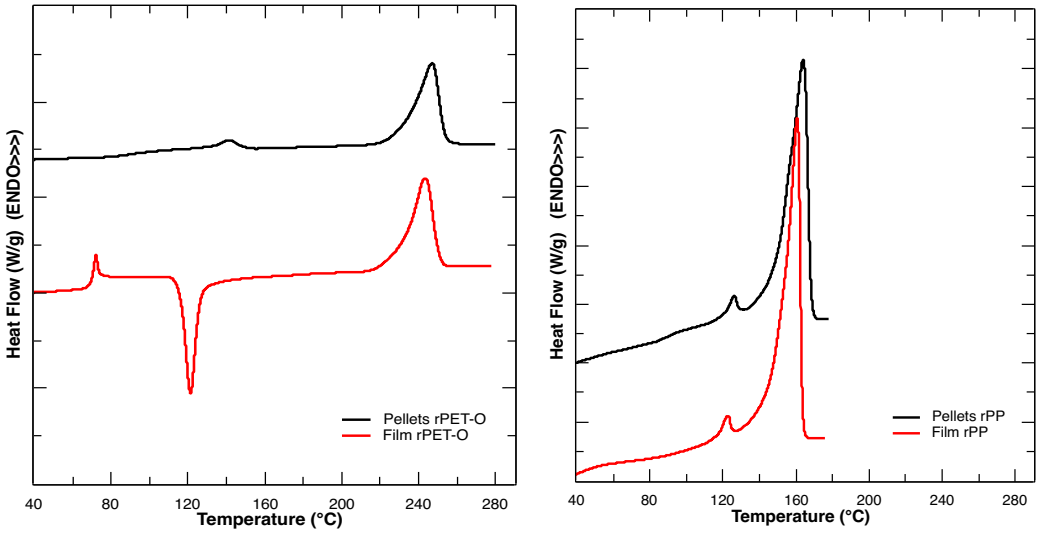

Nel caso dell'rPET-O è evidente che la curva relativa al film (curva rossa), a differenza di quella dei pellets, presenta un picco esotermico che può essere dovuto a un invecchiamento fisico. Non a caso, infatti, è presente nella lamina e non nei granuli, avendo subito un ciclo di raffreddamento brusco e poco controllato durante il processo di calandratura per la sua realizzazione.

Per quanto riguarda il Polipropilene riciclato non vi sono particolari differenze tra i risultati ottenuti per i pellets e quelli ottenuti per la lamina, va sottolineato che la presenza di due picchi endotermici è dovuta alla presenza minoritaria di polietilene all'interno di rPP.

Si riportano le tabelle con i risultati ottenuti dall'analisi termica:

Treatment	Transition	Parameters	rPP (pellets)		rPET-O (pellets)
			PP	PE	
C1	Glass	[°C] T_{g-0}	-	-	80,0
		[°C] T_{g-m}	-	-	87,6
		[W/g] ΔHF	-	-	0,045
	Cold crystallization	[°C] T_{cc}	-	-	-
		[J/g] ΔH_{cc}	-	-	-
		[%] X_{cc}	-	-	-
	Melt	[°C] T_m	164,5	126	247,2
		[J/g] ΔH_m	69,7	7,4	42
		[%] X_m	33,7	2,5	31,7
		[%] X_{total}	36,2		31,7
R1	Cooling	[°C] T_c	124,9	111	194
		[J/g] ΔH_c	80	5,7	38,6
		[%] X_c	38,6	1,9	29,1
C2	Glass	[°C] T_{g-0}	-	-	74,9
		[°C] T_{g-m}	-	-	80,7
		[W/g] ΔHF	-	-	0,038
	Melt	[°C] T_{m-1}	163	126	238,7
		[°C] T_{m-2}	-	-	246,3
		[J/g] ΔH_m	76,1	9,7	38,5
		[%] X_m	36,8	3,3	29,0
		[%] X_{total}	40,1		29

Treatment	Transition	Parameters	rPP (film)		rPET-O (film)
			PP	PE	
C1	Glass	[°C] T_{g-0}	-	-	73,2
		[°C] T_{g-m}	-	-	74
		[W/g] ΔHF	-	-	0,109
	Cold crystallization	[°C] T_{cc}	-	-	124,8
		[J/g] ΔH_{cc}	-	-	31
		[%] X_{cc}	-	-	23,4
	Melt	[°C] T_m	163,5	125,7	246,6
		[J/g] ΔH_m	72,2	4,3	40,8
		[%] X_m	34,9	1,5	30,8
		[%] X_{total}	36,3		7,4

Un'ulteriore confronto si è effettuato tra i due compound:

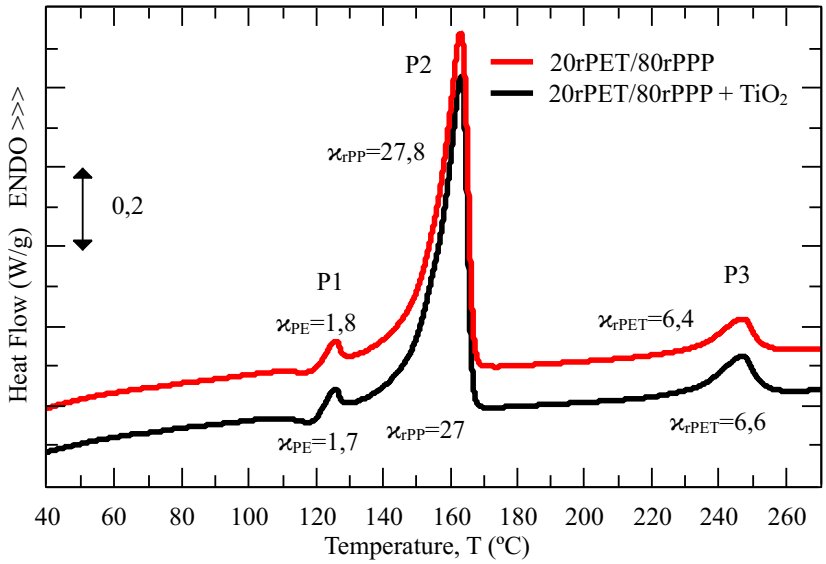

In generale, si osservano tre segnali endotermici massimi relativi alla fusione di ciascun elemento contenuto nei composti (rispettivamente PE, rPP e rPET-O). Anche se lo sviluppo delle curve mostra un alto livello di somiglianza tra i due compound, la miscela con TiO_2 mostra una leggera diminuzione del flusso termico prima del segnale di fusione del PE (125ºC), questo processo chiamato cristallizzazione a freddo è caratteristico del PET e obbedisce ai processi di cristallizzazione esotermica. Sebbene questo processo sia mascherato dalla fusione del PE, ha i suoi inizi intorno ai 112ºC.

Si riportano le tabelle con i risultati ottenuti dall'analisi termica:

Treatment	Transition	Parameters	20/80			20/80 + 5%TiO_2		
			PP	**PE**	**rPET-O**	**PP**	**PE**	**rPET-O**
C1	Glass	[°C] T_{g-0}	-	-	-	-	-	-
		[°C] T_{g-m}	-	-	-	-	-	-
		[W/g] ΔHF	-	-	-	-	-	-
	Cold crystallization	[°C] T_{cc}	-	-	-	-	-	-
		[J/g] ΔH_{cc}	-	-	-	-	-	-
		[%] X_{cc}	-	-	-	-	-	-
	Melt	[°C] T_m	163	125,4	247,4	163	125,3	247,2
		[J/g] ΔH_m	57,6	5,2	8,4	56	5	8,3
		[%] X_m	27,8	1,8	6,4	27,0	1,7	6,6
		[%] X_{total}	36,0			35,3		

Infine, si è analizzato il comportamento meccanico e di frattura. Nello specifico si è effettuato test di trazione, valutazione del CTOD (crack tip opening displacement) e determinazione del lavoro essenziale di frattura (EWF).

Per quanto riguarda il test di trazione, si sono costruite le curve sforzo-deformazione sia delle materie prime che dei compound, al fine di determinare il modulo elastico, la resistenza allo snervamento e la deformazione a rottura. Le curve e i valori ottenuti vengono riportati rispettivamente nel grafico e in tabella:

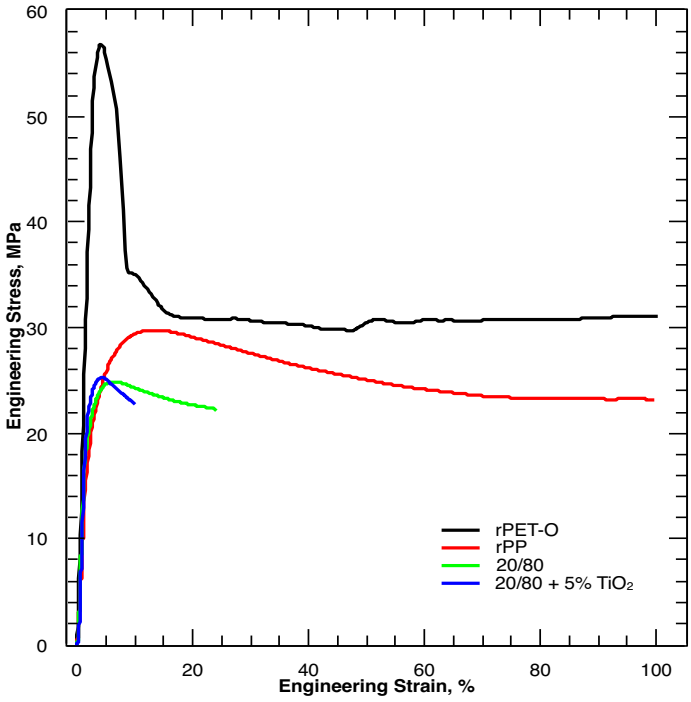

Samples	Elastic Modulus	Yielding strenght	Yelding strain	Strain at break
	GPa	MPa	%	%
rPP	1,16 ± 0,04	28,8 ± 0,6	13,0 ± 0,6	350 ± 22
rPET-O	2,2 ± 0,03	57,3 ± 0,5	3,9 ± 0,04	203 ± 16
20rPET-O/80rPP	1,22 ± 0,03	24,9 ± 0,2	10,94±0,03	33,9 ± 9,6
20/80 + 5% TiO_2	1,24 ± 0,03	25,1 ± 0,3	7,7 ± 0,2	23,5 ± 13

Facendo un confronto tra i materiali analizzati, rPET-O presenta sia modulo elastico che resistenza allo snervamento maggiori rispetto agli altri. Questo risulta coerente con la natura stessa del PET, infatti tale materiale ha un elevato potenziale di cristallizzazione conferito dalla regolarità della sua struttura molecolare; presenta inoltre una minore deformazione allo snervamento percentuale, tale moderata flessibilità molecolare nelle catene polimeriche è dovuta all'esistenza di una struttura di grande volume nel monomero di partenza (anelli aromatici). Facendo riferimento ai compound, si nota come l'aggiunta di TiO_2 faccia aumentare circa del 3% E e σ_y, ma considerando l'errore statistico del calcolo, tale aumento non risulta avere rilevanza significativa. Un aspetto da sottolineare è la deformazione a rottura in entrambi i composti, nonostante la variabilità percentuale tra loro è bassa, il coefficiente di variazione nel calcolo della rottura supera il 35% in entrambi i casi, il che suggerisce una eterogeneità fisica nelle miscele, sia nelle fasi polimeriche che nel filler inorganico.

In generale, incorporando il 20% di rPET nella matrice rPP si ottiene un aumento della rigidità del sistema (+6%) e del 9,5% se si aggiunge il 5% di TiO_2. Al contrario, la σ_y diminuisce rispettivamente del 13,5% e dell'11,4% con la seconda fase polimerica e con l'aggiunta di TiO_2. Anche la deformazione a rottura è influenzata dalla presenza della

seconda fase (rPET-O), che ne provoca una diminuzione del 16% che arriva a valori del 41% con l'aggiunta del diossido di Titanio.

Successivamente si è effettuata la valutazione del CTOD, tale misura permette di comprendere quanto le pareti della cricca si separino prima che avvenga la frattura, lo studio si basa dunque sulla determinazione dell'apertura della cricca poco prima dell'inizio della propagazione instabile della cricca stessa, quando un difetto è causato intenzionalmente (taglio).

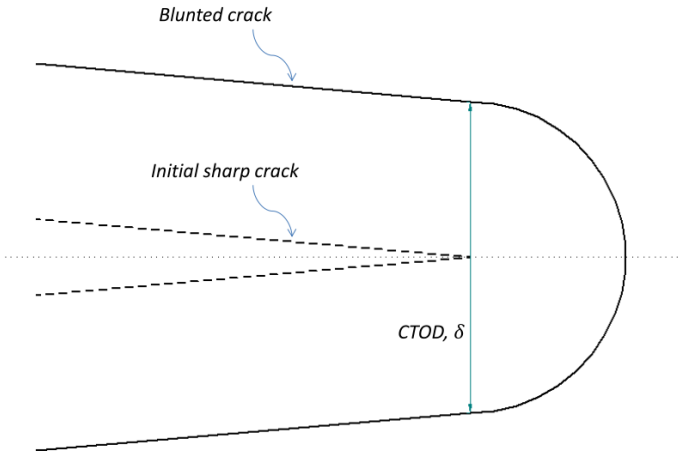

Si riportano in seguito, il grafico ottenuto e la tabella rappresentativa dei valori più significativi:

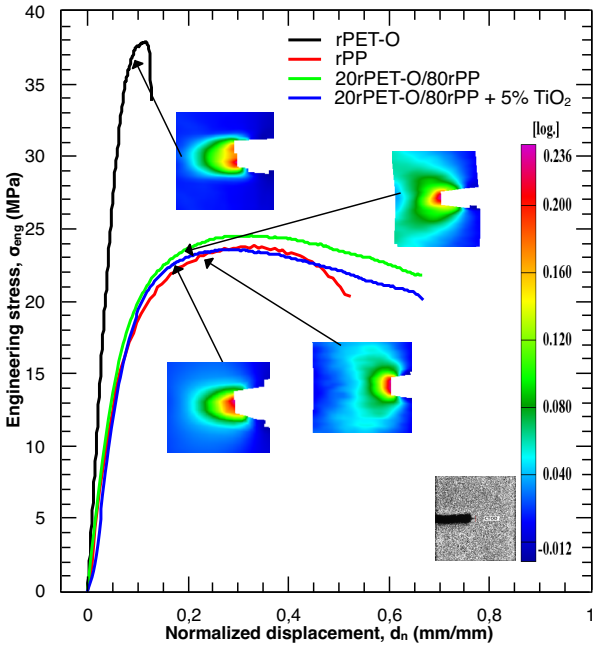

Materials	Thickness, *th* (mm)	Real Ligament, *l* (mm)	Load CTOD, *F* (N)	Stress CTOD, σ_c (Mpa)	Time, CTOD, *t* (sec)	**CTOD, δ_c (mm)**

rPET-O	0,615±0,007	20,03±0,03	408±20	32,6±1,2	8,6±1,3	**0,415±0,017**
rPP	0,620±0,005	20,01±0,19	240±11	19,5±1,0	13,6±1,3	**0,780±0,024**
20/80	0,607±0,003	5,45±0,19	76,2±3,5	23±0,5	66,4±11	**0,572±0,114**
20/80+5 % TiO_2	0,585±0,002	5,73±0,20	72,1±2,6	21,5±0,8	46,8±2,9	**0,446±0,046**

Da tale analisi si evince che i valori più alti di CTOD (δ_c) sono quelli relativi a rPP, per quanto riguarda rPET-O, σ_c è del 67% superiore a rPP e δ_c diminuisce del 47%: questo valore è conforme alla rigidità che il campione ha nell'intervallo di piccole deformazioni secondo lo studio di trazione monoassiale discusso precedentemente. Quando si aggiunge il 20% di rPET-O al campione rPP, δ_c diminuisce del 45% mentre σ_c aumenta leggermente, circa del 17%. Il campo di deformazioni associato mostra un'evoluzione completamente diversa rispetto alle materie prime, è infatti visibile una biforcazione nell'asse di propagazione della cricca che simula un'ostruzione all'estremità della cricca in modo tale che le sollecitazioni siano reindirizzate diagonalmente a 45° e -45° rispetto all'asse di avanzamento della cricca. Una situazione simile, seppur meno accentuata, si manifesta anche nel compound con l'aggiunta di TiO_2: l'aggiunta di una carica inorganica potrebbe portare ad una concentrazione localizzata di sollecitazioni all'interfaccia TiO_2-Polimero che agisce come un concentratore di sollecitazione che blocca leggermente l'insorgenza di una propagazione instabile della cricca.

L'ultima analisi effettuata è quella relativa al lavoro essenziale di frattura (EWF), questo permette di determinare i parametri di frattura di un film polimerico. Quando si considera un materiale duttile, il cedimento completo del materiale si verifica prima della propagazione della cricca, durante questo processo si possono osservare due fenomeni: il processo di frattura e la deformazione plastica che si riflettono rispettivamente in una regione di frattura interna e in una zona plastica esterna.

Questa tecnica è stata originariamente proposta da Boberg, secondo la quale quando un campione duttile, sottoposto a tensioni di trazione uniformi, presenta una rottura centrale, intorno ad essa la zona plastica ha due zone diverse: una zona interna relativa al processo di frattura (FPZ) e una zona esterna relativa al processo di deformazione plastica (OPZ). Il lavoro dissipato in FPZ è indipendente dal materiale in prova, mentre il lavoro associato a OPZ dipende dalla geometria del campione e dalla lunghezza effettiva del legamento.

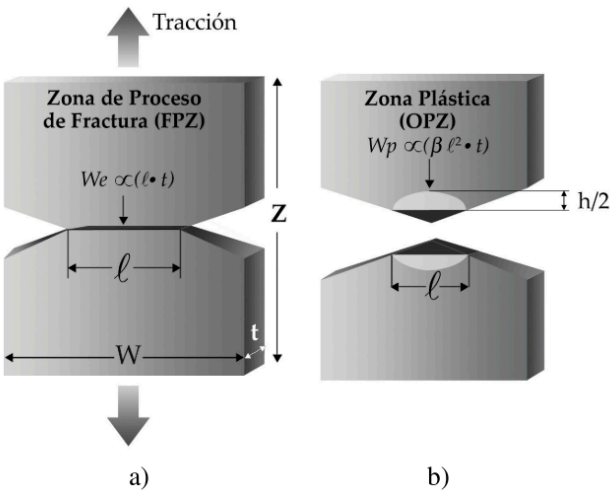

Di conseguenza, quando la parte anteriore della cricca si propaga dopo la generazione della zona plastica, il lavoro necessario per l'intero processo di frattura (W_f) sarà dato dal contributo di due termini, ognuno dei quali si riferisce ad una zona di processo:

$$W_f = W_e + W_p$$

Il primo termine (W_e) rappresenta il lavoro essenziale di frattura, cioè il lavoro necessario a formare una nuova superficie situata in FPZ; W_p rappresenta invece il lavoro di frattura non essenziale, cioè il lavoro causato dai diversi meccanismi di deformazione presenti come ad esempio micro cavità.

L'equazione precedente, in quanto W_e è correlata alla superficie di frattura e W_p al volume di frattura, può essere riscritta come segue:

$$W_f = w_e \cdot lt + \beta w_p \cdot l^2 t$$

con:

- l = lunghezza del legamento reale
- t = spessore del campione
- β = fattore di forma relativo al volume deformato intorno al legamento

Volendo rappresentare il lavoro specifico:

$$\frac{W_f}{lt} = w_f = w_e + \beta w_p \cdot l$$

È possibile ottenere i parametri w_e e w_p inserendo in un grafico la regressione lineare del lavoro totale specifico rispetto alla lunghezza del legamento.

Per quanto riguarda il compound 20/80, facendo inizialmente un'analisi puramente visiva, si è osservato come i campioni mostrassero un cambiamento di tonalità nella zona deformata. In particolare si è notato uno sbiancamento che sembra aumentare longitudinalmente e nella direzione di applicazione del carico all'aumentare della lunghezza del legamento. È importante sottolineare che durante l'esecuzione del test tale sbiancamento è stato osservato prima della propagazione della cricca, in figura si può apprezzare l'evoluzione della deformazione dall'inizio del test all'inizio della propagazione della cricca:

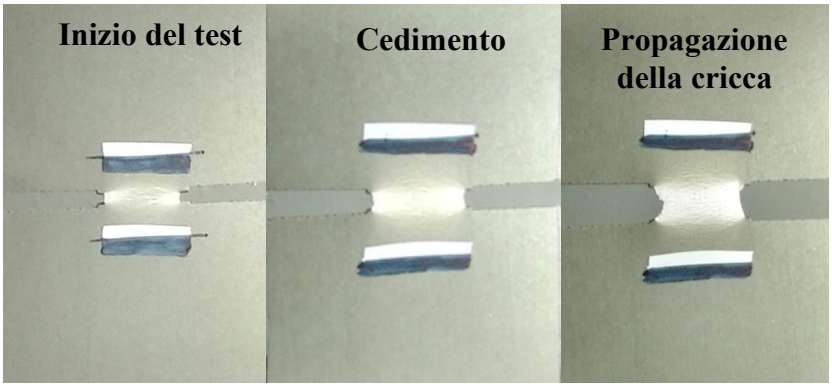

Analizzando l'evoluzione del carico applicato rispetto allo spostamento relativo delle morse del macchinario, si può osservare una crescita sequenziale della curva all'aumentare del legamento:

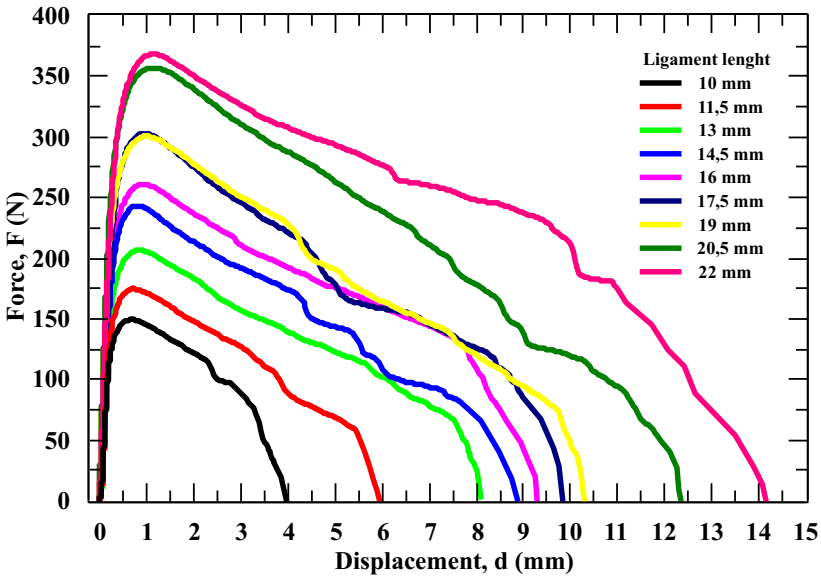

È importante sottolineare che in tutti i casi si è sviluppato un aumento lineare della forza fino alla resa, seguita da una diminuzione del carico applicato fino alla prima brusca caduta della forza nella curva (inizio della propagazione della cricca) ed infine la propagazione instabile e la rottura. Tuttavia nei legamenti da 19 mm a 22 mm, questa crescita non ha obbedito alla sequenza dei legamenti più bassi, una possibile spiegazione è la lunghezza reale del legamento e/o lo stato di tensione sviluppato a queste lunghezze.

Uno dei criteri importanti stabiliti per l'EWF è che la sollecitazione massima del provino in uno stato di sollecitazione planare sia 1,15σy, tuttavia, è stato applicato un intervallo più rigoroso tra 0,9 σy e 1,1 σy per visualizzare la variabilità delle sollecitazioni massime e definire meglio i parametri dell'EWF.

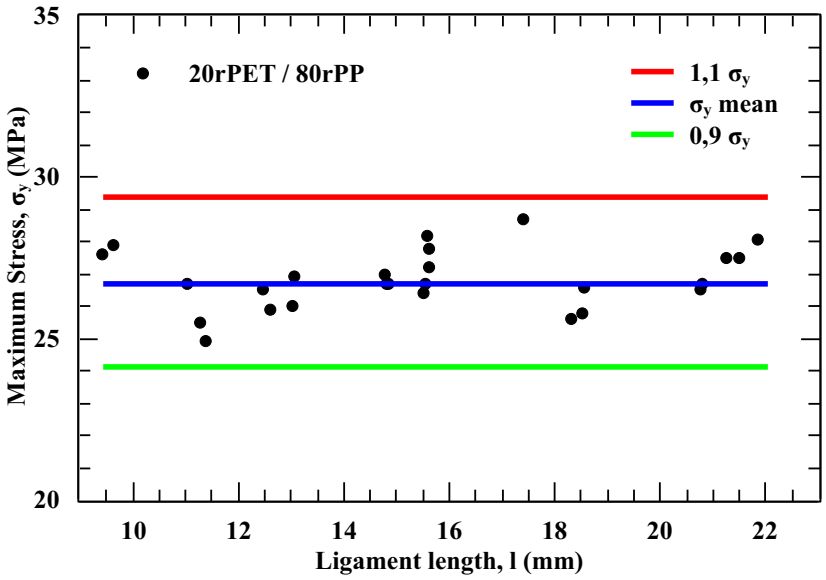

Dal grafico è possibile vedere come tutti i campioni, con tutte le lunghezze di legamento analizzate soddisfino il criterio dello stato di sollecitazione piana.

Come accennato precedentemente, un fattore importante nell'EWF è la dimensione e la forma della zona plasticamente deformata (OPZ) che si sviluppa appena sopra la linea legamentosa. Questa zona è correlata al termine di frattura non essenziale ed è stata calcolata misurando l'altezza h/2 della zona plastica in ogni parte del campione (inferiore e superiore) con l'ausilio di un microscopio ottico.

Come risultato del controllo visivo è stato definito che la geometria sviluppata nella zona plastica è ellittica e quindi il valore numerico costante che ad essa corrisponde è K=1,127:

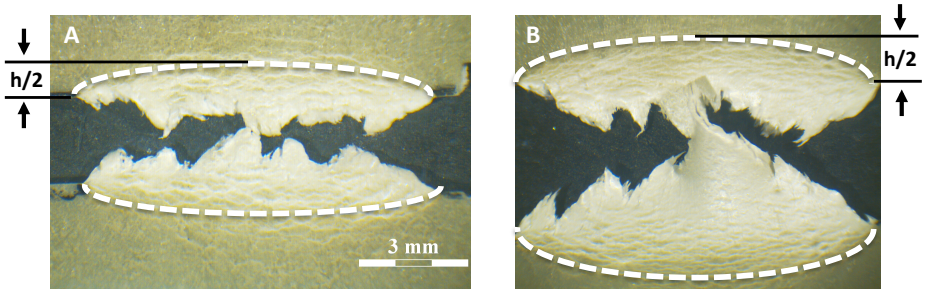

Rappresentando l'altezza h di ogni campione rispetto alla lunghezza effettiva del legamento ed eseguendo una regressione lineare dei punti, la pendenza ottenuta ha stabilito il valore del fattore di forma $\beta = 11x10^{-2}$.

Calcolando l'area sottesa alle curve presentate precedentemente e rapportando questo valore alla sezione legamento (larghezza del campione per lunghezza effettiva del legamento) è stato possibile calcolare il lavoro totale specifico della frattura w_t. Tracciando questo valore

totale rispetto alla lunghezza effettiva del legamento, è stato possibile ottenere i valori dei termini w_e e w_p.

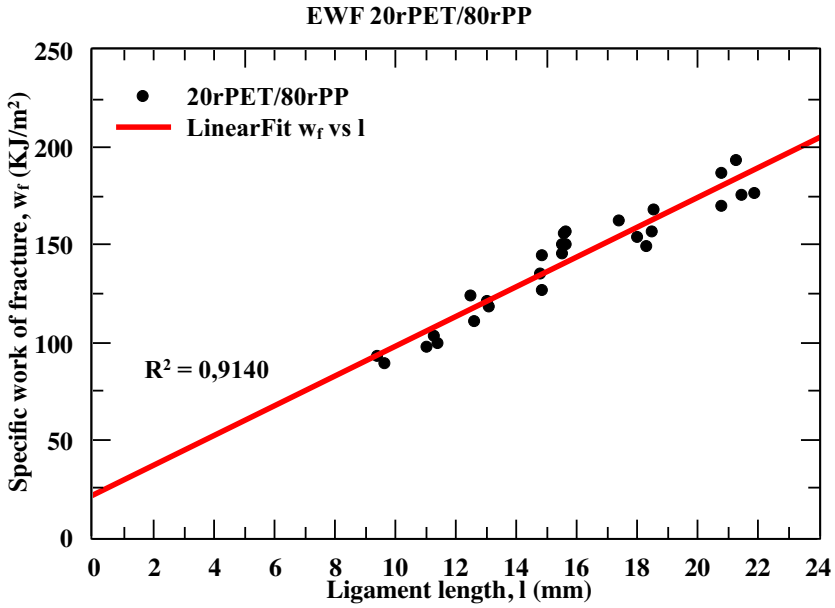

Estendendo la linea di regressione all'ordinata all'origine e applicando le equazioni dell'EWF, è stato calcolato che il valore associato al termine specifico di frattura essenziale $w_p = 21{,}3\ KJ.m^{2-}$ e il termine specifico non essenziale w_p= 69 $MJ.m^{-3}$.

Il medesimo studio si è effettuato sul compound 20/80+5%TiO_2. Si è potuto osservare che le dimensioni della zona di deformazione plastica (OPZ) erano inferiori rispetto ai campioni senza TiO_2. Sebbene lo sbiancamento avvenga prima della rottura, ha un intervallo più piccolo che si traduce in una migliore deformazione generale fino alla rottura.

Tracciando il grafico carico applicato Vs spostamento relativo delle morse:

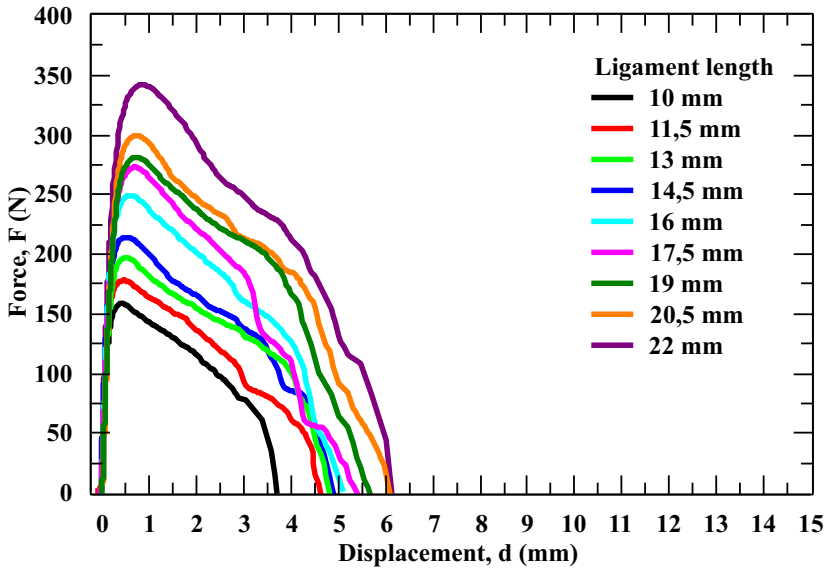

È possibile osservare che vi è un alto grado di linearità nella zona elastica e anche prima della cessione, le sollecitazioni massime aumentano gradualmente con l'aumento del legamento, c'è una diminuzione del carico subito dopo la cessione e un'instabilità tipica della rottura e frattura finale. Tuttavia le sollecitazioni massime, gli spostamenti associati alla cedevolezza e alla rottura sono inferiori. Va sottolineato che, per i legamenti superiori a 13 mm, l'instabilità nelle curve si verifica prematuramente, una spiegazione a ciò potrebbe essere legata alla distribuzione e dispersione del carico inorganico oltrechè agli effetti di concentrazione degli sforzi che questo potrebbe produrre. Inoltre, tale instabilità della frattura, potrebbe essere dovuta al livello di interazione tra le fasi.

Anche nel caso del compound rinforzato, tutti i campioni hanno soddisfatto il criterio di sollecitazione piana, si osserva una leggera e costante diminuzione ogni volta che il legamento aumenta.

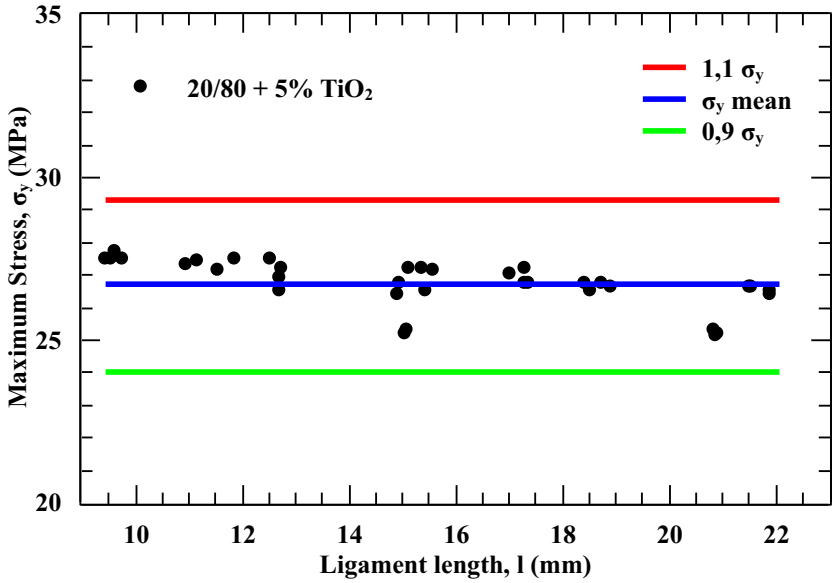

Per la determinazione di h/2, come risultato del controllo visivo è stato definito che la geometria sviluppata nella zona plastica è ellittica e quindi il valore numerico costante che ad essa corrisponde è K=1,127:

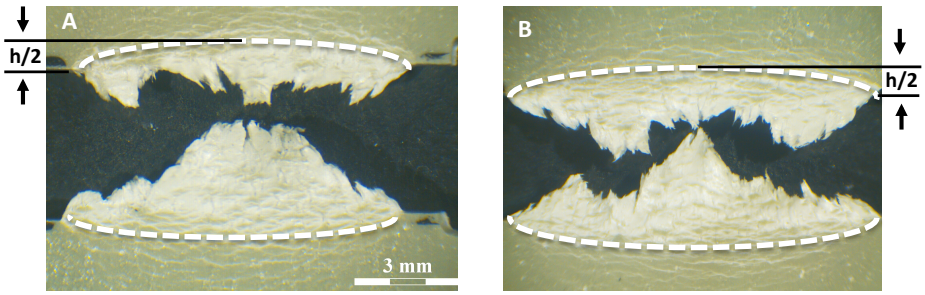

Si è ottenuto un valore del fattore di forma pari a $\beta = 3{,}9x10^{-2}$, circa 3 volte inferiore a quello ottenuto per il compound 20/80.

Analogamente al 20/80 si è calcolata l'area sottesa alle curve e quindi si sono calcolati il lavoro specifico totale e i valori dei termini essenziali e non essenziali specifici. Dalla regressione lineare ed estrapolazione all'ordinata all'origine, il valore relativo al termine essenziale specifico è $w_e = 78{,}9\ KJ.m^{-2}$, mentre quello relativo al termine non essenziale è $w_p = 10{,}2\ MJ.m^{-3}$.

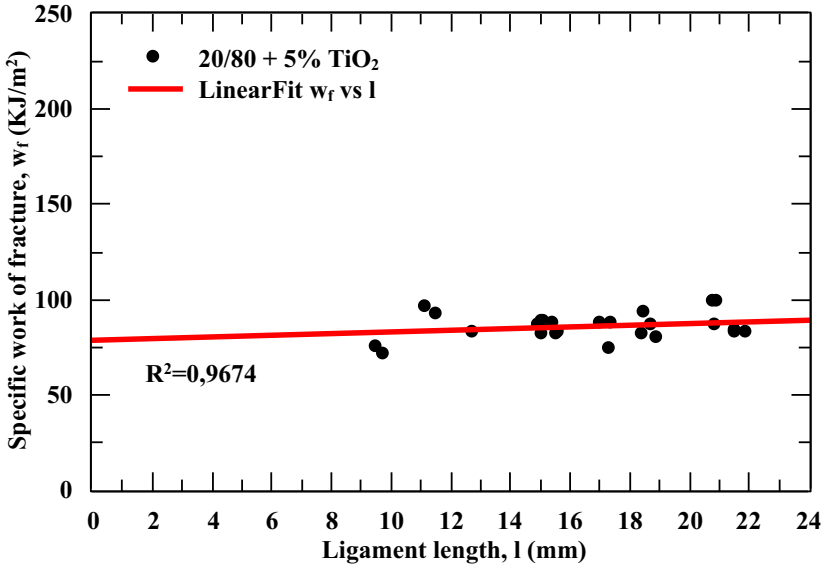

Si riporta una tabella riassuntiva dei valori numerici ottenuti e un grafico comparativo:

Material	w_e	βw_p	$\beta x10^{-2}$	w_P
	$(KJ.m^{-2})$	$(MJ.m^{-3})$	–	$(MJ.m^{-3})$
20rPET/80rPP	21,3 ± 7,5	7,6 ± 0,4	11,0±0,7	69 ± 5
20rPET/80rPP + 5% TiO_2	78,9 ± 8,0	0,4 ± 0,1	3,9 ± 0,4	10,2 ± 0,3

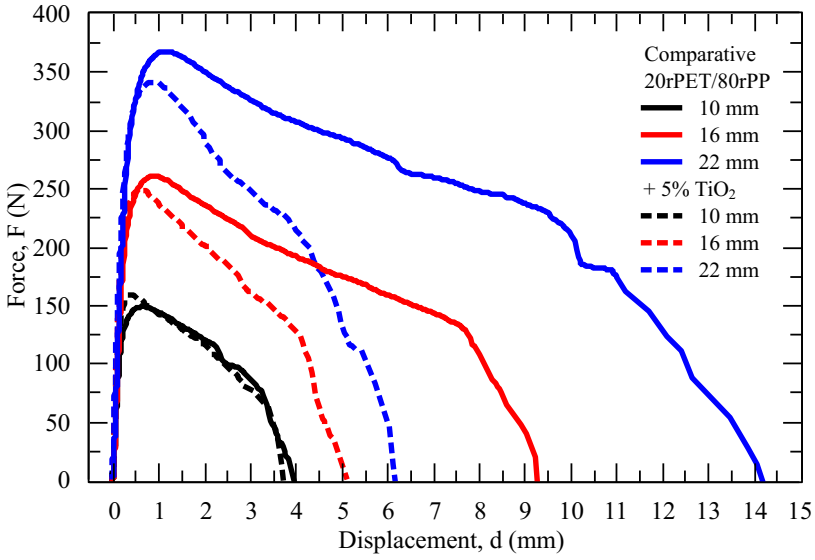

1. OBJECTIVES

The research phase was carried out at the "Centre Català del Plastic" (CCP), a research centre located in Terrassa (Spain), thanks to a collaboration between the “Politecnico di Torino” and the “Universitat Politecnica de Catalunya” (UPC).

This research work is carried out as part of the actions foreseen in the project "Revaluation of recycled opaque PET in innovative materials (RevalPET)" financed by FEDER funds through the INTERREG VA programme.

The main objective of this work is to analyze and compare the mechanical and thermal properties and fracture behaviour of two recycled polymeric materials, polypropylene (rPP) and polyethylene terephthalate (rPET-O), as well as to investigate the morphology-properties relationship of a biphasic system constituted by a matrix of rPP and a second dispersed phase of rPET-O and another system adding a controlled percentage of titanium dioxide (TiO_2).

To this end, the following specific objectives are established:

1. Homogenisation of raw materials and extrusion of sheets
    a. Obtain homogeneous rPET-O granules by means of a co-rotating twin-screw extruder.
    b. Generate a masterbach or rPP concentrate with 5% TiO_2 using a single screw extruder.
    c. Extrude biphasic systems with and without additional TiO_2
    d. Extrude sheets of raw material and compound
2. Mechanical and fracture characterization
    a. Analyze the effect of the second phase dispersed in the rPP matrix on the mechanical parameters by means of uniaxial tensile tests at constant vice displacement speed.
    b. Obtain essential and non-essential fracture parameters through Essential Working Fracture (EWF) trials.
    c. Study the phenomena developed in the fracture process through the protocols of the Mechanics of Linear Elastic Fracture (LEFM) and the critical value of crack opening (CTOD) associated to each compound.
3. Thermal characterization
    a. Determine the characteristic thermal transitions of raw materials and compounds developed through Differential Scanning Calorimetry (DSC) tests.
    b. Determine quantitatively the effective percentage of inorganic filler in each sample using Thermo-Gravimetric Analysis (TGA).
    c. Evaluate the effect of the processing conditions used in the manufacture of the specimens by means of the degree of crystallinity.
4. Morphological characterization
    a. Identify the biphasic nature of the compound as well as the location and distribution of the inorganic filler.

In addition, a mechanical and morphological study was carried out on preliminary r-PP/rPET-O mixtures generated by a collaborating entity of the project.

The thesis work is divided into 5 chapters:

The first chapter discussed the problem of plastic waste, in particular packaging waste, which is of global interest.

In the second chapter, it will discuss PET in general, focusing on the recycling of the same material and on the applications of recycled PET; it will also describe the opaque PET, used for the production of milk bottles as a replacement material for HDPE, focusing on the difficulties of recycling.

In the third chapter, PP will be discussed in terms of properties, synthesis and applications. The focus will also be on recycled PP and its applications.

The fourth chapter will describe the materials, the machinery and the methodologies used for the experiments.

Finally, the fifth chapter will present and discuss the results obtained both from the preliminary phase aimed at deciding the characteristics of the compound to be produced (in terms of the properties of TiO_2 to be used and its percentage to be included in the compound), and the mechanical, thermal and rheological tests of the compound of interest.

2. PLASTIC WASTE

One of the most important issues on the world scene in recent years has been the increasing production of waste and, consequently, its proper management. According to the *"International Solid Waste Association"* today around 4 tonnes of waste are produced worldwide per year and are expected to continue to grow over the years.

This problem has deep roots and, if during almost the entire 20th century there was no preoccupation with the management and disposal of waste, from the 1990s onwards it was necessary to use strategies that were as effective as possible.

The growth of urbanization, in fact, has led simultaneously to an increase in consumption, thus increasing the production of waste, and the reduction of uninhabited areas that were used as landfills.

Not to be underestimated is that the '900 is to be considered the century of the real advent of plastic. In 1910, Bakelite was patented and just two years later the production process of PVC was discovered, which in the following years would find widespread application at an industrial level. In 1913 Cellophane was invented, which can be considered the father of the materials used for packaging, and was in fact the first flexible, transparent and waterproof material. From the 1920s onwards, the real study of the chemistry of polymers began, and then new plastic materials were discovered and the processing techniques adapted to such an innovative and versatile material.

During the 1960s, plastic was seen as an irreplaceable material in everyday life and its applications increasingly extended to cover all sectors, so much so as to irreversibly change society, revolutionising habits that had been established for centuries and making a wide range of products, previously considered niche products, accessible to the masses. Subsequently, up to the modern age, the development of technopolymers, materials with characteristics such as to be able to replace special metals and ceramic materials in different applications.

Figure 1 shows that European and global plastics production from 2005 to 2016 has followed an increasing trend:

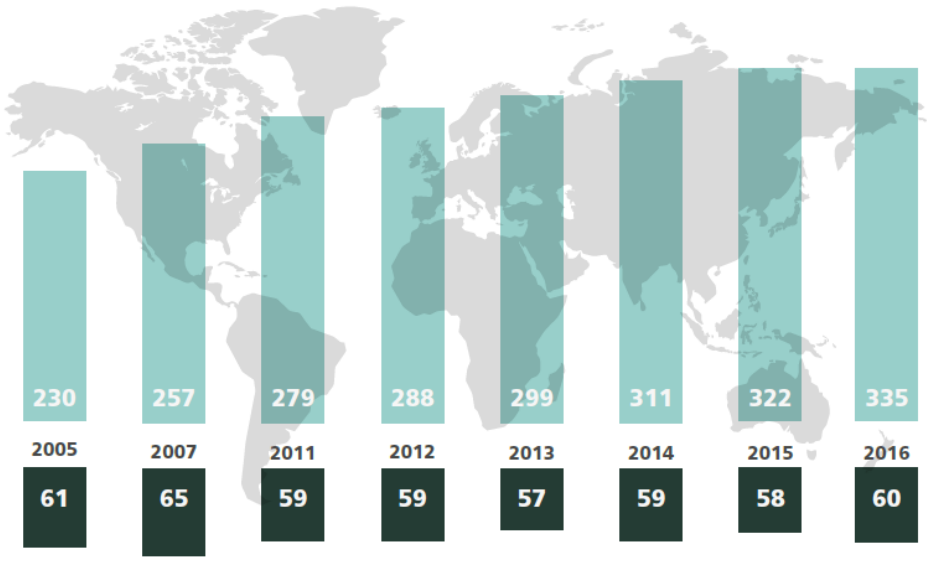

Figure 1: European and global plastics production - 2005/2016

The application sectors in which there is the greatest demand for plastics are shown in Figure 2.

Figure 2: Main market sectors requiring plastic material

Plastics are therefore a fundamental engineering resource, but they carry with them very important environmental issues not due to the material itself, but to post-consumer mismanagement caused by a lack of culture about how consumers handle waste.

In the past, the only solutions adopted were landfill sites and incinerators which, in addition to fuelling the trafficking and illegal disposal of waste, had serious consequences for the environment because of the high concentration of waste in a single area and because of toxic and harmful emissions due to the combustion processes to which plastic waste was subjected.

The possibilities to protect the environment are different, in Figure 3 we observe the descending hierarchical order of desirability in the management of resources and waste.

Figure 3: Hierarchical waste principle

Scientific research today goes in the direction of bioplastics (biodegradable and bio-based) and in the recycling of plastics, for many polymers it is possible to obtain good mechanical properties even after having subjected the material to different re-workings. In 2016, in fact, for the first-time recycling and energy recovery exceeded the amount of material put into landfill (Figure 4).

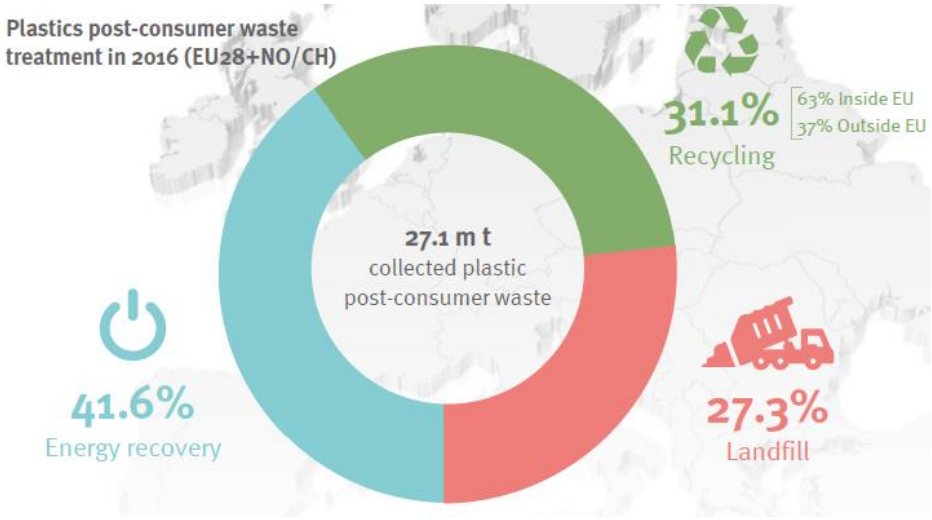

Figure 4: Scheme of destination of post-consumer plastic waste

Despite the fact that many research groups have taken many paths, no definitive solution has yet been found to the problem of plastic waste.

The "RevalPET" project aims both to find the right strategy to recycle a material that is currently not recyclable, and to recycle the recycled material, looking for applications as an innovative material.

3. POLYETHYLENE TEREPHTHALATE

Polyethylene terephthalate, known as PET, is a thermoplastic polymeric material that belongs to the family of polyesters, or polymers obtained by condensation of an acid and an alcohol. In particular, it is obtained by polycondensation of terephthalic acid (PTA) with ethylene glycol (EG).

The structure formula, characterized by ethylene groups (CH_2-CH_2) and terephthalate groups (two ester groups and a benzene ring), is as follows:

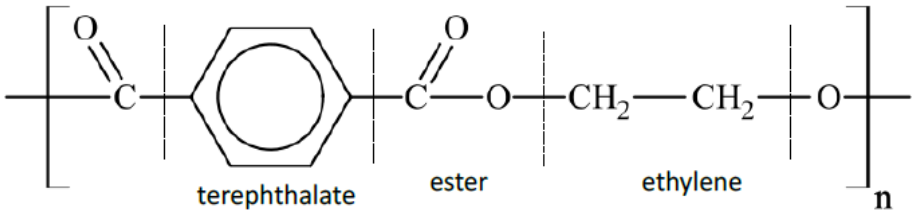

Figure 3.1: PET structure formula [1]

Making a brief historical *excursus*, the first laboratory samples of PET fiber were developed in 1941 by the "*Calico Printers Association*". Immediately after the end of the Second World War, in the United States, the real research activity on this material began. Initially it was based exclusively on the textile sector until 1962, when the first polyester reinforcement was produced [2]. At the end of the 1970s, PET, which had by then become a commercial material, was used for packaging such as films, bottles and coatings. Since then, thanks to the research activities that led to the improvement of the mechanical properties, the consumption of this material in various sectors has grown exponentially. [3]

Nowadays PET is used in a wide range of products such as synthetic fibres, thermoforming applications and technical resins, bottles and food packaging.

In this study, we focused on PET from bottles, for the realization of which this material is considered the favorite thanks to advantages of both technical and economic nature.

The reasons why this material is found to be one of the most used for the production of bottles are:

- mechanical resistance;
- transparency;
- low permeability to odours and CO_2;
- chemical stability;
- possibility of making preforms;
- complete recyclability, the process of which is strongly consolidated.

The polyethylene terephthalate can have both an amorphous and semi-crystalline structure, for the realization of the bottles is aimed at a degree of crystallinity around 20-25% in order to improve the barrier effect to gases and resistance to chemicals and to slow down the absorption of water, also increases the glass transition temperature and the melting temperature, but at the expense of transparency. Crystalline PET has no glass transition, at a temperature of over 250 °C it passes directly from the solid state to the molten state, this allows it to dry, a fundamental and always necessary phase, before processing. PET is in fact a hygroscopic material, i.e. it absorbs atmospheric humidity until its content is in

equilibrium with that of the environment. The factors that influence the absorption of moisture are:

- Temperature and Dew Point of the air;
- Storage conditions and time of exposure of the material to moisture;
- Degree of crystallinity of the material, as amorphous PET absorbs moisture much faster than crystalline PET.

A correct drying of the material is always necessary before it is processed, as the presence of humidity has a considerable effect both on the mechanical characteristics and causes the presence of defects on the final piece.

Another fundamental characteristic of this material is its chemical inertia, which makes it particularly suitable for contact with food. However, it is important to point out that a by-product of the degradation reactions of PET, which occur during its production and during the molding process, is Acetaldehyde (CH_3CHO), which can alter the taste of beverages. Acetaldehyde is a highly volatile product and therefore its presence can be minimized by vacuum or drying processes. [4]

3.1 PET Recycling

Recycling is defined as all those strategies that aim, rather than at landfill, at the recovery of material coming from waste that could still be potentially useful. Clearly, this leads not only to a reduction in the consumption of raw materials, but also to a reduction in energy use and consequently in the emission of greenhouse gases, the main cause of global warming.

As a general rule, when a polymeric material is subjected to processing and reprocessing there is a decrease in its properties, this implies that it cannot be recycled endlessly as it will reach the point where there will be no more useful applications for it and then it will be disposed of in landfill. This shows how, from an environmental point of view, recycling cannot be the definitive solution to a problem that can no longer be underestimated, which could instead be represented by the use of biopolymers.

There are different types of recycling for plastics, the most common are:

- Mechanical Recycling: can be divided into primary recycling (pre-consumer) and secondary recycling (post-consumer). In the first case, the material comes from scraps or processing waste, so in this case, the recycled material has the same properties as the virgin material from which it comes and can therefore be used for the same applications. In the second case, it is a matter of recycling material from objects that have already had a useful life, in this case generally the recycled material finds applications that have lower properties than the material of origin.
- Chemical Recycling: the plastic is subjected to chemical treatments in order to obtain various products such as starting monomers and synthesis gases. When the starting monomer is recovered, the applications and properties are similar to those of the virgin material. Chemical recycling involves a series of pre-treatments and necessary operations that increase its costs, which is why it is often limited for economic reasons.
- Energy Recovery: the polymeric materials are brought to combustion and the energy released during the process is recovered. By subjecting domestic solid waste to mechanical treatment, it is possible to create secondary solid fuel (RDF) which is

marketed in the form of polymer pellets. Energy recovery can be a viable alternative for all materials that cannot be recycled sustainably.

Neither landfill nor incineration, which does not involve energy recovery, are considered as recycling techniques. In the first case, in fact, there is certainly a waste of potentially reusable material, in addition to the need for large areas that could be used for other purposes; in the second case, instead, the incineration of waste can lead to the emission of toxic substances harmful to the environment and to the people.

As regards PET, in consideration of the enormous growth in the use of PET bottles, over the years there has been a strong worldwide interest in recycling and in the possible uses of recycled flakes.

Figure 3.2: Bottles before and after the process [5]

As already mentioned, PET is a 100% recyclable material and recycling processes, both chemical and mechanical, are now highly consolidated.

From a chemical point of view, depolymerization can take place using different agents and therefore with different mechanisms:

- Hydrolysis: obtaining terephthalic acid which, by repolymerization, makes it possible to obtain PET again, or obtaining ethylene glycol which, combined with terephthalic acid, makes it possible to obtain PET;
- Glycolysis: obtaining dihydroxyethylterephthalate, which by repolymerization allows PET to be obtained, or obtaining polyols, which by polycondensation leads to unsaturated polyesters and polyurethanes;
- Methanolysis: obtaining dimethylterephthalate or ethylene glycol which, by repolymerization, leads to the production of PET;
- Ammonolysis: obtaining amides.

As far as mechanical recycling is concerned, it is possible to speak of an "*open loop*" when the recycled material is used for different applications compared to those for which the virgin material was destined, for example PET bottles are recycled for the production of mixed plastic fibres; instead, it is spoken of a "*closed loop*" when the recycled material is used for the same applications as the virgin one, in the case of PET there is the "*bottle-to-bottle*" which means PET bottles are recycled to make other bottles generally as containers for detergents.

As already mentioned, when a polymer is reworked its mechanical properties vary. In particular, the mechanism of degradation of PET involves the scission of the chain, which results in a decrease in the molecular weight of the polymer and therefore as the number of

processing cycles increases, a decrease in mechanical properties. The Tensile Strength has a sudden decline already after the second cycle of reworking, while the Elongation at Break from the third onwards.

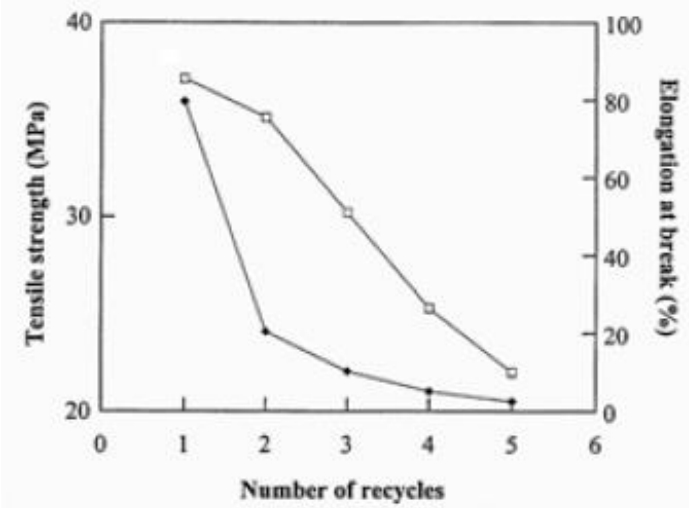

Figure 3.3: Tensile strength and Elongation at break of PET versus recycling steps

As far as Young's Modulus is concerned, since decreasing the length of the chain results in an increase in crystallinity, it can increase or remain constant with the number of cycles. Therefore, by evaluating ductility, it decreases as the molecular weight decreases until the critical molecular weight is reached, at which point the ductile-fragile transition takes place. In addition, in terms of intrinsic viscosity, it decreases as the number of rework cycles increases due to the decrease in the average molecular weight.

To mechanically recycle PET, although each company can customize its own recycling process, there are steps that certainly need to be taken:

- The plant is fed with PET bottles;
- Pre-washing to eliminate any residue of the liquid contained in them;
- Manual and automatic selection by means of NIR spectroscopy through which the bottles are separated according to colour and materials other than PET are discarded;
- Grinding through the use of mills to reduce the bottles into flakes;
- Washing and flotation, to remove any contaminants and residues of adhesive and paper and to separate from any foreign materials residues;
- Drying to eliminate water and moisture present as a result of washing;
- Second grinding to further reduce the size followed by dedusting in order to eliminate the fraction too fine;
- Storage in silos;
- Quality control;
- Packaging of the second raw material.

The obtained second raw material (rPET) can be used for different purposes, but to this end must meet certain requirements such as: low levels of contaminants and the intrinsic viscosity must not vary excessively with respect to both virgin material and between different production batches. In particular, rPET is used in:

- 95,6% fibres

- 1,3% strapping
- 0,3% Engineered resins
- 0,9% film and coatings
- 0,9% beverage containers
- 0,5% non-food containers
- 0,5% Other

From an environmental point of view, to treat one ton of bottles at the inlet, a water treatment process equivalent to a city of about 5000 inhabitants is required, and a consumption of 1.1 m3 of water is expected. However, it is possible to fully recover the incoming ton, generating 760 kg of rPET, 40 kg of caps made of different materials (HDPE, PE), 160 kg of residue for energy recovery, 40 kg of compost.

However, there are some critical issues related to the recycling of this material, such as the presence of residual moisture that leads to a rapid degradation of the material during processing, the high sensitivity to thermal-oxidative degradation that can lead to both aesthetic defects and affect the mechanical properties, pre-process treatments such as drying thrust, the phases of separation from other materials or residues of liquids and glue.

3.2 Opaque PET

Opaque PET is the transparent PET with the addition of a opacifier, usually titanium oxide. The addition of TiO_2 protects the contents of the bottles from UV rays and minimizes the permeation of oxygen inside the bottle itself.

Since 2010, the use of this material has increased considerably, especially for the production of milk bottles previously made of HDPE. [6] In the figure are shown both bottles made of two different materials:

Figure 3.4: a) HDPE milk bottle; b) PET-O milk bottle

The reasons for replacing HDPE with PET-O are [7]:

- PET costs about 20-30% less than HDPE;
- A PET bottle is lighter than a HDPE bottle for the same capacity;

- No more need for aluminium closure;
- Aesthetic finish is brighter;
- Opaque PET bottles increase factory production rates.

The main problem with the use of these bottles lies not only in the non-recyclability of the material but they also disturb the recycling of other bottles because the separation processes are expensive.

Only a small amount of PET-O can be recycled if diluted in the rest of the dark PET stream (maximum 15%), but reduces the quality of dark PET and opaque PET can only be used for the production of fibres or foams.

The problems associated with the recycling of opaque PET lie precisely in the presence of the mineral fillers used to opaque it, although the same fillers in HDPE do not create this type of problem. The reason for this is that PET is more transparent and less dense than HDPE and therefore fillers can prevent recycling due to their colour and properties, as well as when placed in too high a concentration they make PET fibres excessively brittle.

At present, there is no industrial-scale solution for recycling opaque PET in Europe, nor is there an effective method of separation from other plastics; if a recycling solution were to be found, it would be necessary to implement the existing facilities to properly separate packaging made of this material, which would clearly have an economic impact on consumers, sorting centre authorities and recycling companies.

The "RevalPET" project was born with the aim of enhancing the value of opaque PET, to find possible ways to recycle this material by studying the rheological, mechanical and thermal properties for the creation of compounds with other polymers that could find application in innovative sectors.

4. POLYPROPYLENE

Polypropylene, commonly referred to as PP, is a thermoplastic polymeric material that belongs to the family of polyolefins, or polymers obtained by polymerization of vinyl monomers.

The repetitive unit of polypropylene is propylene, i.e. an unsaturated hydrocarbon from the family of alkanes obtained from propane.

In particular, monomers are produced by the cracking of petroleum products such as natural gas or light oils and PP is obtained with the Ziegler-Natta catalysis.

The chemical formula of Polypropylene is shown in the figure 4.1.

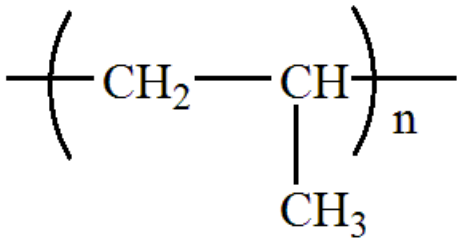

Figure 4.1: Polypropylene Structure Formula

This polymer can show different tactics, i.e. different stereochemical configurations related to asymmetric carbon atoms. During the polymerization process, it is possible to orient the way monomers enter the chain. This means that the methyl groups can be positioned randomly, either symmetrically along the same side of the chain or following a pattern of regular alternation along the chain. There are therefore different types of PP, each with a different molecular weight, crystallinity and tacticity, which strongly influence the characteristics of the final product. Depending on the tactics, it is possible to distinguish between isotactic, syndiotactic and atactic polypropylene.

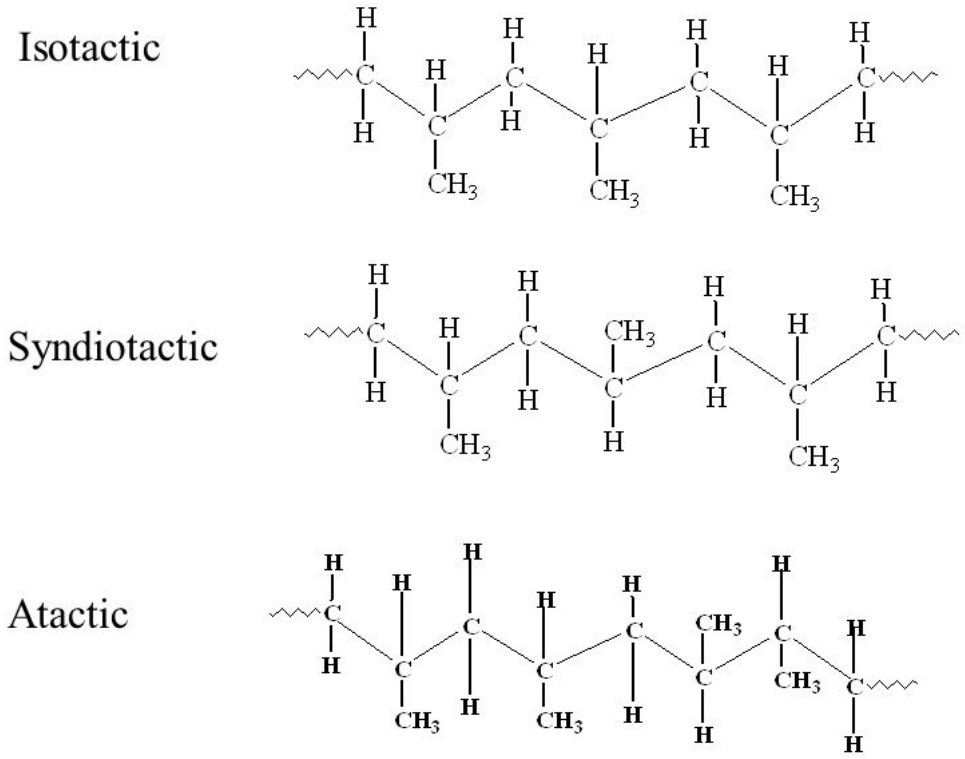

Figure 4.2: Polypropylene formulas with varying tactics

Isotactic Polypropylene is characterized by having all the carbon atoms in the same relative configuration, therefore all the substituents are on the same side; in syndiotactic Polypropylene the adjacent carbon atoms have opposite alternating configurations, therefore the substituents are alternately in one direction and in the other; in atactic Polypropylene the configurations of the carbon atoms are randomly distributed along the chain and therefore the substituents are in one direction or in the other in a random way.[8]

At a commercial level the most interesting is isotactic PP, because it has better mechanical properties due to a higher degree of crystallinity than the other two, in particular it is characterized by high tensile strength, low density (900 kg/m3) and good thermal and abrasion resistance. It is also possible to obtain, using metallocene catalysts, block copolymers consisting of blocks of atactic PP and blocks of isotactic PP in the same chain.

Polypropylene has different optical properties depending on the degree of crystallinity, it can be transparent if in amorphous form or white if in crystalline form. Compared to polyethylene it has an extra methyl group and this makes it better both mechanically and thermally.

Other important characteristics are:

- Good chemical resistance;
- Good electrical insulation;
- Ease of transformation;
- Economical.

Second only to polyethylene is the most produced synthetic plastic in the world with a global market of over 60 million tons per year. All this thanks to its characteristics, its high versatility and compatibility with many processing techniques that make it suitable for many applications in different sectors, such as: automotive sector for the production of

bumpers, dashboards, and other components; components of household appliances; food packaging to make films, trays, containers; as a textile fiber for furniture and linen.

As already mentioned, Polypropylene can be transformed through different processes, the most widely used techniques are:

- Injection moulding thanks to the high fluidity of this material when it is in the molten state, to obtain a wide range of products for everyday use;
- Blow molding, for the production of bottles and jars;
- Extrusion of films, sheets and tubes;
- Thermoforming of sheets to obtain, for example, trays;
- Spinning for the production of synthetic fibres.

4.1 Polypropylene recycling

In view of the very high amount of polypropylene produced, and in the context of what has been said in paragraph 3.1 concerning the importance of recycling plastics, it is clear that recycling of this material is essential.

Most of the material destined for recycling comes from the automotive sector (batteries, bumpers, dashboards) and from packaging, rPP is mainly used in the automotive sector and for the production of geotextiles used in civil engineering.

As already mentioned, recycled material in general has lower properties than virgin material and the properties decrease further as the number of cycles to which it is subjected increases. In the case of polypropylene, in addition to this aspect, the process used must also be taken into account, as the behaviour varies depending on whether the operations take place in an extruder or by injection moulding.

As far as the molecular weight is concerned, taking into account the fact that the dominant degradation mechanism for PP is chain splitting, there is a decrease in both cases already from the first processing cycle.

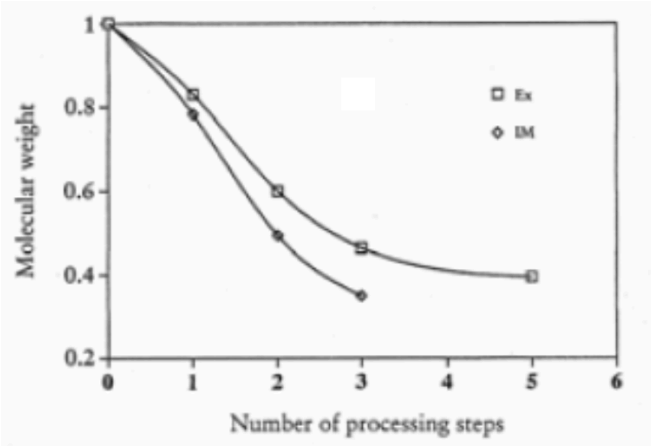

Figure 4.3: variation of the molecular weight of PP according to the number of process steps and the transformation process used.

As far as the elastic modulus is concerned, the behaviour is profoundly different depending on whether it is considered extrusion or injection moulding, as can be seen from the graph shown:

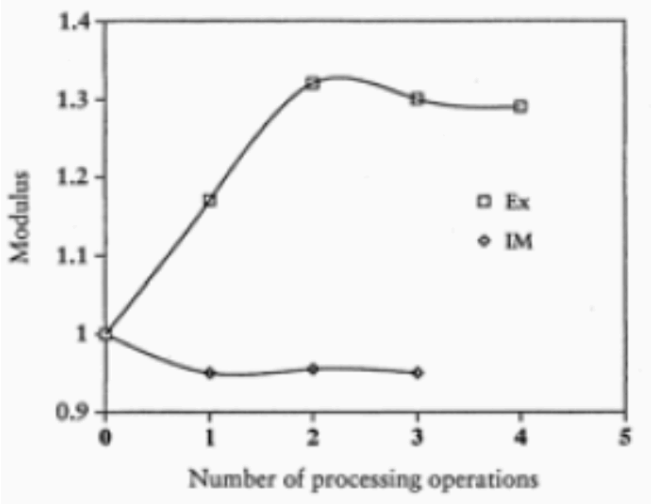

Figure 4.4: variation of the elastic modulus of the PP according to the number of process steps and the transformation process used.

In the case of injection moulding, the modulus remains almost constant, while in the case of extrusion, Young's modulus increases rapidly due to the fact that during extrusion, the chains are increasingly aligned.

Finally, evaluating the elongation at break, in both cases there is a sudden decrease in the second and third cycles respectively for injection moulding and extrusion.

5. EXPERIMENTAL PROCEDURE

During the performance of this thesis work, a preliminary study was initially carried out in order to decide in which percentages and which type of TiO_2 to insert into the polymeric matrix. Subsequently, the compounds of interest were produced and the rheological, thermal, mechanical and morphological characterization was carried out.

5.1 THE MATERIALS

5.1.1 Recycled opaque PET

At the beginning of the RevalPET project, 100% opaque recycled PET (rPET) from milk bottles was used, reinforced with titanium dioxide (TiO_2) nanoparticles and dyes in order to protect the content from UV radiation and minimize the oxygen permeation inside, thus avoiding deterioration of the content. [9]

However, uncontrolled variability in the amount of TiO_2 between batches of material was achieved.

Therefore, to make the material reproducible, a *FLORAL* recycled PET was used, consisting of 10-12% opaque PET and 88-90% conventional colored PET to dilute the TiO_2 concentration. Although it is a less innovative material, it is possible to control the concentration of nanoparticles. In the figure 5.1.1 it is possible to see the material used.

Figure 5.1.1: Flakes of FLORAL rPET

5.1.2 Recycled Polypropylene

The recycled PP used is *rPP QCP™ EXPP 152A*, a recycled copolymer with 95% reused material selected from plastic packaging waste. The grade of this PP combines hardness and impact; however, it has not been previously tested for validation of its use in the food, pharmaceutical or medical sectors.

Figure 5.1.2: Pellets of rPP *QCP™ EXPP 152A*

Density	Kg/m^3	915
Elastic Modulus	MPa	1300
Tensile strength	MPa	27
Tensile strain at break	%	40
Recycled content	%	>95

5.1.3 Titanium dioxide

The highly hydrophobic titanium dioxide used is in the form of nanoparticles with a size of 30 nm and it is covered with silicone oil.

The table below shows its composition:

TiO_2rutile:SiliconeOil	SiO_2	Mg	K+Na	Ca
92+wt%:7wt%	<55ppm	<45ppm	<160ppm	<60ppm

5.1.4 Materials by University of the Basque Country (UBC)

the materials on which a preliminary study was carried out were provided by the University of the Basque Country, namely:

- rPP
- Compound 20rPET-O/80rPP (20/80)
- 20/80+10%TiO_2 hydrophilic
- 20/80+10%TiO_2 hydrophobic
- 20/80+10%TiO_2 modified hydrophobic

5.2 Preparation of samples

5.2.1 Hydraulic Press

The material was supplied by the University of the Basque Country in the form of pellets, so the samples were made using a hydraulic press "IQAP LAP PL-15".

Before the materials were pressed, they were placed in a dryer at 80°C overnight.

The machinery and the mold used are that shown in the figure 5.1:

Figure 5.1: 1) IQAP LAP PL-15 hot plate press equipped with temperature and pressure controlled plates; 2) the mould.

Considering the mold used, plates 140x140x0,5 (mm) were obtained. The conditions under which the materials were processed have been provided by the University of the Basque Country and the Table 1 shows them:

Table 1

Amount of material (g)	Temperature (°C)	First step	Second step	Cooling cycle
13	270	Without pressure t=2min	P=150bar t=5min	water with ice t=2min

In the Figure 5.2 it is possible to observe the samples obtained at the end of the pressing process:

Figure 5.2: Samples of the materials of interest obtained after the pressing process

5.3 Preparation of Compounds

After the preliminary study, it was considered appropriate, in the light of the results obtained and for mainly economic reasons, to use 5% hydrophobic titanium dioxide by weight as reinforcement in the compound.

For the realization of the materials analyzed two different procedures were performed, one related to 20rPET-O/80rPP and one related to 20rPET-O/80rPP + 5% TiO_2.

In both cases, the first step was to homogenize the rPET-O, previously dried in order to eliminate any residual humidity, in a twin-screw extruder. After that, as far as 20rPET-O/80rPP is concerned, the mixing between rPET-O and rPP was carried out in the same extruder, while as far as to 20rPET-O/80rPP + 5% TiO_2 is concerned, the procedure was slightly more complex.

Initially, the recycled PP was mixed with Titanium dioxide in a single-screw extruder, the pellets obtained were then mixed manually with rPET-O and then processed in a twin-screw extruder.

The equipment used to produce the materials and the characterizations carried out are described below.

5.3.1 Compounding

To homogenize rPET-O, in which 2.39% of TiO_2 is present, it was extruded in order to obtain the raw material in the form of pellets.

Before any processing of a material containing PET, it is necessary to dry it, because during storage PET absorbs moisture up to 0.2% by weight. This moisture is not limited to the surface layer only, but spreads inside the grain and if it is present inside the material at the

time of processing, when it exceeds the melting temperature of the material, the water present would have a hydrolysis effect that would degrade the material. Normally, the residual moisture level in the material should not exceed 50 ppm before processing. [10]

Therefore, it was necessary to dry the material at 120°C for 4 hours. The dehumidifier, PIOVAN (DSN506HE, Venice, Italy) visible from the image 5.3, was then used:

Figure 5.3: PIOVAN (DSN506HE, Venice, Italy)

A co-rotating twin-screw extruder KNETER 25X24D, Collin GmbH, Ebersberg, Germany was used to homogenizes the product, with a ratio of L/D=36 and a screw diameter of 25 mm. The extruder has a circular die and consists of seven zones, each of one is maintained at a certain temperature. The extruder works in vacuum to eliminate all gases, at the same time nitrogen is blown in to ensure that the atmosphere is inert.

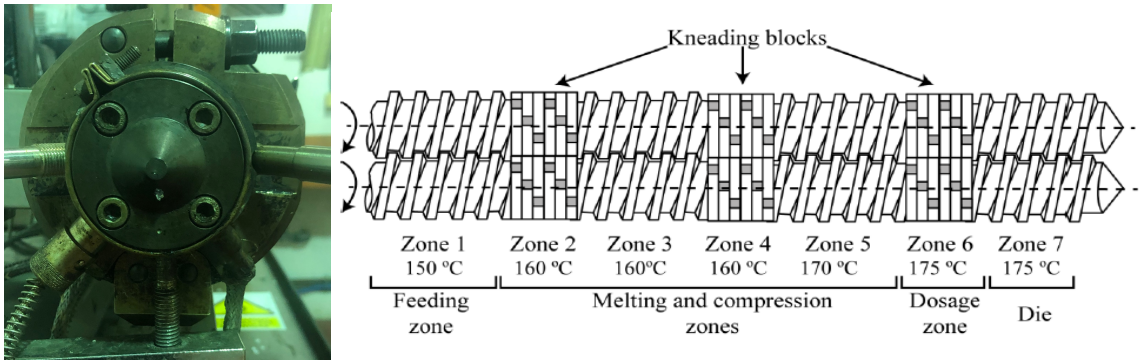

Figure 5.4: 1) Circular die; 2) schematic representation of extrusion

The table 2 shows all the conditions used for extrusion:

Table 2

Zones	1	2	3	4	5	6	7
Temperature ramp (°C)	175	215	230	235	240	245	245
spindle speed	80 rpm						
feeding speed	15,9 g/min						
cutting speed	358 rpm						

After homogenizing rPET-O, two compounds were created. In the first one there is 20% by weight of rPET-O and 80% by weight of rPP (20/80), while in the second one the same ratio by weight between rPET-O and rPP has been maintained, but the 5 % Titanium dioxide hydrophobic (TiO_2) has been inserted as filler (20/80 + 5% TiO_2).

As far as the 20/80 compound is concerned, a mechanical mixing was initially carried out in order to obtain the correct proportion of the two phases, and then it was dried for 4 hours at 100°C.

Subsequently, the same twin-screw extruder described above was used to make the pellets.

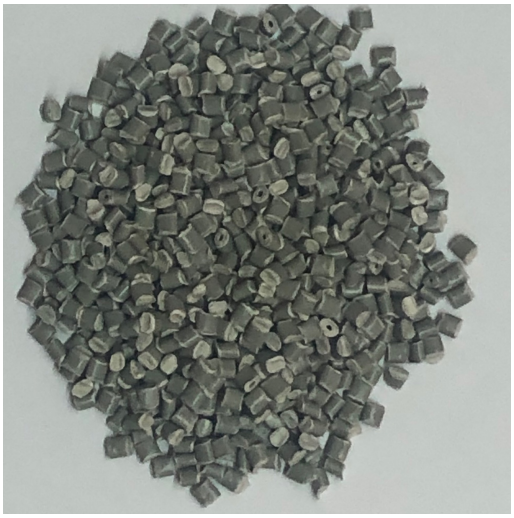

5.5: 20rPET/80rPP compound pellets

In the table 3, it is possible to observe all the conditions used for the extrusion:

Table 3

Zones	1	2	3	4	5	6	7
Temperature ramp (°C)	175	215	230	235	240	245	245
spindle speed	80 rpm						
feeding speed	71,5 g/min						
cutting speed	750 rpm						

As far as the compound 20/80 + 5% TiO2 is concerned, the preparation was more complex. Titanium dioxide has been added in order to obtain an improvement in the mechanical and thermal properties of the recycled material. Initially, this was mixed exclusively with rPP within a single-screw extruder (Figure 5.6).

Figure 5.6: Single-screw extruder

Table 4

Zones	1	2	3	4
Temperature ramp (°C)	140	160	185	210
spindle speed	50 rpm			
cutting speed	840 rpm			

Therefore, after obtaining the pellets, the desired compound (20/80+5%TiO_2) was obtained using the twin-screw extruder.

Figure 5.7: 20rPET/80rPP + 5%TiO_2 pellets

The table 5 shows all the extrusion conditions:

Table 5

Zones	1	2	3	4	5	6	7
Temperature ramp (°C)	175	215	230	235	240	245	245
spindle speed	80 rpm						
feeding speed	59,7 g/min						
cutting speed	750 rpm						

5.3.2 Extrusion: Sheet Preparation

After the production of the pellets of the two compounds of interest (20rPET-O/80rPP and 20rPET-O/80rPP + 5% TiO_2), the process continued in order to obtain, starting from them, the foils on which the mechanical tests were then carried out.

For this purpose, the twin-screw extruder described above was used, replacing the circular head with a flat head and then connected to the calender to obtain sheets with a thickness of 0,6 mm and a width of 100 mm.

In the image 5.8 it is possible to observe a diagram of the system used, while in the table there are all the calendering conditions, which were the same for both compounds.

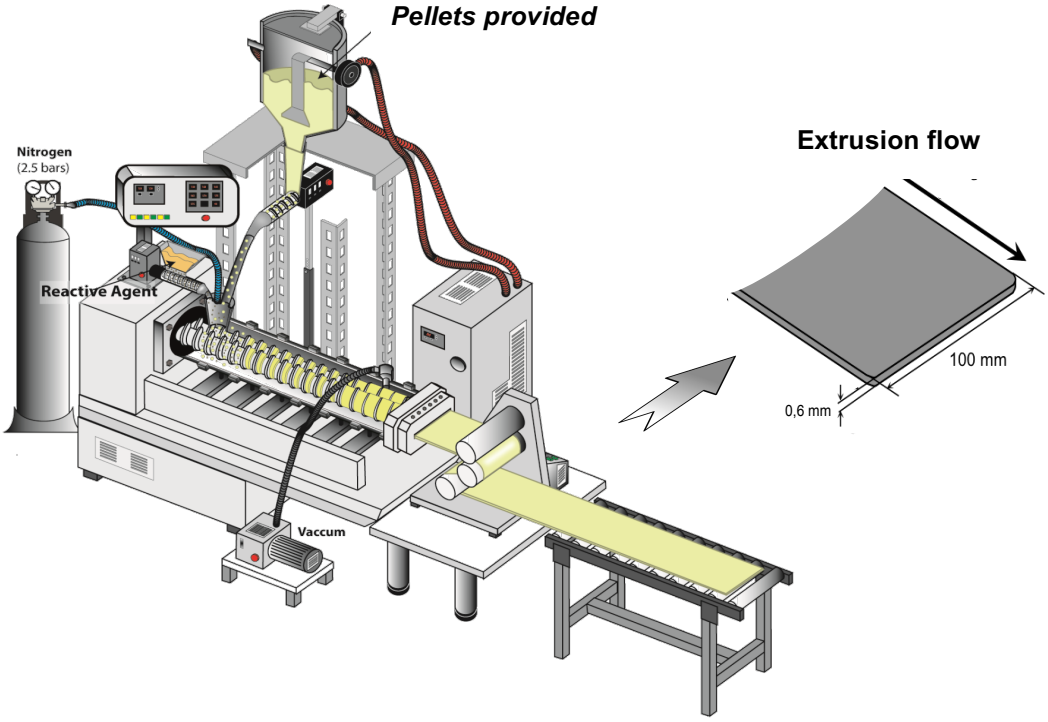

Figure 5.8: Scheme of the system used

Table 6

Zones	1	2	3	4	5	6	7
Temperature ramp (°C)	140	180	195	205	215	215	210
Screw speed	55 rpm						
feed speed	55 g/min						
calender speed	0,4 rpm						
Temperature calender	50 °C						

5.4 Rheological Characterization

It was decided to carry out the rheological characterization on the materials produced in order to better understand their behavior and to be able to appreciate any changes due to the processing cycles and processing conditions.

5.4.1 Capillary Viscosimetry

The capillary viscometer was used to analyze the viscosity of the previously homogenized rPET-O, in order to carry out a quality control of the material obtained and a comparison with the same virgin material. The viscometer used is Ubbelohde Type 1B. The amount of

material analyzed was 0.25 g and the reference used was a solvent consisting of 60%$_{wt}$ phenol and 40%$_{wt}$ tetrachloroethane according to the ASTM D 4603-03 standard.

First of all, a solution consisting of 0.25 g of r-PET-O with 25 ml of solvent was created, which was stirred at 60 rpm and 110°C for 15 minutes in order to obtain perfect dissolution of the r-PET-O in the solvent. As soon as the solution reached room temperature, an additional 25 ml of solvent was added in order to have the exact concentration of rPET-O desired in the solution, which must be equal to 0.5% as per the regulations.

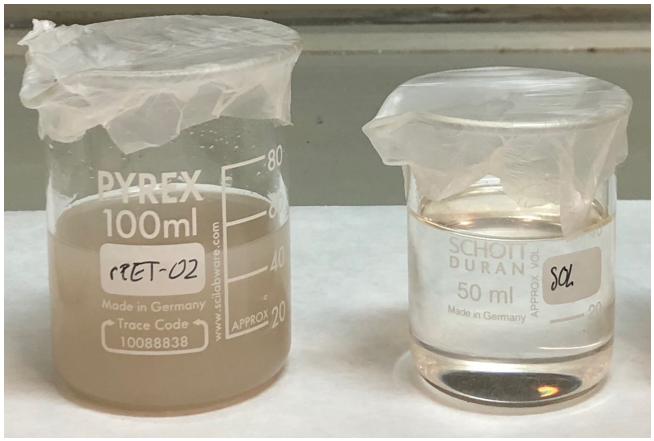

Figure 5.9: 1) Solution containing PET-O; 2) solvent

After that, the empty viscometer was placed in a water bath which must be kept at a temperature of 30°C during the whole execution of the test.

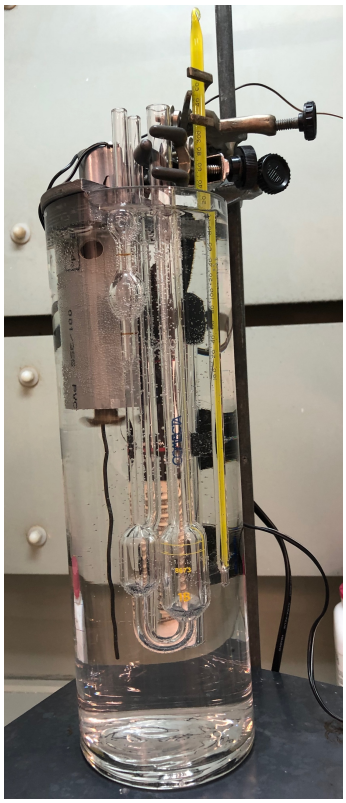

Figure 5.10: Ubbelohde Type 1B

The first measurement to be made is that of the solvent used as a reference only. Then the solvent was placed in the viscometer and the latter in the bath, waiting for the thermal equilibrium to be reached at 30 °C, and the measurement was carried out.

Before to start with the measurement to the solution, it was necessary to filter the solution because, as is well known, inside the rPET-O there is TiO_2, which we want to exclude from our analysis.

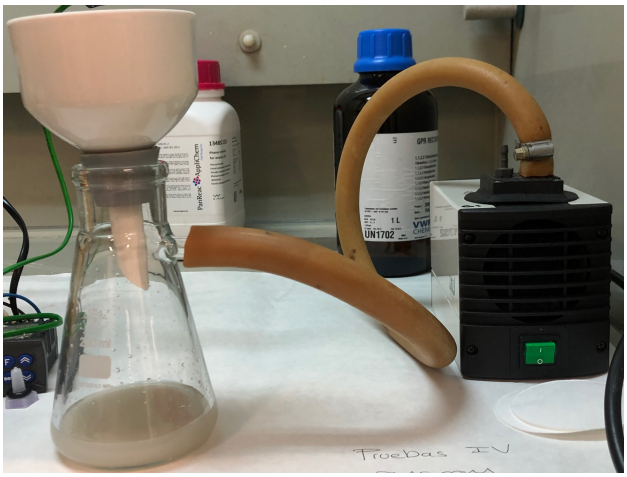

Figure 5.11: Filtering of the solution

After filtration, the analysis was carried out. This consists of timing as the time the solvent arrives from the first to the second line, this measurement is repeated five times and it is necessary to have a standard deviation at most equal to 0,2.

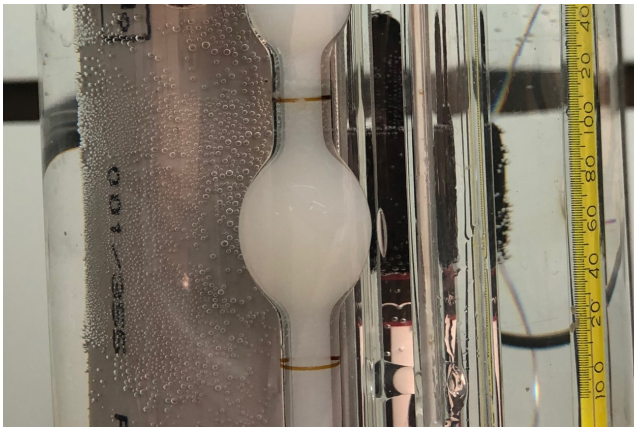

Figure 5.12: Representation of the first and second lines on the viscometer

The formula used for intrinsic viscosity calcium is the Billimer relationship:

$$\eta = 0.25\ (\eta_r - 1 + 3 \ln \eta_r)/C$$

where:

η_r= relative viscosity= t/t_0,

t= average solution flow time, s,

t_0 = average solvent flow time, s,

C= polymer solution concentration, g/dL

5.4.2 Melt Flow Index

The samples for which the MFI was analysed are:

- rPP
- 20/80 (dry & not dry)
- 20/80 + 5% TiO_2 (dry & not dry)

The test was carried out in accordance with ISO 1133 at Temperature of 230°C. The materials analyzed are in the form of pellets, in particular, for each sample, 4 g of material were analyzed and a cutting time of 7 seconds was applied.

In order to know the flow index of the materials processed, a series of MFI tests were carried out on the starting raw material (rPP) and compounds generated in the form of pellets. Since the minority phase of the compound is a semi-crystalline polyester, a drying process was applied to both mixtures in order to know the effect of humidity versus a thermal process.

5.5 Thermal Characterization

5.5.1 Differential Scanning Calorimetry (DSC)

The differential scanning calorimetry, known by the acronym DSC, is a technique of thermal analysis that records the changes in enthalpy of the material under examination as a function of temperature or as a function of time at a fixed temperature. Its versatility stems from the fact that most physical transformations or chemical reactions produce energy variations in the system.

The basic principle of this technique is to obtain information on the material by heating or cooling it in a controlled manner, and in particular the DSC measurement detects the difference in heat flow between the sample under examination and a reference, which remains inert to temperature changes, while the two are bound to the same heat treatment.

The differential measurement of the system is important, because the resulting signal can be studied independently of the thermal effects external to the system, i.e. the behavior of the material can be studied independently of the test conditions.

The instrument can be outlined as follows:

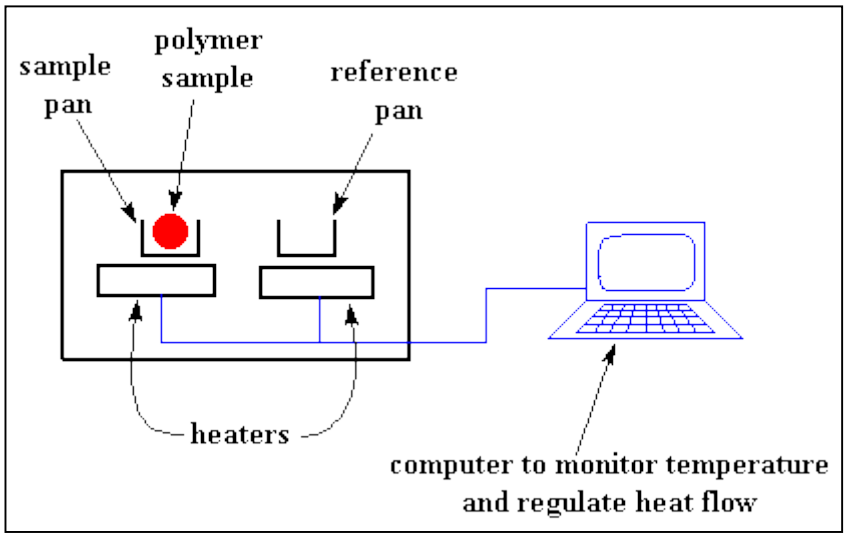

Figure 5.13: DSC operating diagram

The experiment is prepared by placing two identical crucibles on the housings, chosen in such a way as to resist the test temperatures without interacting with the sample under examination. One of the two crucibles will remain empty, as it will serve as a reference for differential measurement.

Once the thermal program (usually a linear temperature ramp) has been inserted into the furnace containing the material to be analyzed, an inert atmosphere with a continuous and uniform flow of argon or nitrogen is created. Once the test has started, the two crucibles are heated in the same way by means of a specific heat flow, for polymers normally 10 °C/min.

Any temperature variation between the two crucibles is due to phenomena arising in the material to be analyzed: an exothermic reaction will raise the temperature of the sample, while an endothermic reaction will do the opposite. During the experiment, a system of thermocouples collects the temperature data and sends them to a computer that through a special software processes them to generate the output - a thermogram - for the user. Specifically, the thermogram consists of a graph in which the temperature is shown on the axis of the abscissae, while the axis of the ordinates shows the variation of the heat flow.

Figure 5.14 shows a typical example of a thermogram in which all the information typically obtained through DSC analysis is contained:

- glass transition temperature of the polymer (Tg);
- melting temperature (Tm);
- crystallization temperature (Tc);
- melting enthalpy (Hm), proportional to the area underlying the peaks;
- determination of the degree of crystallinity of semi-crystalline polymers, proportional to the crystallization enthalpy.

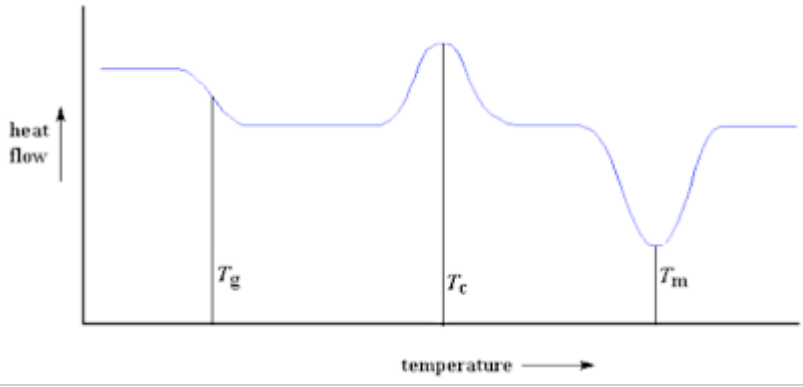

Figure 5.14: Ideal thermogram containing all possible information provided by a DSC analysis

In this thesis, the calorimetric analysis was carried out in order to evaluate the recrystallization temperature and then determine the variation of the enthalpy value at melting and the subsequent degree of crystallinity. The materials analyzed were:

- rPET-O
- rPP
- 20rPET/80rPP
- 20rPET/80rPP + 5% TiO_2

The analysis was carried out by means of a differential scanning calorimeter of TA Instruments, model Q2000, in the figure 5.15:

Figure 5.15: Differential Scanning Calorimeter from TA Instruments Model Q2000

The procedure performed was as follows:

- Preparation of the samples: 6mg of material were weighed and placed inside a special Aluminum crucible.
- The crucible was then inserted into the chamber, using aluminum as the reference material.
- As far as the test is concerned, this has involved several steps:

1. Achievement of equilibrium at 30 °C,

2. isotherm for 2 minutes,
3. start of the temperature ramp at a speed of 10°C/min up to a temperature of 290°C in order to be sure that all the material is perfectly melted,
4. when the T of 290°C was reached, an isotherm was made for 3 minutes,
5. consequently, cooling began at a speed of 10 °C/min from 290°C to 30 °C,
6. isotherm for 3 minutes,
7. start of the second temperature cycle always performed up to 290 °C.

5.6 Mechanical Characterization

5.6.1 Tensile test

The Tensile test was carried out using a universal tensile test machine GALDABINI Sun 2500 (Figure 5.16), both on samples made by pressing and on extruded foils.

Figure 5.16: GALDABINI Sun 2500

With regard to the materials provided by the UBC, in order to carry out the tensile test, it was necessary to make specimens with dog bone, as required by the ISO 527-2:2012 regulations. The Figure 5.17 and the Table 7 show all the characteristics that the specimens must have.

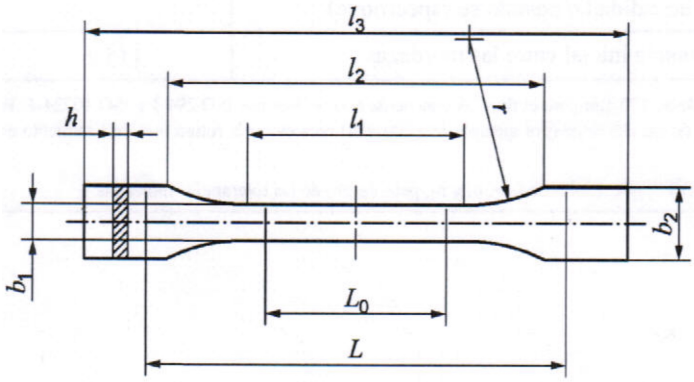

Figure 5.17: Specimen dimensions according to ISO standards

Table 7

	Specimen type	**1BA**
l_3	Overall lenght	≥ 75
l_1	Length of the narrow part of parallel faces	30,0±0,5
r	Radiance	≥ 30
l_2	Distance between the wide parts of parallel faces	58 ± 2
b_2	Width at the extremities	10,0 ± 0,5
b_1	Width of the narrow section	5,0 ± 0,5
h	Thickness	≥ 2
L_0	Reference length	25,0 ± 0,5
L	Initial distance between the jaws	58 ± 2

The geometry was selected based on the dimensions of the plate generated by the compression process and the amount of material disposed.

The samples were extracted from a specific zone of the plates due to the heterogeneous thickness in each one.

The test was carried out in order to know the elastic modulus (E), the yield strength (σ_y), the yield strain (%) and the tensile strength (%).

The conditions under which the tensile test was carried out were as follows:

- Load cell: 1KN
- Distance between grippers: 58 mm
- Distance between marks: 25 mm
- Test speed: 5mm/min
- Specimen geometry: Type 1BA
- Number of samples to be tested: 5 per material
- Temperature: 20 °C

- Humidity: 30%
- Preload: 1,5

According to the standard, in the elastic portion was measured the Young Modulus with a 2D video extensometer coupled to a windows software and the strain between the marks. In the Figure 5.18 it is possible to see all the samples after they have been tested.

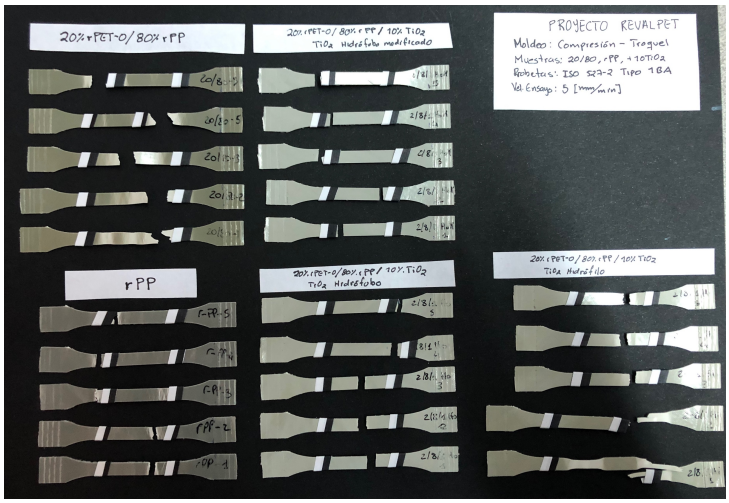

Figure 5.18: Samples after tensile test

As far as the compounds produced are concerned the tensile test was carried out on samples made according to ISO 527-3 "type 5". In the figure 5.19 it is possible to see a sample diagram and in the table 8, all the corresponding dimensions.

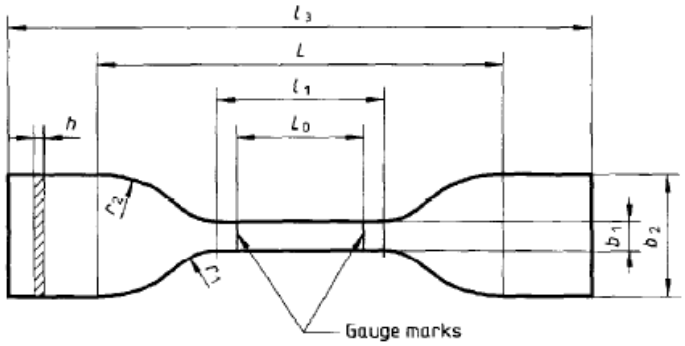

Figure 5.19: Samples ISO527-3 “type 5”

Table 8

Section	Dimensions (mm)
h	≤ 1
L	80 ± 5
L_0	25 ± 0,25
l_3	> 115
b_1	6 ± 0,4

The test was carried out in order to know the elastic modulus (E), the yield strength (σ_y), the yield strain (%) and the tensile strength (%).

The conditions under which the tensile test was carried out were as follows:

- Load cell: 1KN
- Distance between grippers: 80 mm
- Distance between marks: 25 mm
- Test speed: 20 mm/min
- Specimen geometry: Type 5
- Number of samples to be tested: 12 per material
- Temperature: 21 °C
- Humidity: 42%
- Preload: 1,5

According to the standard, in the elastic portion was measured the Young Modulus with a 2D video extensometer coupled to a windows software and the strain between the marks. In the image 5.20 and 5.21 it is possible to see all the samples after they have been tested.

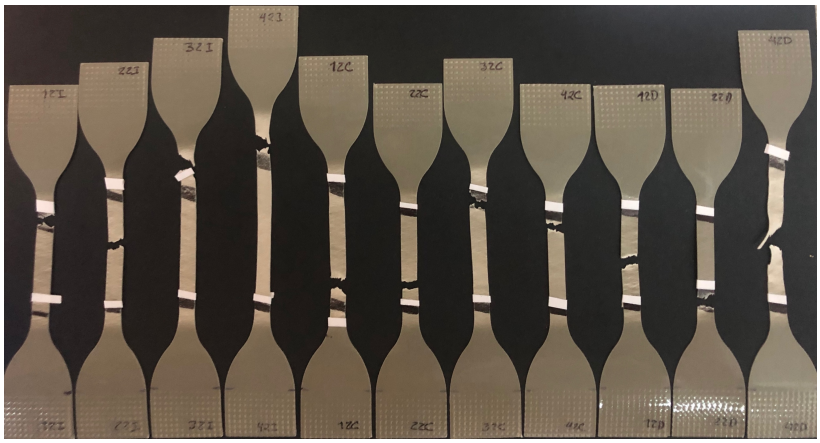

Figure 5.20: 20rPET-O/80rPP

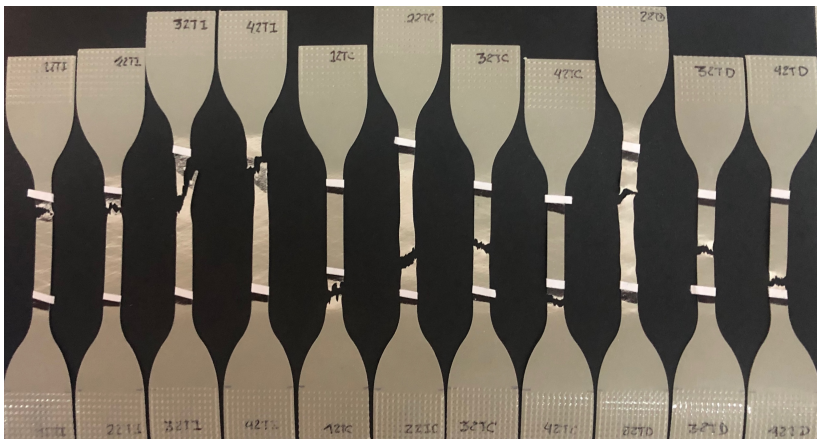

Figure 5.21: 20rPET-O/80rPP + 5% TiO_2

5.6.2 Crack Tip Opening Displacement (CTOD)

Fracture mechanics is a study of the material's fracture resistivity, consisting two main parts: - linear elastic fracture mechanics (LEFM) and elastic plastic fracture mechanics (EPFM). Linear elastic fracture mechanics describes the material's fracture resistance within the elastic yielding region, mainly represented by stress intensity factor, K; the elastic plastic fracture mechanics considers post yielding where the crack deforms plastically, represented by the J-integral and crack tip opening displacement, CTOD.

CTOD is a measure of the physical opening of an original crack tip in a standard fracture toughness test specimen at the point of stable or unstable crack extension. Material exhibiting elastic-plastic properties would experience plastic deformation at the crack tip before fracture. The maximum opening of the crack tip before cleavage fracture or plastic collapse is the CTOD.

One of the best-known definition for CTOD is the opening of the original crack tip when the crack opens due to loading. It is a measure of displacement of the crack tip, where the original crack tip (produced by machining or fatigue pre-cracking) experiences blunting as the crack opens, resulting in a finite displacement at the original crack tip:

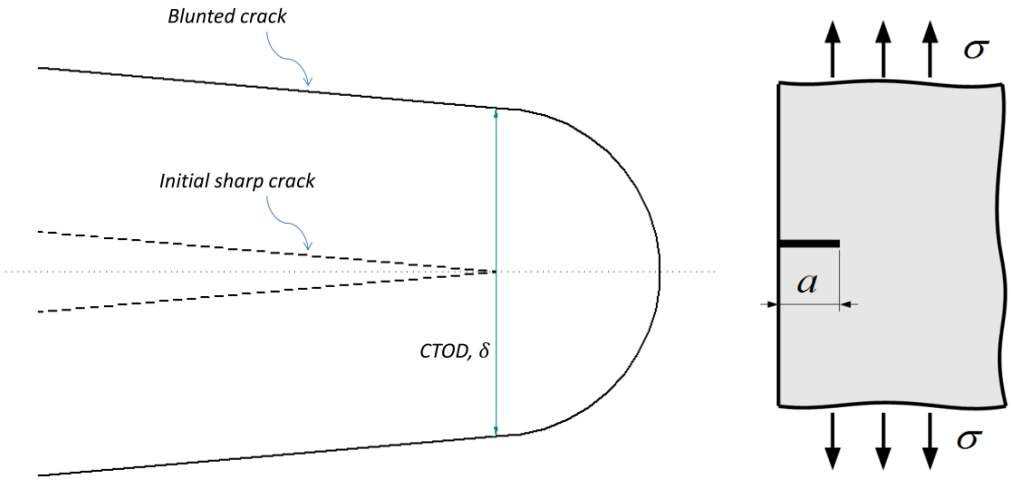

Figure 5.22: SENT geometry

The geometry of the specimens used for the CTOD study corresponds to the so-called SENT with the dimensions described in the figure 5.22. The ratio crack length - specimen width (a/W) was 0,5 in all cases. Once the notch was made, it was sharpened by means of a razor blade up to a length of 1,5 mm in each of the samples in order to standardize the preparation sequence before the test.All the samples are characterized by CTOD.

The instrument used is AMSLER HC 25 by Zwick/Roell (figure 5.23)

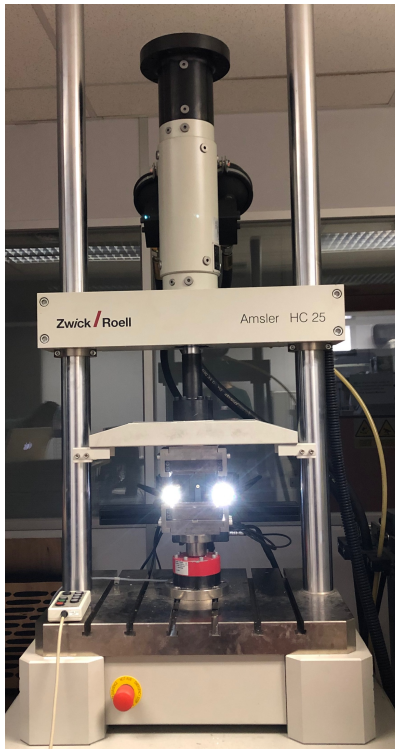

Figure 5.23: AMSLER HC 25 by Zwick/Roell

The machinery is characterized by load cells of 2.5 and 25 KN and a maximum stroke of 100 mm in which it is possible to perform tensile and bending tests as well as high number of cycle fatigue. It has fixed and movable clamps for clamping flat and cylindrical samples. The operation of the equipment consists of a servo-hydraulic mechanism that, by varying the voltage, transforms and sends the acquired signal in terms of applied load, time and displacement through a load cell.

The monitoring of the deformation in the specimen was carried out by means of an optical analysis system of deformation in 3D (ARAMIS) of high temporal and local resolution, without contact, developed by GOM (Gesellschaft für Optische Messtechnik) that determines the coordinates, displacements and deformations in the surface of the piece along the tensile test under the decomposition of the tensor gradient of deformation in two dimensions.

Since the output data must be extremely accurate, the digital image correlation system requires accurate calibration based on the parameters shown in the figure 5.24.

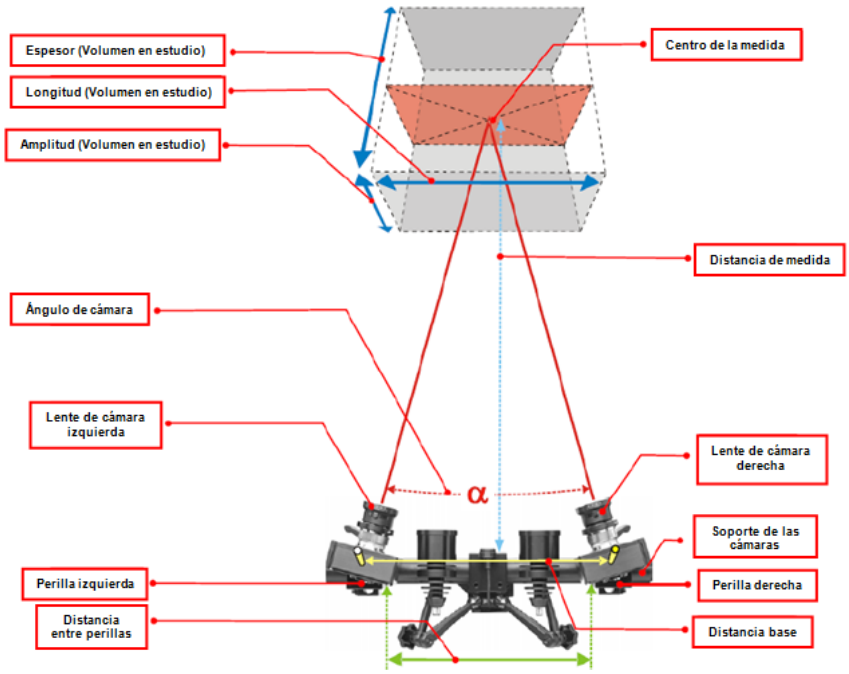

Figure 5.24: Calibration parameters of the GOM optical system and the spatial arrangement of the volume under study

The values of each parameter are established based on the type of cameras and dimensions of the lenses available. Similarly, there is a series of values for a given volume of study, i.e., depending on the geometry of the specimen to be analyzed, a previous calibration is carried out applying the calibration code corresponding.

As far as the tests carried out in the present work are concerned, the optical device consisted of two stereoscopic cameras of 2M configuration.

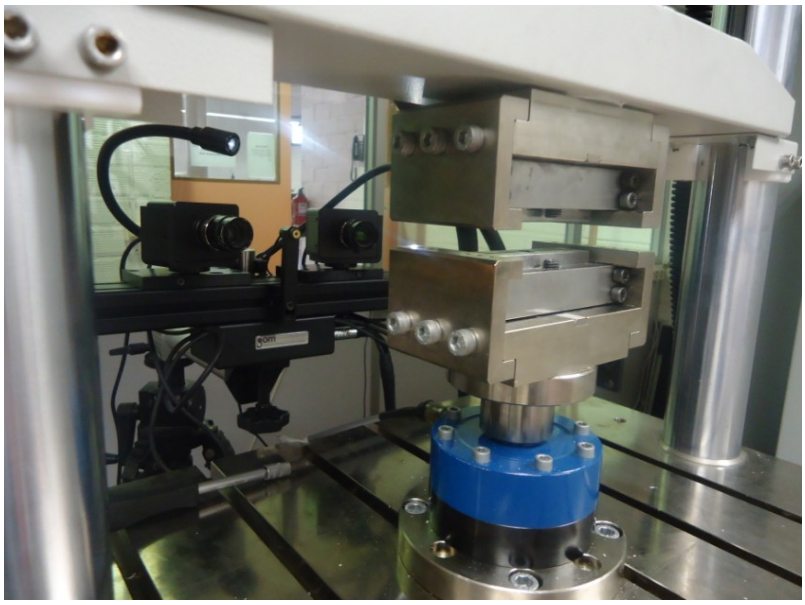

Figure 5.25: Optical analysis system used to study the materials

Each configuration has a calibration standard. This pattern is an informative scale panel under an organized distribution of secondary points and specific location of primary points with interpoint separations of 1mm delimited by the rectangular dimensions that its name establishes. Thus, the standard used for the current calibration (figure 5.26) corresponds to

65mm x 52mm (1mm).

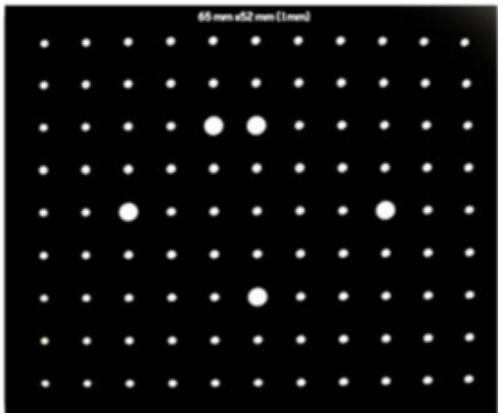

Figure 5.26: Calibration pattern used for the study of specimens with halter geometry

The calibration sequence is also determined by the type of study to be performed. For a 2D analysis, calibration with a single camera and a sequence in the positioning of the associated standard is sufficient. When the analysis is in 3D, as it is the case of this work, the sequence and the number of steps for the optimal calibration is clearly increased. The calibration is based on the capture of images of the pattern in different positions established by the program (figure 5.27), thus detecting the distance and orientation of the primary and secondary points.

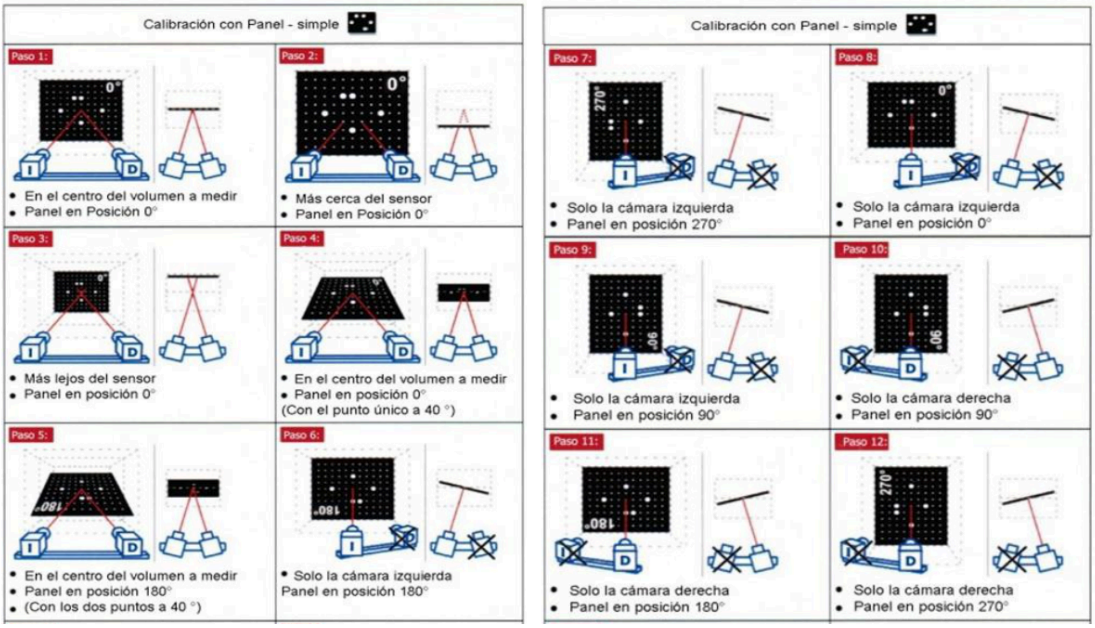

Figure 5.27: Graphical calibration sequence for a 3D analysis with the corresponding pattern.

Once the calibration is completed, the program sends a result deviation to quantify its accuracy. If the accuracy is between 0.01 and 0.04 pixels, it will be Calibration guarantees the reliability of the data obtained in retrospect.

One of the preliminary aspects on which the GOM system is based is the variation of the distance between characteristic points, which is why the surfaces of the specimens were conditioned to achieve a correct recording of dimensional changes without altering their morphological or chemical properties. Two coats of paint were applied to the surface of the specimens by spraying: matt white paint as a base and then stochastic black paint generating

a fine pattern of evenly distributed points.

In the figure 5.28 it is possible to observe one of the samples used before and after painting:

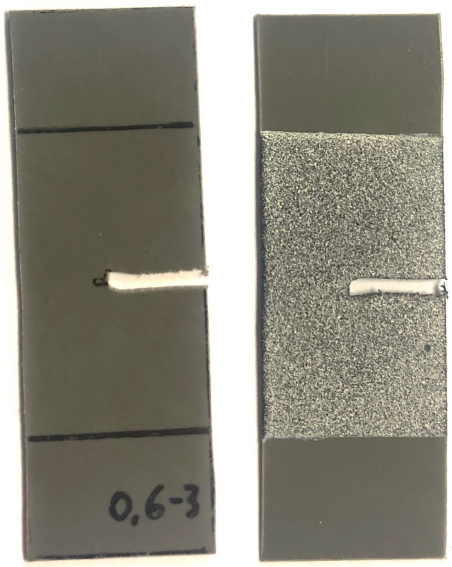

Figure 5.28: Samples before and after painting

After having carefully calibrated the machinery and correctly prepared the samples, the test for the evaluation of the CTOD was carried out.

The table 9 shows all the conditions used during the test:

Table 9

Load cell	25 KN
Distance between jaws	25 mm
Test speed	1 mm/imn
Speciemen geometry	SENT
Number of samples to be tested	10
Temperature	20 °C
Humidity	30%
Pre Load	1,5 N

In the figure 5.29 it is possible to observe the samples after they have been tested:

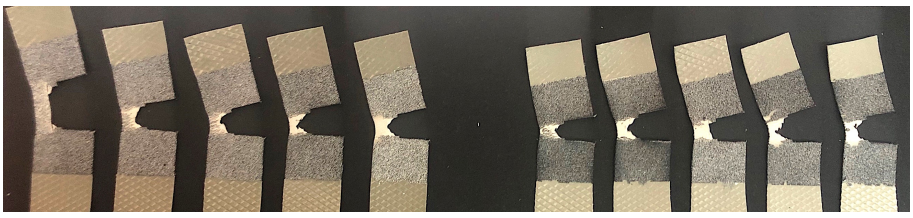

Figure 5.29: Samples after the test

5.6.3 Essential Work Fracture (EWF)

Essential Work Fracture (EWF) is a technique by which the fracture parameters of a polymeric film can be determined. When considering a ductile material, the complete failure of the material occurs before the crack propagates. Two phenomena can be observed during this process, namely the fracture process and the plastic deformation that are reflected respectively in an internal fracture region and in an external plastic zone. [11;12]

This technique was originally proposed by Boberg, according to which when a ductile sample, subjected to uniform tensile stresses, has a central rupture, around it the plastic zone has two different zones: an internal zone related to the fracture process (FPZ) and an external zone related to the plastic deformation process (OPZ). The work dissipated in FPZ is independent of the material being tested, while the work associated with OPZ depends on the geometry of the sample and the actual length of the ligament.[13;14] In the figure 5.30 it is possible to observe the two zones just described.

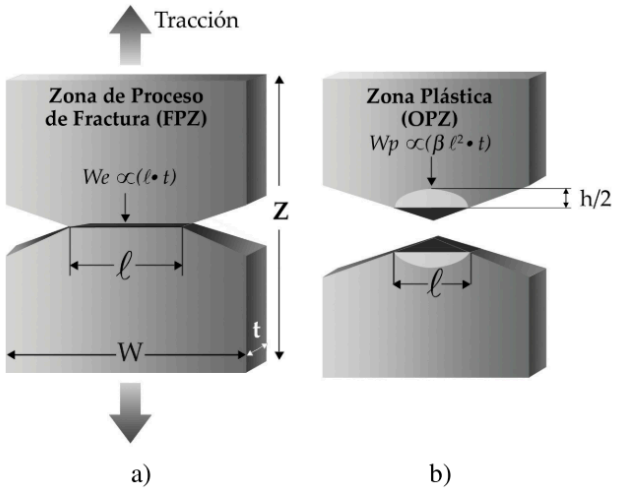

Figure 5.30: Specimen diagram DDENT a) before testing and b) after testing

Consequently, when the front of the crack propagates after the generation of the plastic zone, the work necessary for the entire fracture process (W_f) will be given by the contribution of two terms, each of which refers to a process zone:

$$W_f = W_e + W_p$$

The first term (W_e) represents the essential fracture work, i.e. the work necessary to form a new surface located in FPZ; W_p instead represents the non-essential fracture work, i.e. the work caused by the different deformation mechanisms present such as crazing and micro cavity. [14;15]

The previous equation, as W_e is related to the fracture surface and W_p to the fracture volume, can be rewritten as follows:

$$W_f = w_e \cdot lt + \beta w_p \cdot l^2 t$$

with:

- l = lenght of the real ligament
- t = sample thickness
- β = shape factor relative to the deformed volume around the ligament

Wanting to represent the specific work:

$$\frac{W_f}{lt} = w_f = w_e + \beta w_p \cdot l$$

It is possible to obtain the parameters w_e and βw_p by placing in a graph the linear regression of the specific total work *vs* length of the ligament [16]

The test was performed on the previously extruded sheets, i.e. on the compounds 20rPET-O/80rPP and 20rPET-O/80rPP + 5% TiO_2. The samples were then produced, 45 for each compound, DDENT with double incision, the diagram of which can be seen in the figure 5.31:

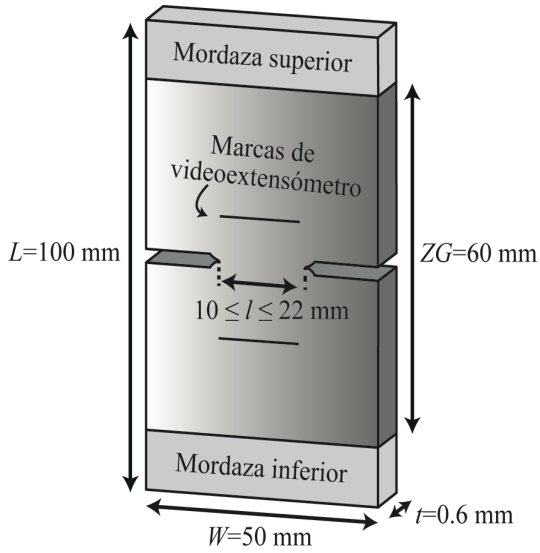

Figure 5.31: DDENT geometry

As required by ESIS TC-4 [17], to ensure a plane deformation, nine different ligament lengths were made in mm: 10; 11.5; 13; 14.5; 16; 17.5; 19; 20.5; 22, and also the two notches were made in the TD direction, applying the load in the MD direction.

The study of the essential fracture work (EWF) was carried out following the guidelines established by the ESIS which highlight the state of stress to which the specimens must be subjected (pure state of planar stress) as well as the complete yield of the ligament before the beginning of crack propagation.

Fracture analysis was performed on DDENT specimens with 9 different ligaments ranging from 10mm-22mm and intervals of 1,5 mm; the thickness was previously established in the extrusion-calendering process and fixed at 0,6 mm. The distance between black and white contrast marks for the deformation measurement corresponded, in each case, to the length of the ligament, i.e., for a 13mm ligament, the distance between marks was 13 mm.

Specimens were obtained from extruded sheets in flow direction (MD) and the ligament section was established in transverse flow direction (TD). The test speed in all cases was 10 mm/min with a load cell of 5 KN.

5.7 Morphological Characterization

5.7.1 Scanning Electron Microscope (SEM)

The Scanning Electron Microscope (SEM) is an instrument through which it is possible to conduct a non-destructive investigation through the interaction between an electron beam and a sample. Thanks to SEM it is possible to obtain morphological and structural information of the sample, but also information related to the chemical nature of the same.

SEM is born from the limit of the resolving power of the optical microscope. In fact, the resolving power "d" - i.e. the minimum distance between two distinguishable points - is substantially linked to the wavelength λ of the radiation used. In particular, the resolving power is defined by the following relation:

$$d = 0.61 \frac{\lambda}{nsen\alpha}$$

where:

n = refractive index of the medium in which the lens operates;

α = angular aperture of the lens.

Since the value of the angular aperture - depending on the type of lens and the medium in which the radiation is propagated - generally varies between 0.95 and 1.40, in order to increase the resolving power, it is necessary to vary the wavelength of the radiation with which the analysis is made. Therefore, since the resolving power increases proportionally to the decreasing of the wavelength of the radiation used and since the electrons have a radiation of very low wavelength, it is possible to use electron beams to obtain higher resolving powers than a normal optical microscope.

In fact, with a d.d.p. of 100kV values of wavelength equal to 0.04 Å, a resolving power of 5 Å and a depth of field of 5 m are obtained; instead, typical values of the resolving power of an optical microscope are never higher than 2000 Å.

The experimental apparatus (figure 5.32) is essentially composed of an electronic column at the top of which is placed the emitter of electrons (usually an incandescent filament of tungsten or lanthanum exaboride that emits electrons by thermoelectronic effect) and a device that gives strong acceleration to the beam of electrons emitted, subjecting them to a high voltage in a range ranging from 20 to 100 thousand volts. The accelerated electron beam crosses a condenser (electrostatic or magnetic), affects the sample, is collected on a lens (electrostatic or magnetic) and passing through an eyepiece goes to incise either on a fluorescent screen or on a photographic plate forming the image for visual observation. The process described above takes place in the ultra-high vacuum provided by a system of pumps.

Under these conditions, the wavelength of the electrons ranges from 0.1 to 0.005 Å (1 angström = 10-10 meters) so as to be several tens of thousands of times smaller than the visible light.

The optical system of the instrument consists of two magnetic lenses: a condensing lens and an objective lens. The first (consisting of one or more lenses) is used to control the electron beam that reaches the target; the second determines the electron beam incident on the surface of the sample.

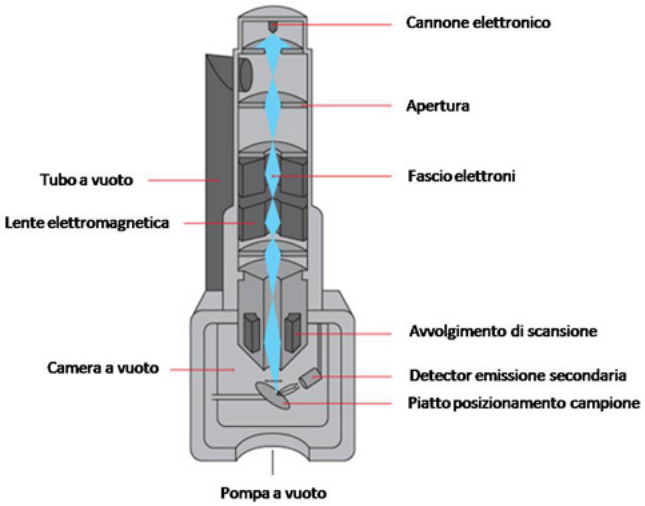

Figure 5.32: SEM functional scheme

The principle of image formation is sequential, in the sense that an electron beam (probe) is focused on the surface of the sample and made to slide on it according to close parallel lines, as is the case for the electronic brush of a television tube.

The interaction of the electron beam (primary electrons) with the material generates, in addition to the transmitted electrons, also different forms of energy (figure 5.33) such as:

- electronic energy (secondary electrons, backscattered electrons or Auger electrons);
- photon emission (infrared and visible);
- X-ray emissions.

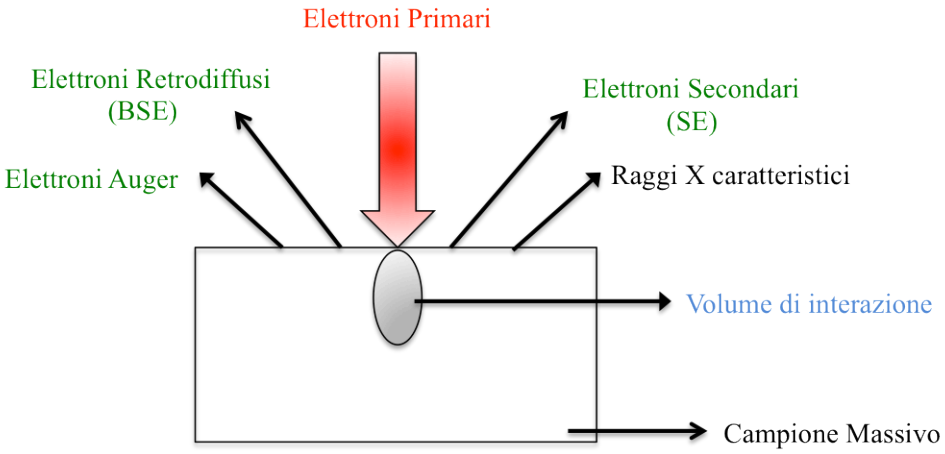

Figure 5.33: Scheme of interaction of the electrons with the sample

Each of these forms of energy is able to provide indications on the nature and morphology of the material, but the most commonly exploited sources are the emission of secondary and backscattering electrons.

Secondary electrons with low energy - less than 50 eV - come from the interaction of the primary beam and the backscattered electrons with the valence electrons. These electrons provide information on the morphology of the sample and on the presence and distribution of magnetic or electric fields. A scintillator/phototube preceded by an accelerator stage is used to detect them. The image provided by these electrons appears in relief, as if the observer were at the same level as the internal diaphragm and looked at the object illuminated by a hypothetical source located at the detector.

As for the back-scattered electrons, or BSE (Back-Scattered Electron) signals, with high energy - higher than 50 V - derive from the primary beam following the interaction with the atomic nuclei. These electrons provide information about the average atomic number of the interaction volume (about a few μm), the topography and the crystalline structure of the sample. This results in different shades of gray, such that heavier elements (with a high Z) appear in lighter shades of gray.

The products of the interaction are then collected by appropriate detectors and transformed into electrical signals, which, once amplified, are sent to modulate the intensity of the beam of the cathode ray tube.

The scanning movement of the probe and the electronic brush of the tube takes place by means of two pairs of electromagnetic coils placed inside the lenses of the lens, which move the electronic brush on the Cartesian coordinates X and Y of the surface of the sample through the electrical signal sent to it, making each position of the probe on the sample correspond to a position defined by the brush on the screen of the tube, whose brightness therefore depends on the intensity of the signal collected.

The elements making up the final image are called image points or pixels (0.01 mm2). The magnification obtained with such an optical system, is given by the ratio between the width of the screen of the cathode ray tube and the length of the corresponding tract traversed by the probe on the surface of the sample. The resolving power of the SEM is due to the size of the geometric diameter of the probe, which can be improved (at the same current intensity of the beam, which determines the contrast) by using sources of high brightness and / or large angles of opening of the cone of electrons converging on the surface.

While not reaching theoretical limits, the electron microscope provides up to 150,000 to 200,000 magnifications, with a resolving power of the order of one millionth of a millimeter (millimicron).

SEM provides information on the appearance, nature and surface properties of samples, with an average resolution of 2,5 nanometers (referred to the signal "generated" by secondary electrons).

The design of the sample chambers is carried out in such a way as to facilitate the exchange of the samples themselves, with little change in pressure from the ambient to the working pressure. The sample holder can also vary in X, Y and Z directions, rotating around the samples to examine them at any point.

The most common technique for obtaining SEM images from non-conductive samples is to coat the surface of the sample with a thin metal film produced by sputtering or vacuum evaporation.

In this thesis, the analysis of the SEM images was obtained with a microscope MEB JSM-7001F (JEOL) coupled to an image capture system controlled by the program. The samples were observed in the two directions, perpendicular (Transversal direction - TD), and horizontal to the flow (Melting direction - MD) as well as in the center and skin areas of the sample as indicated in the figure 5.34:

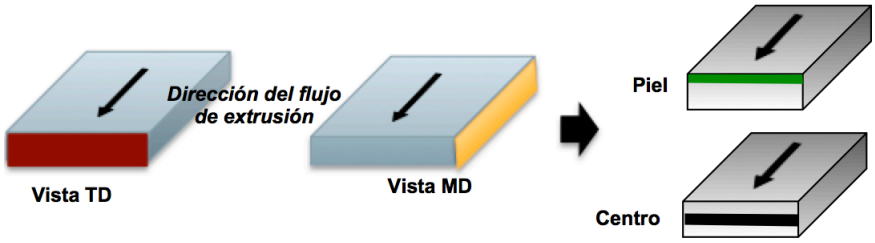

Figure 5.34: Representative diagram of the fracture zones analysed in SEM

The samples analyzed at SEM were those for which the essential work of fracture (EWF) had been evaluated:

- rPP
- rPET-O
- 20rPET/80rPP,
- 20rPET-O/80rPP + 5%TiO_2.

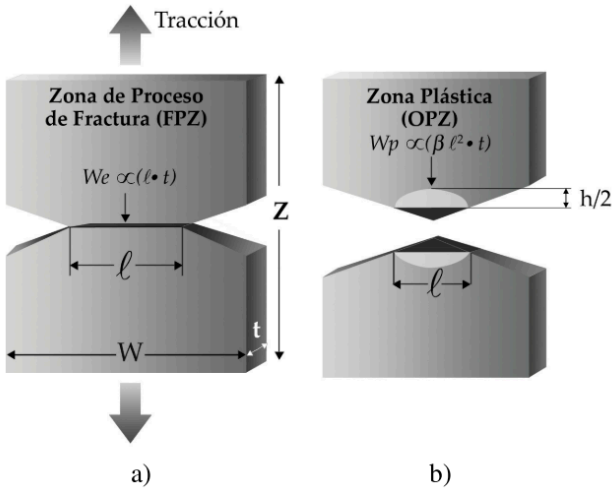

Figure 5.35: Specimen diagram DDENT a) before tensile testing and b) after testing

To analyze the essential work fracture, the samples were made with a ligament between 10 mm and 22 mm. However, only the sample with a ligament of 16 mm was tested for SEM.

Table 10 shows the parameters used for rPP and 20/80, table 11 shows the parameters used rPET-O and 20/80+5%TiO_2 respectively:

Table 10

Voltage	10 KV
Vacuum	0,25 mbar
Vacuum time	25 sec
Gas	Argon
Metallic	Platinum & Palladium (80/20)
Metallic time	60 sec
Standby time	20 sec
Current	28-29 mA
Coating thickness	10 nm

Table 11

Voltage	10 KV
Vacuum	$2x10^{-2}$ mbar
Vacuum time	10 min
Gas	Argon
Metallic	Gold
Metallic time	60 sec
Standby time	20 sec
Current	28-29 mA
Coating thickness	10 m

6. RESULTS AND DISCUSSION

In this chapter of the thesis will be analyzed and discussed the results of experimental tests conducted on the following materials:

- UBC Materials
  - rPP
  - 20rPET-O/80rPP
  - 20rPET-O/80rPP + 10% TiO_2 hydrophobic
  - 20rPET-O/80rPP + 10% TiO_2 modified hydrophobic
  - 20rPET-O/80rPP + 10% TiO_2 hydrophilic
- Compounds
  - 20rPET-O/80rPP
  - 20rPET-O/80rPP + 5% TiO_2

6.1 Materials by University of the Basque Country (UBC)

6.1.1 Tensile test

The Young Modulus, Yielding stress and breaking strain were determinate in the engineering stress-strain curve. The imagine 6.1 shows the representative Engineering Stress-strain curves for each sample tested.

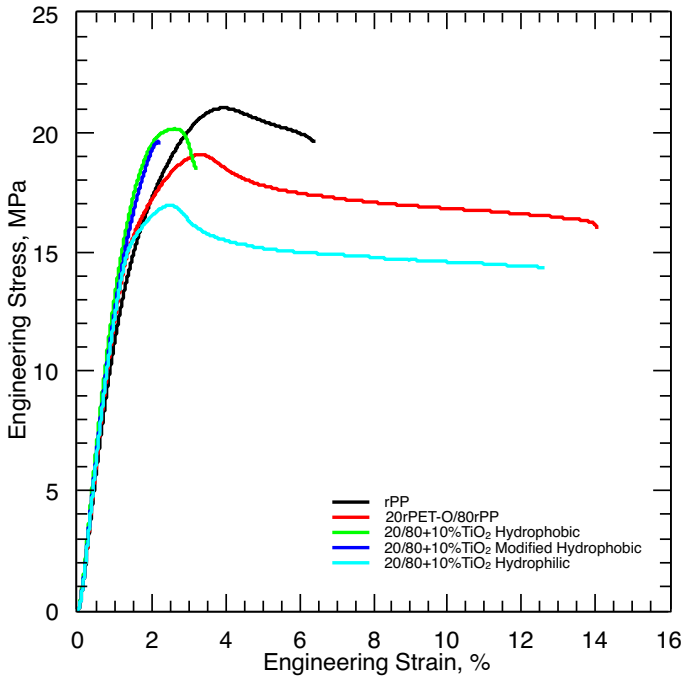

Figure 6.1: Engineering Stress-strain curves

It is possible to see that the starting material (rPP) presents breakage just after the deformation softening process with a low elongation level. When 20% rPET-O is added to the sample, it gives a certain elongation level beyond 14%, i.e., an increase of almost 100% with respect to the rPP.

In reference to the yield stress and associated deformation, although the point value differs by 11% in favor of rPP, the statistical variability makes this change unrepresentative.

Rigidity, however, presents a slight increase when the second polymer phase (rPET-O) is added; a fact that can be motivated by the presence of 2.39% of TiO_2 in the minority raw material.

When 10% hydrophobic TiO_2 is added to the 20/80 mixture, the system presents an increase in stiffness, i.e., the elastic module increases by 11% which indicates that TiO_2 limits the movement of the polymeric chains in the elastic region and also, the yield stress is slightly favored. An important feature to mention is the fragile behavior that imprints the addition of the inorganic load since it decreases drastically from 14.4% to 3.9%.

When this 10% inorganic load is modified superficially, there are no considerable changes in the elastic region, however, it presents a fragile behavior just when the maximum effort is reached. As far as the breaking process is concerned, this is reduced by 40% when TiO_2 is modified.

Finally, and changing the affinity of the inorganic load, the rigidity of the system with 10% hydrophilic TiO_2 does not present considerable changes, however the yield stress is reduced by up to 20% with respect to the hydrophobic sample. Deformation at break is a property that is highly favored since it reaches levels of elongation at break similar to sample 20/80.

The table 12 reports the final results of the tensile test:

Table 12

Samples	Elastic Modulus GPa	Yielding strength MPa	Yielding strain %	Yielding time sec	Strain at break %
rPP	1,1 ± 0,1	21,0 ± 1,2	4,9 ± 0,6	28 ± 4	7,8 ± 2,0
20rPET-O/80rPP	1,26 ± 0,01	19,1 ± 0,5	4,3 ± 0,4	23 ± 2	14,4 ± 1,8
20/80+10%TiO_2 modified hydrophobic	1,3 ± 0,1	19,1 ± 1,0	2,0 ± 0,6	15 ± 1	2,4 ± 0,3
20/80+10%TiO_2 hydrophobic	1,4 ± 0,1	20,9 ± 0,8	3,2 ± 0,1	19 ± 1	3,9 ±0,4
20/80+10%TiO_2 hydrophilic	1,3 ± 0,1	17,8 ± 0,5	3,9 ± 0,5	21 ± 5	12,7 ± 3,1

6.1.2 Crack Tip Opening Displacement (CTOD)

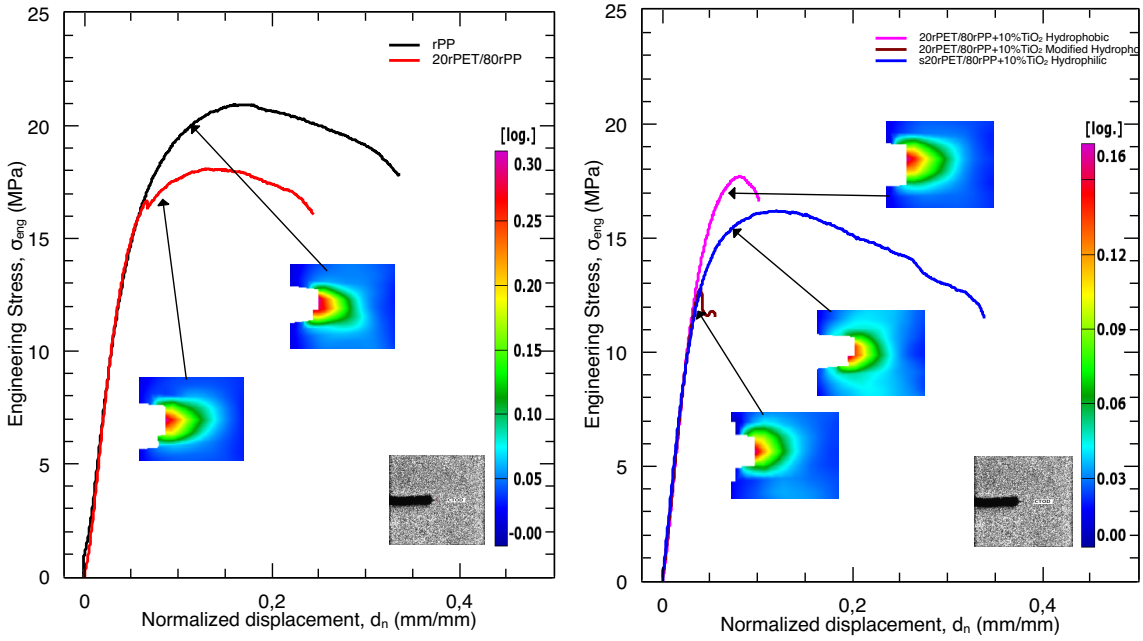

Figure 6.2: Representative graphic of the CTOD 1) rPP and 20/80; 2) 20/80+10%TiO_2

Table 13

Materials	Tickness (mm)	Real ligament (mm)	Load CTOD (N)	Stress CTOD (MPa)	Time (sec)	CTOD
rPP	0,39	7,38	59	20,50	63,9	0,53
20/80	0,4	7,60	52,4	17,24	52,4	0,51
20/80+10% TiO_2 Ho	0,45	7,35	58,3	17,63	35,5	0,33
20/80+10% TiO_2 HoM	0,44	7,38	41,5	12,78	18,7	0,17
20/80+10% TiO_2 Hi	0,46	7,55	55,2	15,89	40,3	0,41

Derived from the uniaxial tensile test on SENT specimens, figure 6.2 shows the Engineering Tension vs. normalized displacement curves (by *l* of 7.5 mm). In reference to the samples without percentage increase of TiO_2 (figure a), the rPP reaches the critical value of crack opening CTOD δ_C=0,53 mm at a load of F_C=59 N while the mixture 20/80 gave a value of δ_C=0,51 mm at a load of F=52,4 N.

Although in both scenarios there is a relatively similar field of crack tip deformations prior to catastrophic propagation, the intrinsic ductility of the rPP allows propagation to occur at 12% greater load F and 10 seconds prior to the catastrophic failure of the 20/80 mixture. Normalizing the load applied to δ_C by the actual ligament section has an increase of 19% in the effort σ_{CTOD} of the rPP versus the mixture before crack propagation.

On the other hand, figure b shows the curves corresponding to the samples with different types of TiO_2. It is noticeable that the sample with TiO_2 Hydrophobic presents a critical load F_C=59 N and develops a deformation field at the tip of the crack of similar dimensions to the sample rPP and 20/80 but with half in magnitude in the true deformation ε_t. While ε_t of rPP and 20/80 has a value close to 0,3 s^{-1}, the Ho mixture has it over 0,16 s^{-1}. Similarly, the value of δ_C decreases by up to 40% to δ_C=0,33 mm.

By normalizing the load by the cross section analyzed, σ_{CTOD}, it can be seen that the effort required to initiate propagation does not vary significantly but the time to which it occurs. A possible explanation may be that the TiO_2 fraction in the sample acts as a stress concentrator promoted by a low level of cohesion between TiO_2-polymer phases.

When TiO_2 is modified superficially (HoM), the load and associated critical effort are significantly affected, decreasing up to 30% with respect to the Ho sample. The critical opening δ_C=0,17 mm and the time in which t_C=0,17 s occurs are also detrimentally pronounced, decreasing up to 50% with respect to the sample without superficial modification of the load.

A visual review of the field of deformations at the tip of the crack shows that the HoM sample develops a slightly smaller field than the hydrophobic sample accompanied by a circular geometry in the plastca flow zone of larger dimensions.

In the curve σ_{Eng} vs d_n important differences can be appreciated for the sample with hydrophilic TiO_2, Hi; a high level of ductility before rupture, the value d_n at which the critical crack opening occurs and the stress associated with this parameter. Although the σ_{CTOD} is in the middle of the other samples, the time at which t_C=40,3 s occurs increases 12% with respect to Ho and doubles with respect to Hi; a similar fact happens with the value of CTOD that changes from 0,17 to 0,41 mm.

As far as the field of deformations is concerned, the HoM sample develops a circular plastic zone at the tip of the crack with a greater transition in the region of small defromations, i.e., the material has the ability to distribute the applied load over a larger zone before the catastrophic growth of the crack. This phenomenon may be due, among other things, to the polarity of the majority phase, chemical affinity between elements of the compound as well as the level of distribution and location of TiO_2 in the sample.

6.2 Compounds

6.2.1 Rheological Characterization

The obtained intrinsic viscosity value for PET-O, as a result of our analysis, by applying the formula in the paragraph 5.4.1 and averaging over five measurements is as follows:

$$\eta_{rPET\text{-}O}= 0,619$$

Regarding the evaluation of the MFI, Figure 6.1 shows the weight of the samples in each cut against the accumulated test time. A similar behaviour is shown in all curves, however there are differences in the initial weight of each sample (higher for samples with additional inorganic filler) and in the total duration of the test (higher for samples without inorganic filler).

In the compound 20/80 without TiO_2 drying (red curve) a stability in the weight is appreciated until the 70 seconds of test, followed by a linear increase in the weight of 22% for 30 seconds (0,7% per second) and finally a smaller slope until the 200 seconds. When

the sample is not dried, the initial weight increases by 33% and a stability of 75 seconds, followed by a steep increase of 20% of the weight for 15 seconds, i.e. 1.3% per second; although there is no change during stability, degradation accelerates when the sample is not dried.

Similarly, the compound with dried TiO_2 (intermittent red curve) has a stability period of 60 seconds, followed by a 21% increase in weight for 35 seconds (0,6% per second). Finally, when the compound is not dried, it has a stability of 50 seconds and a weight increase of 9% for 20 seconds.

Analysing the effect of humidity, in both compounds there is an increase in the weight of each cut when the compounds were not dried (blue curves), i.e., under equal weight and temperature conditions, at the same cutting time the amount of molten material is greater for the samples not dried, which exposes the possible hydrolytic degradation of the second phase (rPET).

An important fact to emphasize is the use of the stable time of each sample, since this can give us an idea of the maximum time of exposure of the sample in a source of thermal energy, or relate it with the optimal residence time in an extrusion or injection process.

As a result of the fluidity study, Table 9 summarizes the data obtained for each compound, the sample without additional inorganic filler has a fluidity index of 3,8 (g/10min) with a previous dryness. However, when the sample is not dried the MFI increases to a value of 5,6 (g/10min), i.e. 47%. The inorganically loaded dried sample yielded a value of 8,0 g/10min, in the absence of the drying process the MFI increases to a value of 9,4 (18%).

Finally, by adding 5% TiO2 to sample 20/80 the MFI increases by 110% when a drying process is applied; similarly, the MFI increases by 68% when no pre-drying is applied.

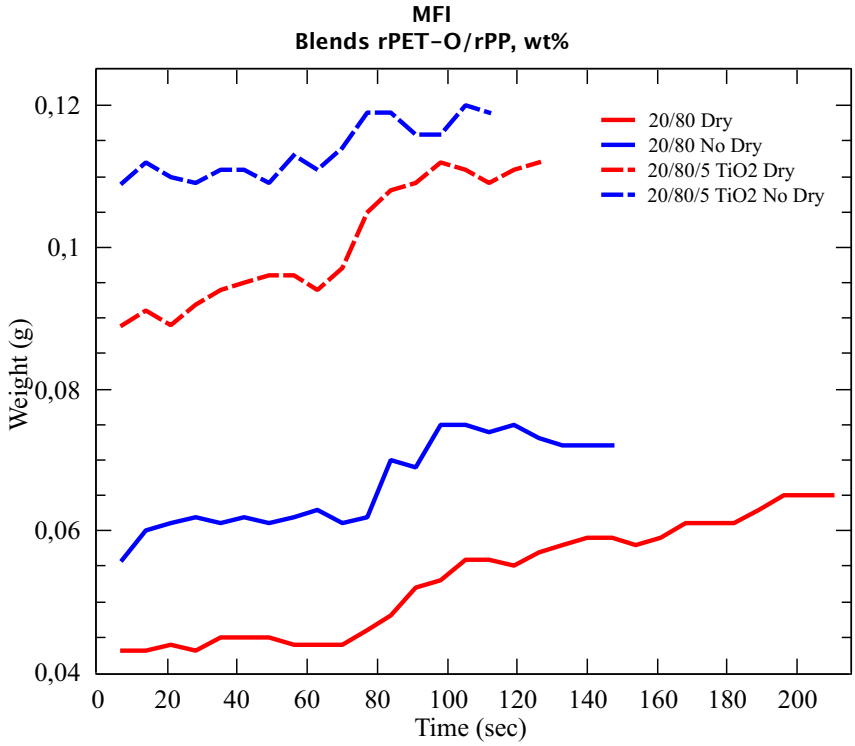

Figure 6.3: Graph representing the trend of the MFI of the compounds of interest

As a statistical argument for sampling, the reliability of the results is adequate given the low standard deviation since the percentage variation is below 5% (CV).

Table 14

Samples	MFI (g/10 min)	Std. Dev. -	CV %
Ref. rPP	*17,7*	*0,7*	*4%*
20/80 Dry	3,8	0,1	3%
20/80 No Dry	5,6	0,3	5%
20/80 + 5%TiO2 Dry	8,0	0,2	3%
20/80 + 5%TiO2 No Dry	9,4	0,3	3%

6.2.2 DSC

Comparative Pellets 3 cycles

In order to know the specific thermal transitions of the starting material, a standard thermal sweep of the two main materials was carried out.

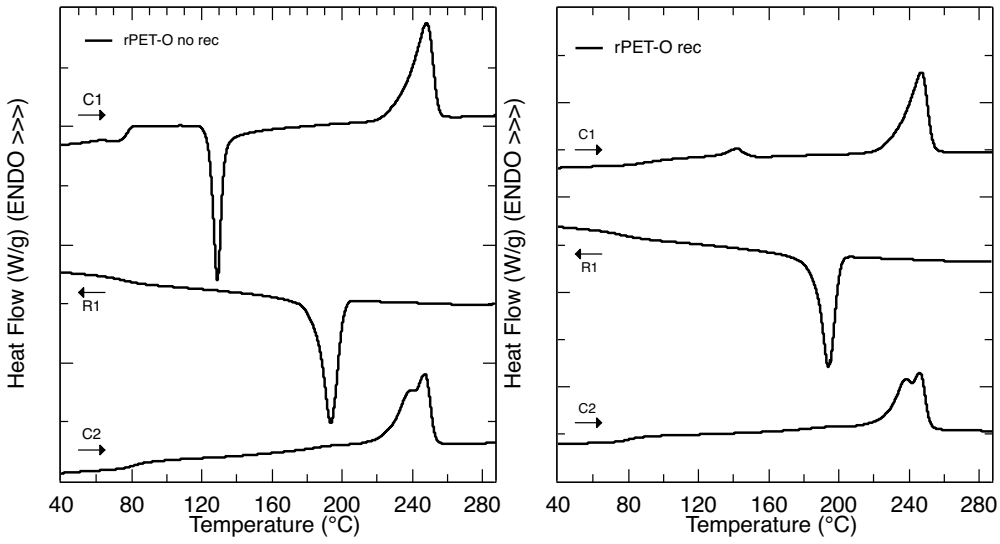

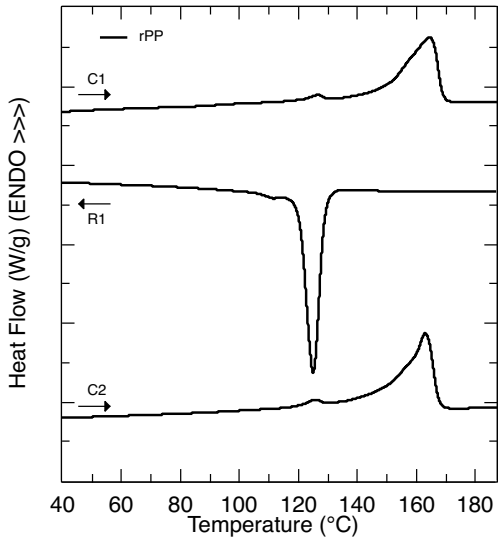

Figure 6.4: Thermal behaviour of the starting material rPET-O after the homogenisation process (a), after the recrystallisation process (b) and of the rPP (c). The nomenclature of each cycle is defined as C1: First heating cycle, R1: Controlled cooling and C2: Second controlled heating cycle, in all cases at 10ºC/min.

In the case of rPET-O, two thermal sweeps, i.e., were performed at the end of the homogenization process (no rec) in order to know the degree of crystallinity obtained after the extrusion process. The second thermal sweep was performed on the same sample after the isothermal recrystallization step controlled at 120 ºC. The second thermal sweep was performed on the same sample after the isothermal recrystallization step controlled at 120 ºC. This temperature was defined based on the cold crystallization peak of the thermometer (a). In both cases, the thermal range of analysis was 40 to 280 [ºC].

In the first heating cycle (C1) of figure 6.4 (a), the vitreous transition region without enthalpic relaxation typical of PET is observed in the initial temperature range of $T_{g\text{-}0}$=74 ºC and $T_{g\text{-}m}$ =77,7 ºC on average. This is followed by the cold crystallization region between $T_{cc\text{-}0}$ =117 ºC and $T_{m,i}$=180 ºC, the latter being defined as the *Cold Crystallization to Fusion Transition Temperature* that represents an exothermic transition in the system, and a minimum in the T_{cc}=129 ºC signal defined as *Peak Cold Crystallization Temperature* and an associated enthalpy of ΔH_{cc}=29.9 J/g quantified by a cold mass crystallinity index of χ_{cc}= 22.6 %. This behaviour is due to an abruptly cooled PET sample, which was carried out during the cooling of the rPET-O flakes homogenization process.

Finally, under an endothermic process, a maximum melting signal at T_m =248 ºC and associated melting enthalpy of ΔH_m=40.7 J/g and melting crystallinity index of χ_m=30.7 % are observed. As a result of this first heating cycle, the homogenised rPET-O sample has a total crystallinity index of χ_{total}= 8,1 %.

In the second cooling cycle from melt R1 the exothermic crystallization process is observed in a temperature range of 205 - 170 [ºC] and a minimum in the signal of T_c=193,6 ºC and χ_c= 25,9 %.

With respect to the second heating cycle C2, there are not very significant differences in the values of $T_{g\text{-}0}$, however there is a slight increase of 3 ºC in $T_{g\text{-}m}$ and a decrease of 30% in the enthalpy variation (ΔCp), phenomenon associated with intermolecular factors such as symmetry and flexibility of the main chains. Thus, ΔCp is less significant the higher the degree of crystallinity of the polymeric system. In this sense, given the absence of the exothermic process of cold crystallization, the crystallinity at the end of C2 has a value of χ_{total}= 24.5 %.

Figure 6.4 (b) shows the thermogram of the recrystallized rPET-O. A fact to be highlighted in the first heating cycle C1 is the absence of the exothermic peak since after eliminating the new polymeric crystals generated in the abrupt cooling by means of an isothermal recrystallization process at a temperature well above T_{g-m}, the amorphous section and the cold crystallization zone present a structural reorganization.

Thus, the glass transition region is in the initial temperature range of T_{g-0}=80 ºC and T_{g-m}=87.6 ºC on average, i.e., an average increase of 6 and 10 ºC, respectively, compared to the sample without recrystallization as well as a decrease of 26 % in ΔCp. Regarding fusion, there are no significant variations in the maximum signal and the associated enthalpy, i.e., in both samples the melt crystallinity index is χ_m=31%.

In R1, there are no significant differences in the temperature range of the crystallization process compared to sample 1a, however, the values of ΔH_c and χ_c show an increase of 12%, with values of 38.6 J/g and 29.1 %, respectively, for the recrystallized sample.

Finally, in C2 a similar response is observed in the vitreous transition of both samples; however, the intensity of the endothermic signal of the recrystallized sample gives a ΔH_m=38.5 J/g and final crystallinity of χ_m=29 %, representing an increase of 18.5% with respect to the non-crystallized sample. This increase is due to the amplitude of the fusion signal, which is greater in this case. Some authors attribute this behaviour to the fact that the molecular weight distribution of long chains is greater. An important fact to emphasize is that, in both samples, there are two maximum signals in the fusion attributed to the formation and fusion of imperfect crystals.

The same three-cycle sweep was performed on the rPP sample (Figure 6.4 (c)). The thermal analysis range for this material was 40 to 180 ºC based on the general thermal transitions of this type of polyolefin which means that only the melting behaviour of the material was analysed.

In the first heating cycle C1, two endothermic signals at T_m=126 ºC and T_m=164.5 ºC can be seen within the characteristic ranges of polyethylene (PE) and PP, which indicates the existence of two phases in the sample. However, the enthalpic contribution of each transition differs significantly, ΔH_m=7,4 and 69,7 J/g respectively. In terms of crystallinity, PE provides a crystallinity index of χ_{m-PE}=2.5% versus χ_{m-PP}=33.7% of PP giving a total rPP index of χ_{TOTAL}=36.2%, so the percentage of the majority phase in the compound (PP) is 93%.

In the second cooling cycle from the melt R1 there is the exothermic crystallization process in the temperature range of 134 to 112 [ºC] for PP and 112 to 98 [ºC] for PE, and a minimum in the signals T_{c-PP}=124,9 ºC and T_{c-PE}=111 ºC. However, the baseline in the thermogram does not recover from one transition to another which suggests a certain level of miscibility between phases. The total crystallinity value at cooling is $\chi_{c-TOTAL}$= 40.6%.

As a result of the inspection of the second heating cycle C2 the most significant variation is given by the enthalpy of both phases and the associated crystallinity index; thus, the crystallinity at the end of C2 is χ_{TOTAL}= 40,1%. Table 15 summarizes the results obtained in the thermal sweep performed on the starting materials.

Table 15

Treatment	Transition	Parameters	rPP		rPET-O Homogenised	rPET-O Recrystallized
			PP	PE		
C1	Glass	[°C] T_{g-0}	-	-	74,2	80,0
		[°C] T_{g-m}	-	-	77,7	87,6
		[W/g] ΔHF	-	-	0,061	0,045
	Cold crystallization	[°C] T_{cc}	-	-	129	-
		[J/g] ΔH_{cc}	-	-	29,9	-
		[%] X_{cc}	-	-	22,6	-
	Melt	[°C] T_m	164,5	126	248	247,2
		[J/g] ΔH_m	69,7	7,4	40,7	42
		[%] X_m	33,7	2,5	30,7	31,7
		[%] X_{total}	36,2		8,1	31,7
R1	Cooling	[°C] T_c	124,9	111	193,6	194
		[J/g] ΔH_c	80	5,7	34,3	38,6
		[%] X_c	38,6	1,9	25,9	29,1
C2	Glass	[°C] T_{g-0}	-	-	75,5	74,9
		[°C] T_{g-m}	-	-	80,1	80,7
		[W/g] ΔHF	-	-	0,043	0,038
	Melt	[°C] T_{m-1}	163	126	239,6	238,7
		[°C] T_{m-2}	-	-	247,2	246,3
		[J/g] ΔH_m	76,1	9,7	32,5	38,5
		[%] X_m	36,8	3,3	24,5	29,0
		[%] X_{total}	40,1		24,5	29

The starting materials in the form of pellets were then calendered using an extruder to produce the foils. It was considered appropriate to make a comparison between the behaviour of the materials in the form of pellets and of the same after a further transformation process. Figure 6.5 shows the graph for rPET-O.

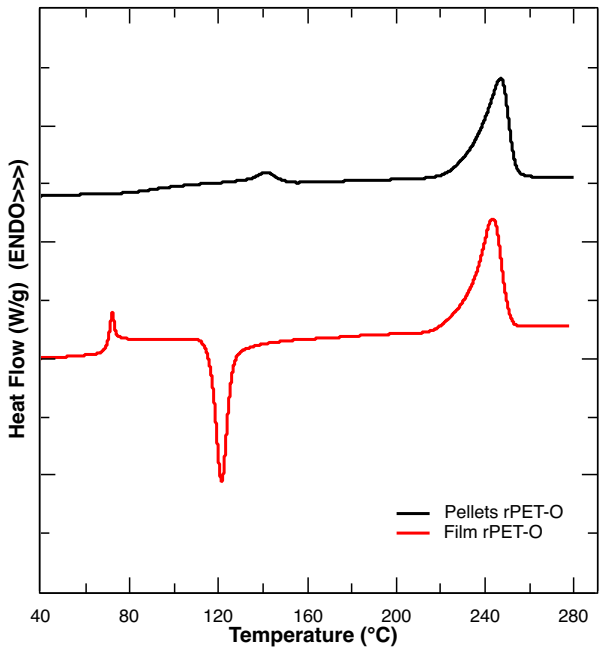

Figure 6.5: Comparison of the thermal behaviour of rPET-O in the form of pellets and films

Observing the behaviour of rPET-O (film), we can notice the glass transition region in an initial range $T_{g\text{-}0}$=73,2 °C and $T_{g\text{-}m}$=74°C. It is evident, when comparing with the same material in the form of granules, that both the glass transition region and the variation of T decreased in terms of T, which in this case is slightly less than 1°C, whereas previously we had observed a difference of almost 10°C.

It is possible to notice the presence of an esothermic peak, which is not present in the curve relative to the granules, this peak is an index of enthalpy relaxation, or a physical aging phenomenon. It is not by chance that it is present in the lamina and not in the granules, since it has undergone an abrupt and poorly controlled cooling cycle during the calendering process for its realization.

Following the glass transition region, we can observe the zone of cold crystallization that presents a minimum at T_{cc}=124,8 °C and an associated enthalpy ΔH_{cc}=31 J/g quantified by an index of crystallinity χ_{cc}=23,4%.

Finally, we note the maximum signal of the melting peak at T_m=246,6 °C and the associated melting enthalpy ΔH_m=40,8 J/g, and the melting crystallinity index ΔH_m=30,8. These values do not differ much from those related to the granules of rPET-O, what instead differs greatly is the value of the total crystallinity index which in this case is χ_{tot}=7,4%.

As far as rPP is concerned, the results obtained for the material in the form of pellets and for the filmed material do not show any particular differences.

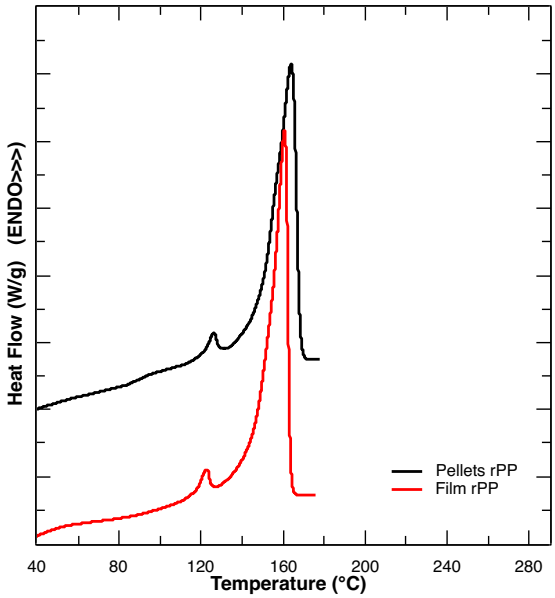

Figure 6.6: Comparison of the thermal behavior of rPP in the form of pellets and films

Also in the case of rPP (film) only the behavior in fusion has been analysed and we note the peaks relative to PE and PP respectively at temperatures $T_{m\text{-}PE}$=125,7°C and $T_{m\text{-}PP}$=163,5; the enthalpic contribution is equal to $\Delta H_{m\text{-}PE}$=4,3 J/g and $\Delta H_{m\text{-}PP}$=72,2 J/g and therefore the crystallinity indices $\chi_{m\text{-}PE}$=1,5 and $\chi_{m\text{-}PP}$=34,9, it follows that the total crystallinity index is χ_{total}=36,3%.

The table 16 shows the values for the materials discussed in film form:

Table 16

Treatment	Transition	Parameters	rPP		rPET-O
			PP	PE	
C1	Glass	[°C] $T_{g\text{-}0}$	-	-	73,2
		[°C] $T_{g\text{-}m}$	-	-	74
		[W/g] ΔHF	-	-	0,109
	Cold crystallization	[°C] T_{cc}	-	-	124,8
		[J/g] ΔH_{cc}	-	-	31
		[%] X_{cc}	-	-	23,4
	Melt	[°C] T_m	163,5	125,7	246,6
		[J/g] ΔH_m	72,2	4,3	40,8
		[%] X_m	34,9	1,5	30,8
		[%] X_{total}	36,3		7,4

After analysing and comparing the starting materials in both pellets and foil form, the analysis was also carried out for the compounds:

- 20/80

- 20/80 + 5% TiO_2

As a result of the differential scanning calorimetry (DSC) study carried out on the extruded sheets in a first heating cycle, the thermogram of figure 6.7 was obtained. In general, three maximum endothermic signals are observed related to the fusion of each element contained in the compounds (PE, rPP and rPET-O, respectively).

The 20rPET/80rPP sample develops a first maximum endothermic (**P1**) at 125 ºC and enthalpy of 5,2 J/g associated with the small portion of PE contained in the compound. Next, and of greater magnitude, a second peak (**P2**) appears over 160ºC corresponding to the majority phase of rPP (57,6 J/g and 27,8%, enthalpy and crystallinity, respectively). The third endothermic maximum (**P3**) referring to the second minority phase rPET (8,4 J/g and 6,4, *idem*) takes place further away at 250ºC.

Similar to the sample without TiO_2, the first endothermic signal (**P1**) of the compound with TiO_2 addition refers to the small portion of PE contained in the compound and reveals crystallinity values of 1,7 associated with a fusion enthalpy of 5 J/g. Immediately thereafter a second endothermic peak (**P2**) develops and of greater magnitude exhibits the rPP matrix in the compound with a crystallinity value of 27 and fusion enthalpy of 56 J/g. The third endothermic peak (**P3**) is related to the presence of the minority phase of rPET and yields a degree of crystallinity of 6,6.

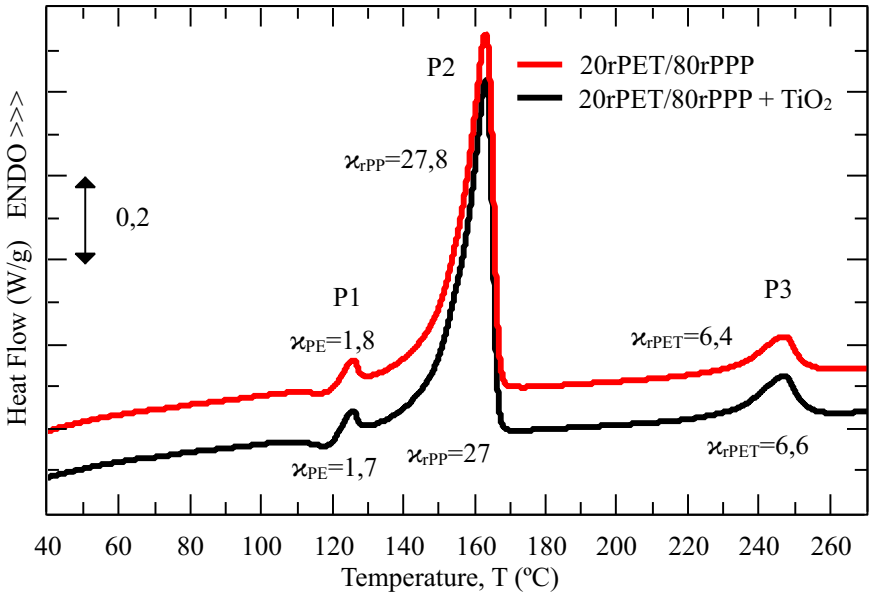

Figure 6.7: Comparison of the thermal behaviour of 20/80 and 20/80+5%TiO_2

Finally, the extrude sheet of 20rPET/80rPP yielded a total crystallinity of 36% where 5%, 77% and 18% is generated by PE, rPP, rPET, respectively. On the other hand, the sample with 5% TiO_2 presented a 35,3% of total crystallinity where 18,5% corresponds to the minority phase of rPET, 76,5% to rPP and 5% to PE, proportion that corresponds to the percentage of each element in the compound.

Although the development of the curves shows a high level of similarity between the compounds, the mixture with TiO_2 shows a slight decrease in the heat flow (exothermic of heat) before the melting signal of the PE (125ºC), this process called cold crystallization is characteristic of PET and obeys exothermic crystallization processes. Although this process is disguised by the fusion of PE, it has its beginnings around 112ºC.

The crystallinity values depend to a large extent on the forming process, which is why only a first heating cycle was performed in order to relate the mechanical response and fracture of the sheets with the degree of crystallinity developed during the extrusion-calender process.

Table 17 shows a summary of numerical results obtained by thermal characterization.

Table 17

Treatment	**Transition**	**Parameters**	**20/80**			**20/80 + 5%TiO2**		
			PP	**PE**	**rPET-O**	**PP**	**PE**	**rPET-O**
C1	Glass	[°C] T_{g-0}	-	-	-	-	-	-
		[°C] T_{g-m}	-	-	-	-	-	-
		[W/g]ΔHF	-	-	-	-	-	-
	Cold crystallization	[°C] T_{cc}	-	-	-	-	-	-
		[J/g]ΔH_{cc}	-	-	-	-	-	-
		[%] X_{cc}	-	-	-	-	-	-
	Melt	[°C] T_m	63	125,4	247,4	163	125,3	247,2
		[J/g] ΔH_m	57,6	5,2	8,4	56	5	8,3
		[%] X_m	27,8	1,8	6,4	27,0	1,7	6,6
		[%] X_{total}	36,0			35,3		

Thermogravimetric analysis was also carried out to evaluate the percentage of residual material following the thermal cycle, in order to verify the correct realization of the compounds. Table 18 shows this data, resulting from the test carried out in air.

Table 18

Material	Residual (%)
rPP	2
rPET-O	2,5
rPP+6,2%TiO_2	9,95
20/80	2,1
20/80+5%TiO_2	5,7

As far as rPP is concerned, there is a residue equal to 2%, having conducted the test in air the presence of Oxygen is relevant because it is possible that there were cyclization reactions that led to the formation of aromatic rings that are stable even in O_2 up to higher temperatures.

rPET-O shows a residue of 2.5%. The residue is due to the presence of Titanium dioxide in this material as mentioned in paragraph 5.1.1. Being in the presence of oxygen, in fact, the aromatic rings present in the polyester chain at a higher temperature is also consumed.

As far as compounds are concerned, the observable residue corresponds to the quantity of TiO2 present. The fact that the percentages do not correspond exactly may be due to a not perfectly controlled dispersion of the inorganic charge within the polymer matrix.

6.2.4 Tensile Test

The Young Modulus, Yielding stress and breaking strain was determinate in the engineering stress- strain curve. The figure 6.8 shows the representative Engineering Stress-strain curves for each sample tested and the table 19 summarizes the main data for each samples.

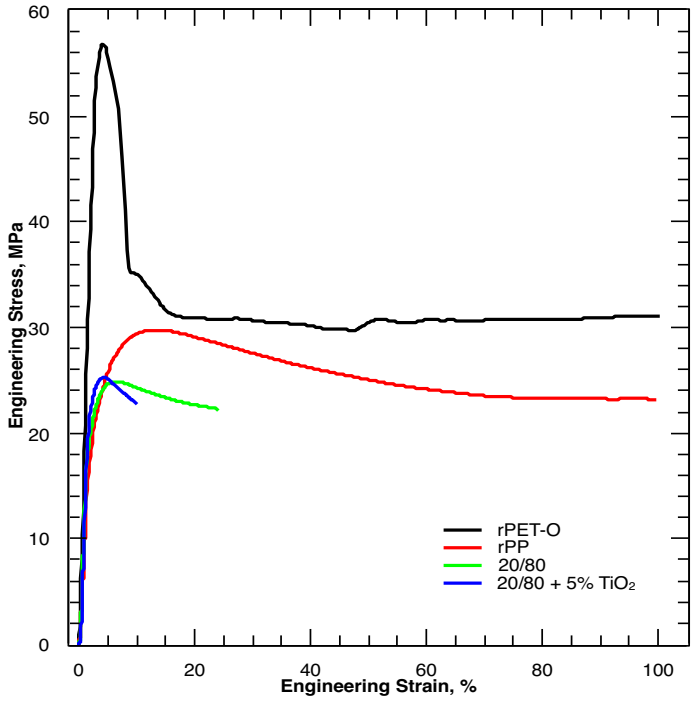

Figure 6.8: Engineering stress-strain curves of raw materials and compounds

Table 19

Samples	Elastic Modulus	Yield strenght	Yeld strain	Strain at break
	GPa	MPa	%	%
rPP	1,16 ± 0,04	28,8 ± 0,6	13,0 ± 0,6	350 ± 22
rPET-O	2,2 ± 0,03	57,3 ± 0,5	3,9 ± 0,04	203 ± 16
20rPET-O/80rPP	1,22 ± 0,03	24,9 ± 0,2	10,94±0,03	33,9 ± 9,6
20/80 + 5% TiO2	1,24 ± 0,03	25,1 ± 0,3	7,7 ± 0,2	23,5 ± 13

From a limited viewpoint and considering rPET-O as a reference material, it presents a high level of rigidity with an elastic modulus (E) of 2,2 GPa and yield stress (σ_y) of 57,3 MPa, the highest compared to the rest of the samples, accompanied by an associated deformation (ε_y) of 3.9%.

On the other hand, the rPP presented an E and σ_y almost 50% lower (1,2 GPa and 28,8 MPa, respectively) accompanied by one ε_y 13%, four times higher than the rPET-O. In both materials, there was a deformation at break that exceeds 200% of the nominal deformation and a high level of confidence (low standard deviation).

The nature of PET responds to the results obtained since the high level of rigidity of rPET-O is sustained by the high crystallization potential conferred by regularity in its molecular structure. Once the elasto-plastic regime (28 MPa) and even σ_y has been reached, the mobility of the amorphous part contained in the microstructure of the system begins in a deformation range of 4%. This moderate molecular flexibility in the polymer chains is due to the existence of a large volume structure in its starting monomer (aromatic rings).

A similar behavior in the elastic range is found in the rPP, with the difference in deformation in the elasto-plastic range where the recycled nature of PP contributes to the reduction in yield stress but with the increase in ε_y.

In reference to the compound 20rPET/80rPP, the module gave a value of 1,23 GPa with a maximum stress of around 24,9 MPa at a yield deformation of 10.9%. However, by incorporating 5% TiO_2 in the sample, both E and σ_y showed an increase of 3% compared to the sample without TiO_2, which, within the statistical error of the calculation, does not present significant relevance. Contrary to what happened with its associated deformation (ε_y), where the decrease was 30%.

A fact to emphasize is the deformation at break (ε_b) in both compounds, although the percentage variability between them is low, the coefficient of variation (VC) in the calculation of breakage exceeds 35% in both cases which suggests a physical heterogeneity in the mixtures, both in the polymer phases and in the inorganic filler.

In general, incorporating 20% rPET into the rPP matrix results in an increase in system rigidity (+6%) and 9.5% when 5% TiO_2 is added. On the contrary, the σ_y decreases by 13,5% and 11,4% with the second polymer phase and the addition of TiO_2, respectively. In the same sense, ε_y is affected with the second phase of rPET-O (-16%) and with the addition of TiO2 (-41%). Finally, in both systems (with and without TiO_2) there is a 90% decrease in ε_b.

6.2.5 Crack Tip Opening Displacement (CTOD)

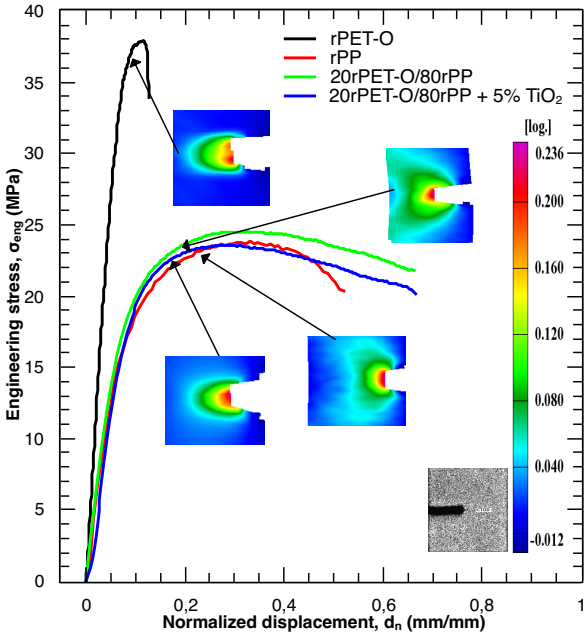

Figure 6.9: Representative graphic of the CTOD of raw materials and compounds

Table 20

Materials	Thickness, *th* (mm)	Real Ligament, *l* (mm)	Load CTOD, *F* (N)	Stress CTOD, σ_c (Mpa)	Time, CTOD, *t* (sec)	**CTOD, δ_c (mm)**
rPET-O*	0,615±0,007	20,03±0,03	408±20	32,6±1,2	8,6±1,3	**0,415±0,017**
rPP*	0,620±0,005	20,01±0,19	240±11	19,5±1,0	13,6±1,3	**0,780±0,024**
20/80	0,607±0,003	5,45±0,19	76,2±3,5	23±0,5	66,4±11	**0,572±0,114**
20/80+ 5% TiO_2	0,585±0,002	5,73±0,20	72,1±2,6	21,5±0,8	46,8±2,9	**0,446±0,046**

-*the tests on these materials were carried out prior to the CCP, so I took them as a reference.

The figure 6.9 shows the curve stress vs. normalized displacement (σ_{eng}-d_n) that represents the evolution of the applied force (F) by the transversal section of the real ligament (*lxth*) versus the relative displacement of the normalized jaw by the real length of the ligament (*l*).

The deformation field developed at the time the CTOD of each sample is reached is also represented.

Table provides a summary of the results of the CTOD test carried out on the samples. Two important facts to highlight are:

1. The difference in the real ligament (l) and the load at which the value of CTOD (F) is reached both in the raw material and in the compounds, this is due to the fact that two different geometries of specimens were used, however the cut/width ratio of the specimen (a/w) remained constant with a value of 0,6.

2. The difference in the time to which the CTOD (t) is reached both in the raw material and in the compounds, this is due to the fact that two test speeds were used: 10 mm/min for the raw material and 1 mm/min for the compounds.

Since the CTOD study is based on the determination of the crack opening just before the onset of unstable crack propagation when a defect is intentionally caused (cut), the test conditions are defined based on the ductility of the sample and the acquisition of images throughout the test in order to have a photographic record during the opening and propagation of the crack.

As a result of the CTOD analysis it was obtained that the rPP yielded the highest aperture value before the onset of unstable propagation (δ_c =0,78 mm) at a critical stress (σ_c) of 19,5 MPa and a deformation gradient in front of the spherical crack suggesting a homogeneous distribution of uniaxial stress. On the other hand, rPET-O had a value of δ_c=0,415mm and a σ_c =32,6 MPa. Although σ_c is 67% higher than rPP, δ_c decreases 47%. This value conforms the stiffness that the sample has in the range of small deformations according to the uniaxial tensile study carried out in section 6.2.4.

However, the field of deformations at the tip of the crack is slightly smaller in the direction of load application and more far-reaching in the direction of crack propagation. i.e., there is an accumulation of localized stresses such that beyond σ_c unstable propagation will begin.

When 20% rPET-O is added to the rPP sample, δ_c is highly decreased by 45% and σ_c slightly favored by 17%. On the other hand, the associated field of deformations shows a completely different evolution than raw materials. A bifurcation can be seen in the axis of crack propagation simulating an obstruction at the tip of the crack such that the stresses are redirected diagonally at 45º and -45º with respect to the axis of crack advance.

A similar event occurs when 5% TiO_2 is added to the sample; a value of δ_c =0,572 mm and σ_c=23 MPa, however, the deformation field developed at the tip of the crack yields an angular bifurcation but less far-reaching than its counterpart without TiO_2. The addition of an inorganic charge could result in a localized concentration of stresses at the TiO_2-Polymer interface acting as a stress concentrator that slightly stops the onset of unstable crack propagation.

6.2.6 Essential Work of Fracture (EWF)

-20rPET / 80rPP

As a result of a visual review of the 20/80 samples tested, it can be seen that in all cases there was a change in tonality in the deformed zone. The whitening seems to increase longitudinally and in the direction of the application of the load as the length of the ligament increases. Figure 6.10 shows one specimen for each ligament analysed.

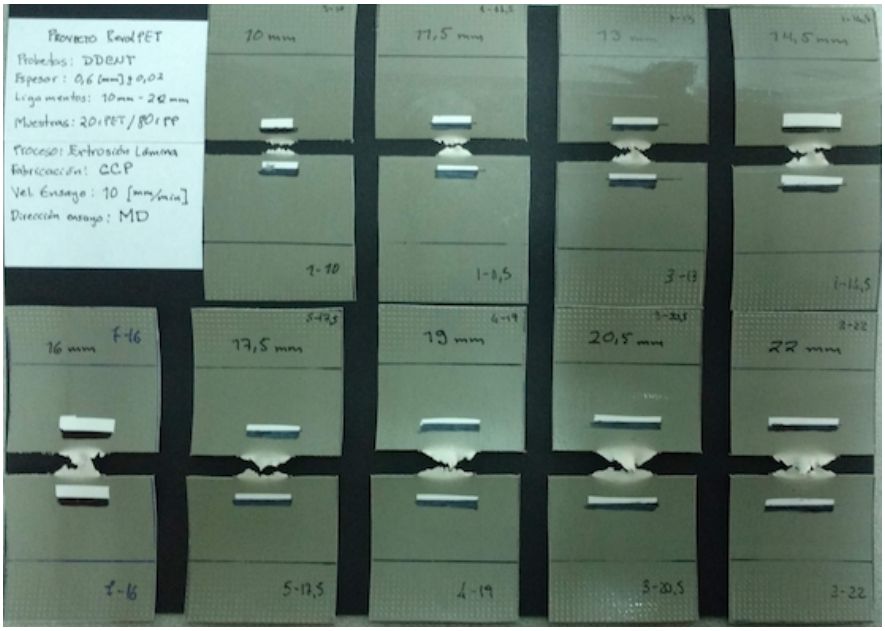

Figure 6.10: Samples after the test

It is important to emphasize that during the execution of the test this whitening (ligament yield) was observed before the propagation of the crack, in the image sequence of figure 6.11 the evolution of the deformation from the beginning of the test to the beginning of the propagation of the crack can be appreciated.

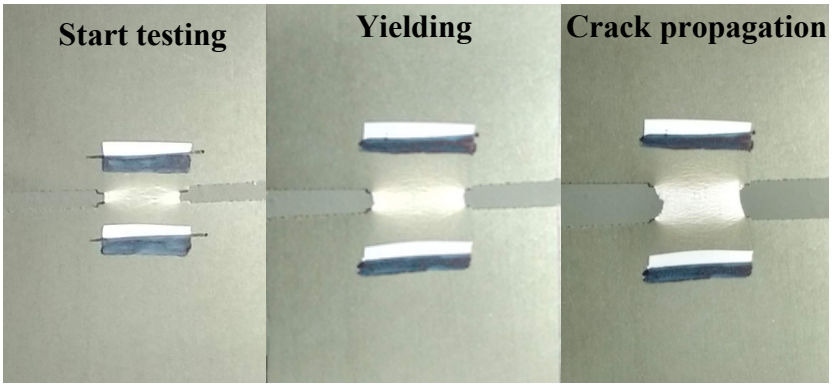

Figure 6.11: Evolution of the deformation from the beginning of the test to the beginning of the propagation of the crack

Analysing the evolution of the applied load against the relative displacement of the jaws, a sequential growth of the curve can be seen in the whole range as the ligament increases, that is, both the maximum load, posterior tear zone, final rupture and displacements associated with each point increased according to the length of the ligament.

Two important facts to emphasize is that in all the cases a linear increase of the force was developed until the yield followed by a decrease in the applied load until the first abrupt fall of the force in the curve (beginning of crack propagation) and finally the unstable propagation and rupture, however in the ligaments 19 mm to 22 mm, this growth did not obey the sequence of the lowest ligaments, a possible explanation is the real length of the ligament and/or the state of tensions developed at these lengths.

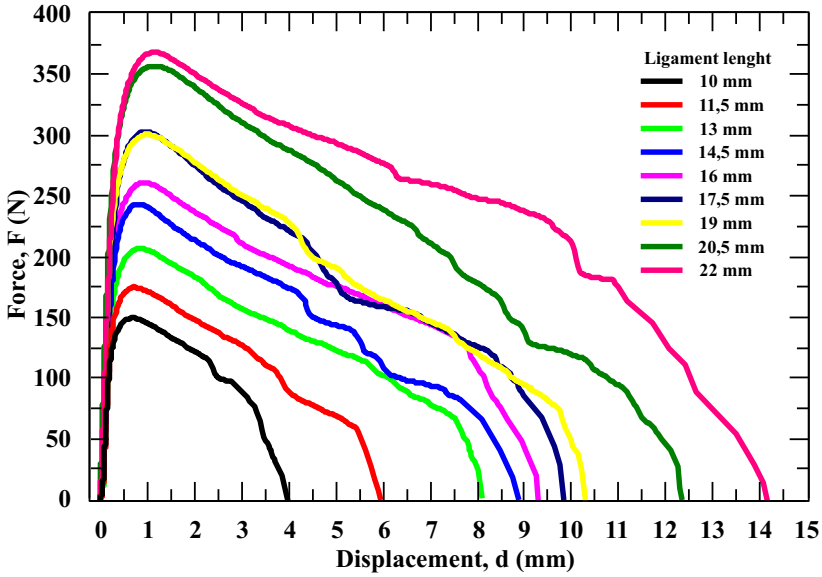

Figure 6.12: Load-displacement curves associated with the study of EWF in the selected ligaments

One of the important criteria established for the EWF is that the maximum stress of the DDENT specimen under a planar stress state is 1,15 σ_y, however, a stricter range between 0,9 σ_y and 1,1 σ_y was applied in order to visualize the variability of the maximum stresses and better define the EWF parameters.

It can be seen in Figure 6.13 that the maximum stress criteria are met throughout the range of ligaments studied and it is verified that all the specimens considered in the post-cedence fracture study meet the flat stress state criterion.

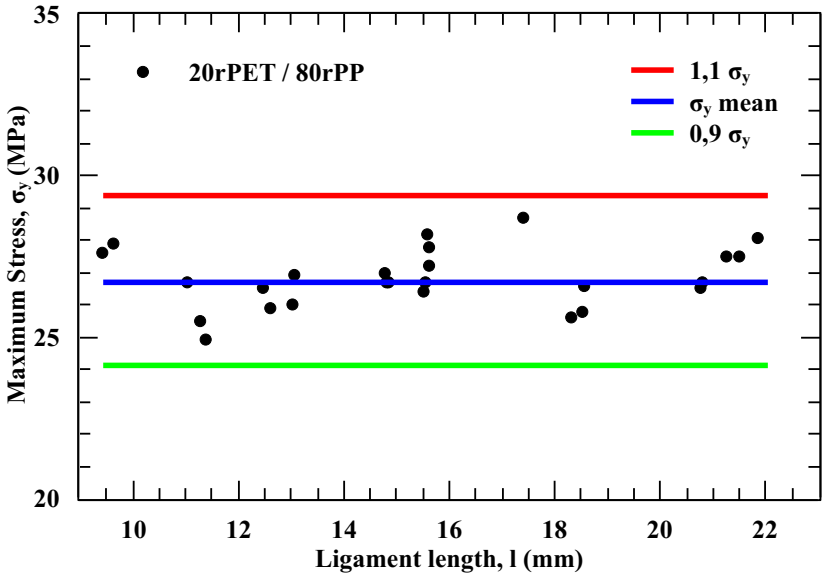

Figure 6.13: Graph of maximum stresses in 20/80 samples for validation of stress states

As mentioned in section 5.6.3, an important factor in the EWF is the dimension and shape of the plastically deformed zone (OPZ) that develops just above the ligament line. This zone is related to the non-essential fracture term and is calculated by measuring the height h/2 of the plastic zone in each part of the specimen (lower and upper) with the aid of an optical microscope.

Figure 6.20 shows the section h/2 measured in two different specimens (10 mm and 13 mm) in order to visualize the growth of the OPZ according to the increase of the ligament. As a

result of the visual inspection it was defined that the geometry developed in the plastic zone is elliptical so the constant numerical value that corresponds to it is K=1,127. By representing the height h of each specimen against the actual length of the ligament and performing a linear regression of the points, the slope obtained established the value of the shape factor $\beta = 11x10^{-2}$

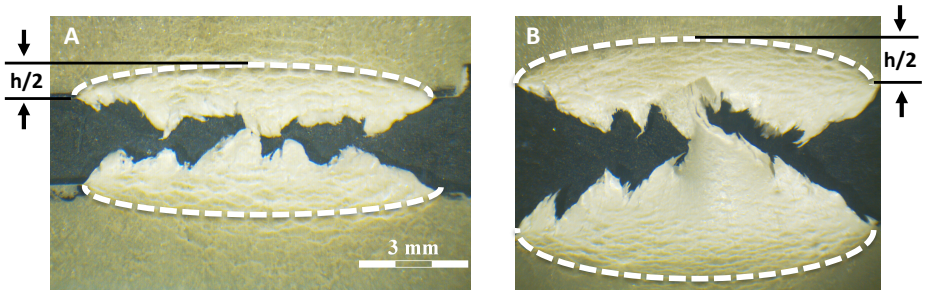

Figure 6.14: Images taken with the optical microscope to measure h/2

By calculating the area under the figure 6.12 curve and relating this value to the ligament section (specimen width by actual ligament length) it was possible to calculate the fracture-specific total work w_t. By plotting this total value against the actual ligament length, it was possible to obtain the values of the terms specific essential w_e and non-specific fracture essence w_p.

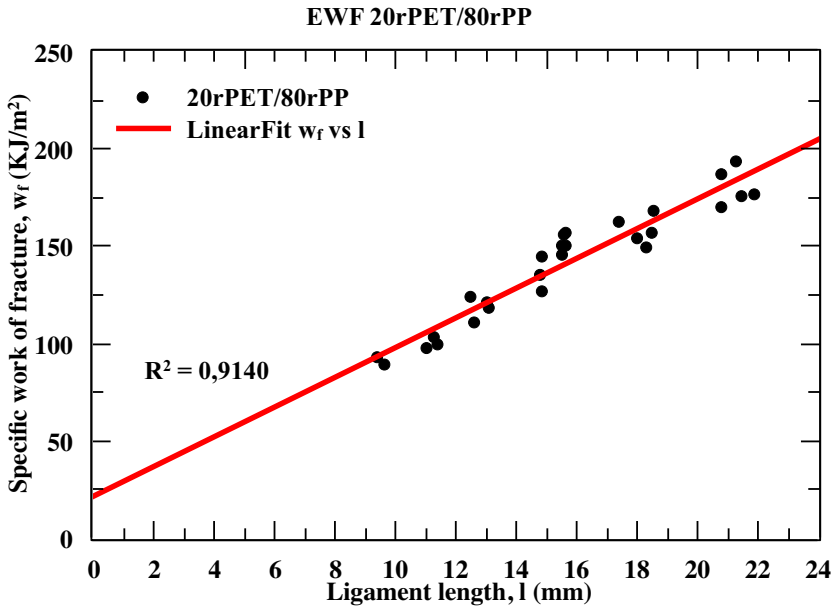

Figure 6.15: Representation of specific work fracture versus ligament length for sample 20/80.

By extending the regression line to the ordinate at the origin and applying the EWF equations, it was calculated that the value associated with the specific essential fracture term is $w_e = 21{,}3\ KJ.m^{2-}$ and the specific non-essential term or plastic work (w_p) was 69 $MJ.m^{-3}$.

-20rPET / 80rPP + 5% TiO_2

Similar to sample 20/80, the EWF study was applied to the compound with additional TiO_2. However, the dimensions of the plastic deformation zone (OPZ) were lower than the sample without TiO_2 even though the real ligament increased (figure 6.16). Although the whitening occurs in the area prior to the rupture, it has a smaller range which translates into a better general deformation until the rupture.

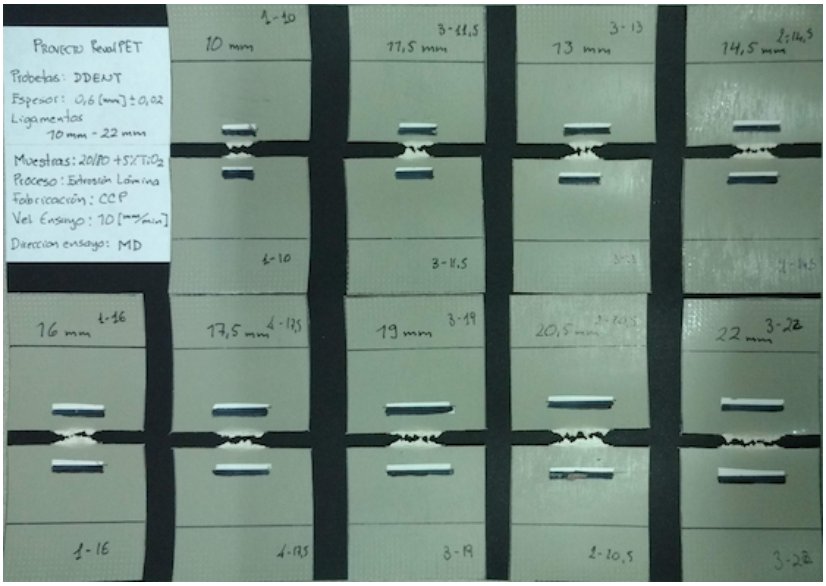

Figure 6.16: Samples after the test

Once the applied load has been plotted against the relative displacement of the jaws (figure 6.17), remarkable facts can be seen in each of the curves; there is a high degree of linearity in the elastic zone and even before the cession, the maximum stresses gradually increase with the increase of the ligament, there is a decrease in the load immediately after the cession and an instability typical of the final tear and fracture.

However, and in all the phenomena described above, these are lower in all cases compared to sample 20/80, i.e., the maximum stresses, displacements associated with cedence and rupture are lower. This fact underlines what was exposed in the figure 6.16 where the whitening zone is smaller than the 20/80 samples.

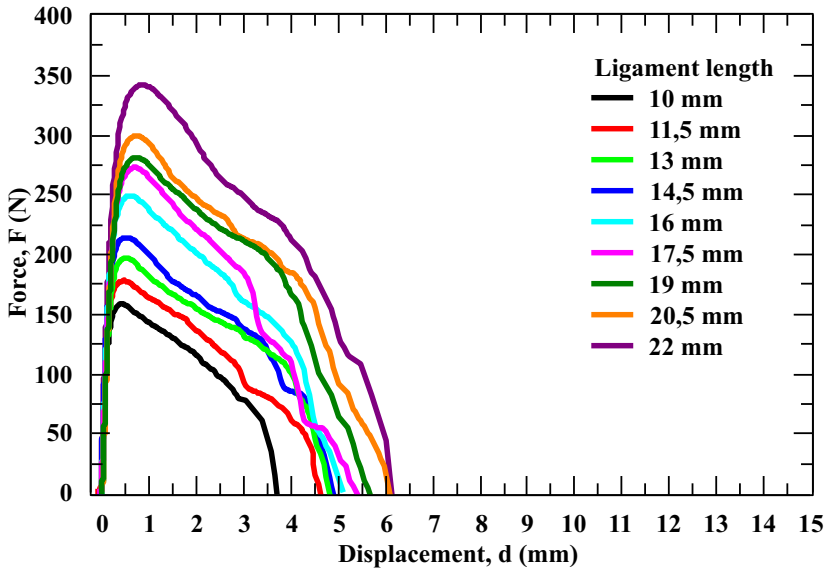

Figure 6.17: Load-displacement curves associated with the study of EWF in the selected ligaments

It is important to mention that instability in curves occurs prematurely, i.e., once the load decreases, unstable propagation processes take place in ligaments greater than 13mm. An explanation could focus on the distribution and dispersion of the inorganic load and the stress concentrating effects it could produce. Also, the level of interaction between phases could be a phenomenon that explains this instability of fracture.

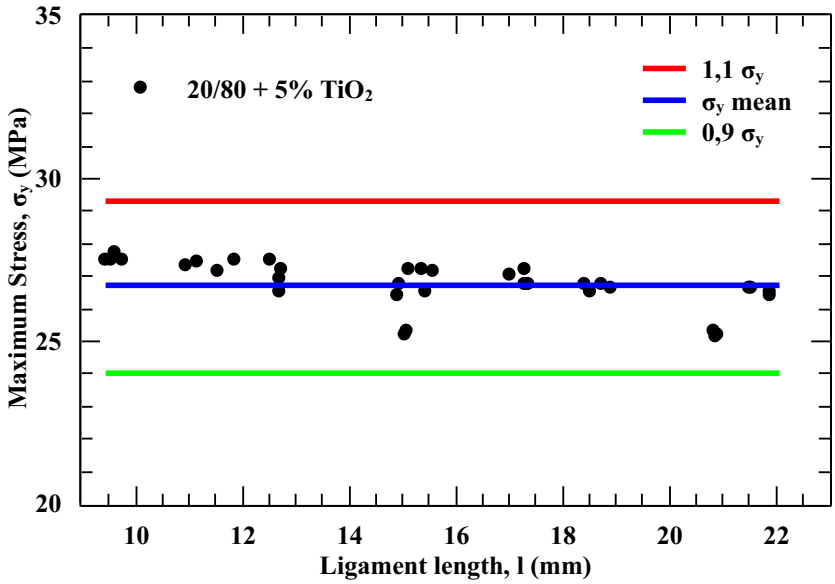

Figure 6.18: Graph of maximum stresses in 20/80+5% TiO_2 samples for validation of stress states

In reference to the maximum stress criterion, a range between 0,9 σ_y and 1,1 σ_y was established to ensure the state of flat stress in the samples. These efforts are between 24 and 29 MPa with an average of 27 MPa. In the figure 6.18 it is possible to see that the points are within the defined range so the flat stress state for this batch is formed. Analysing the trend of the points, there is a high degree of confidence in the statistical result, however, there is a slight constant decrease each time the ligament increases.

The height h/2 of each specimen was measured with the aid of an optical microscope. In the figure 6.19 the sections of ligaments 10 and 13 mm are shown in a representative way; in equality of conditions of the test, it is appreciable that the difference in the zone of plastic deformation (OPZ) does not suggest significant changes reason why the value of h/2 yields a slight increase of total h opposite to the real ligament (figure 6.20).

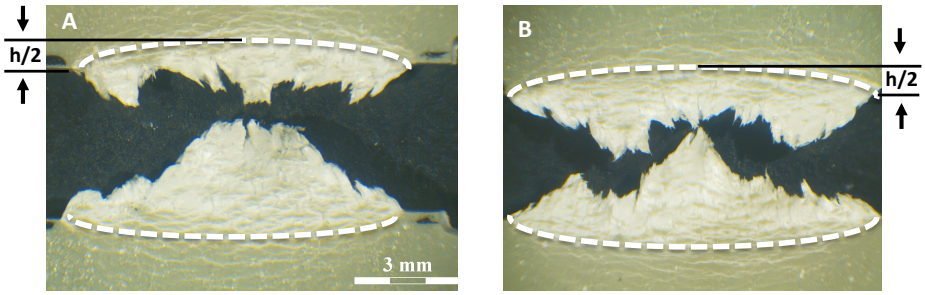

Figure 6.19: Images taken with the optical microscope to measure h/2

As a result of the visual inspection it was defined that the geometry developed in the plastic zone is elliptical (K=1,127). By representing the height h of each specimen against the actual length of the ligament and performing a linear regression of the points, the form factor yielded a value of $\beta = 3{,}9x10^{-2}$, almost reduced by a factor of 3 with respect to sample 20/80.

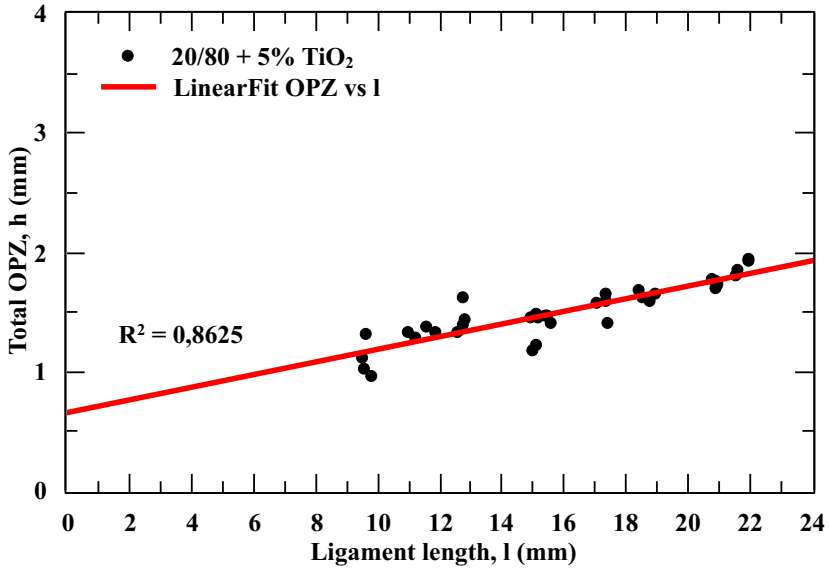

Figure 6.20: Shape factor

Analogously to sample 20/80, the area under the curve of the test specimens figure 6.17 was calculated. By relating this value to the cross section of the ligament and plotting it against the actual length of the ligament, the total specific work w_t and the values of the terms specific essential w_e and non-specific fracture essence w_p were determined.

From the linear regression and extrapolation to the ordinate to the origin, the value related to the specific essential term is $w_e = 78{,}9\ KJ.m^{-2}$ and$w_p = 10{,}2\ MJ.m^{-3}$ for the non-essential term, including the previously determined form factor, all with an adjustment of 0,96 which gives a high level of confidence in the delivered values.

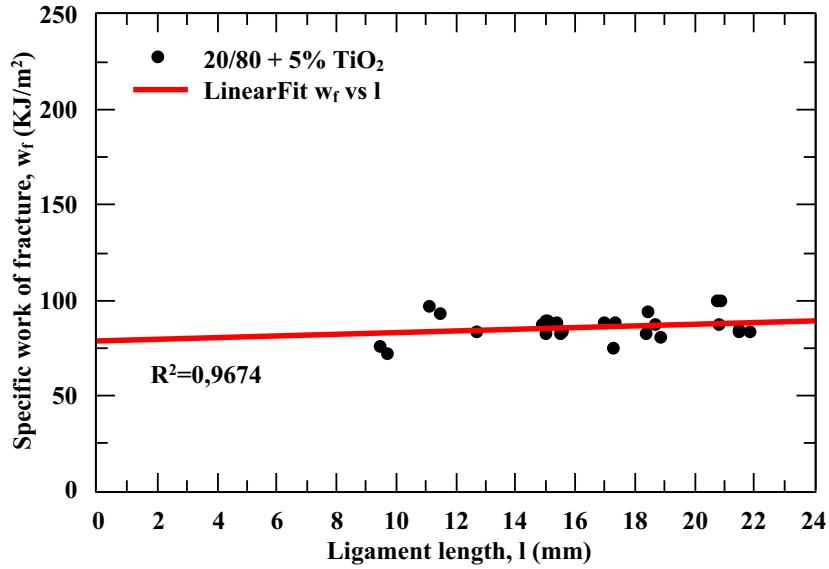

Figure 6.21: Representation of specific fracture work versus ligament length for sample 20/80 + 5% TiO_2.

General results

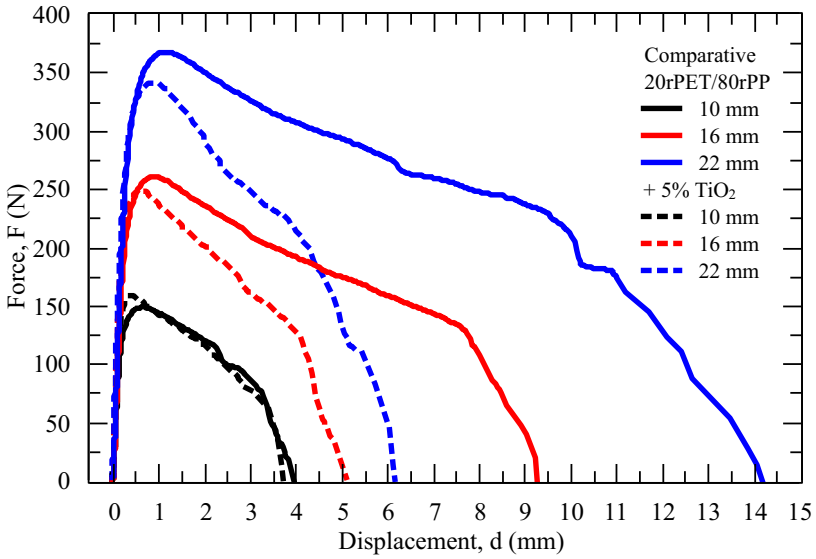

Figure 6.22: Typical curves of Force vs. deformation engineers with ligament lengths of 10, 16 and 22mm for the two compounds studied.

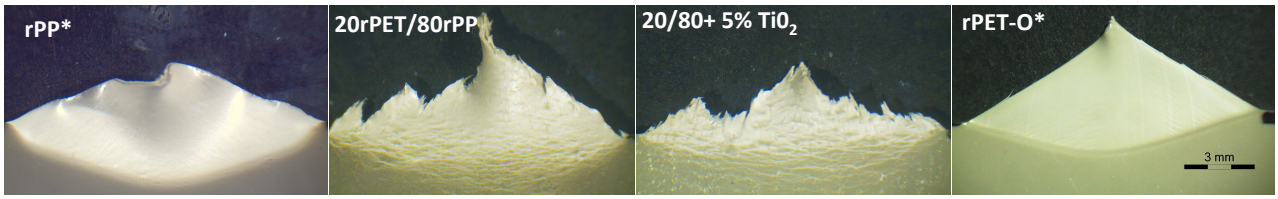

Figure 6.23: Images for the 11,5 mm ligament through the optical microscope

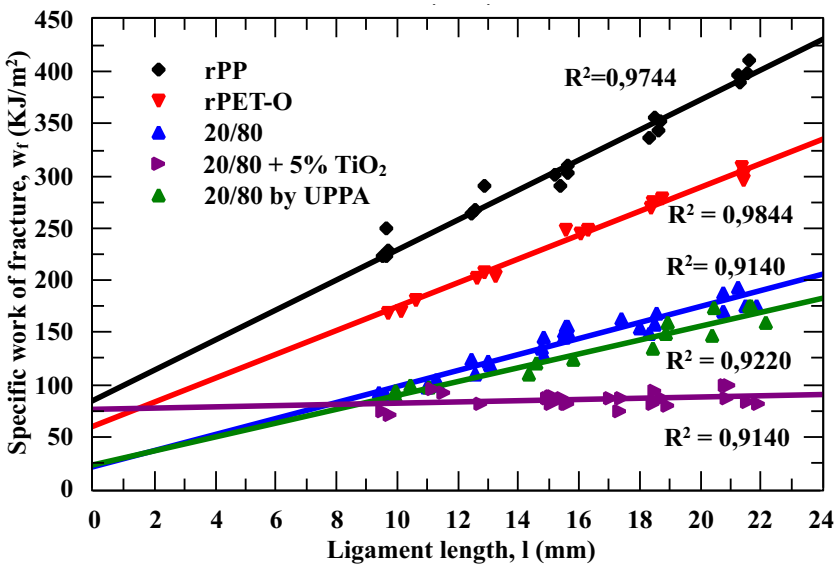

Figure 6.24: Representative curves of fracture-specific work parameters vs. ligament length.

Table 20

Material	w_e	βw_p	$\beta \times 10^{-2}$	w_P
	$(KJ.m^{-2})$	$(MJ.m^{-3})$	–	$(MJ.m^{-3})$
rPP	84,9 ± 10,2	14,4 ± 0,6	13,81 ± 0,01	104 ± 2
rPET-O	*56 ± 4*	*11,6 ± 0,3*	*8,6 ± 0,3*	*135 ± 8*
20rPET / 80rPP	21,3 ± 7,5	7,6 ± 0,4	11,0 ± 0,7	69 ± 5
20rPET/80rPP+5% TiO2	78,9 ± 8,0	0,4 ± 0,1	3,9 ± 0,4	10,2 ± 0,3
20PrET / 80rPP (UPPA)	*23,5 ± 8,8*	*6,6 ± 0,5*	*30,2 ± 7,4*	*22 ± 6,0*

6.2.7 Scanning Electron Microscope (SEM)

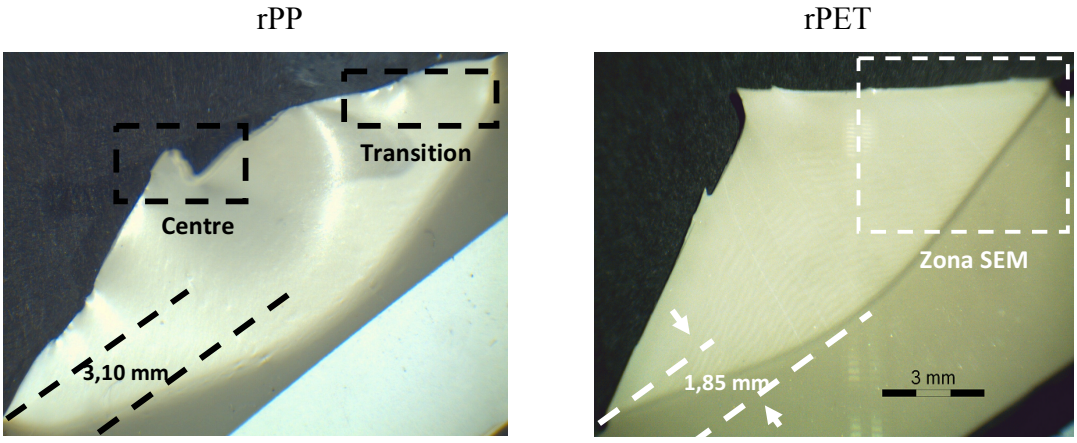

Figure 6.25: General view of the analysed samples

Figure 6.26 shows the images obtained by SEM divided into two zones of interest, central and maximum deformation, and lateral or transition zone; all images were taken at two different magnifications: 50X to select the zone of interest and 1500X for morphological analysis of the selected zone. Two sections were considered for morphological analysis; upper part (A) central part (B).

The 50X images clearly show the formation of a geometrically distributed cavity just at the end of the acute notch (transition zone) and maintained along the plastically deformed zone up to the tip. In section A of the transition zone, a small gradient of micro cavities in direction A - B is observed simulating the presence of inclusions in the system. This gradient seems to reach a maximum point in B where an unstable breaking zone with the appearance of short fibers can be appreciated.

By reviewing the image in detail at 1500 magnifications of the transition zone the presence of small spherical particles of homogeneous dimensions (diameter=1μm) can be seen, both before and after the acute notch. Given the density of these micro-spheres it could be assumed that this is the minority phase (PE).

At the top of the central zone of part A small micro-layers of material can be observed that develop a completely ductile fracture. Section B also presents a highly pronounced cavity and areas with a high level of plastic deformation.

Given the thermo-mechanical degradation that the recycled materials present, the mechanical and fracture behaviour are properties that are directly affected since the total crystallinity that they can develop depends directly on their molecular structure. In this sense, the presence of a second minority phase (PE) in a recycled matrix could promote instability in the plastic flow of the samples.

SEM images made to rPET-O samples are shown in figure 6.27.

In this case four levels of approach were made: 50X to define the areas of general interest (central and maximum deformation, and lateral or transition zone) followed by increments to 150X, 500x and 1500X. The location of the sections of interest was randomly defined as the previous image was analysed since the general morphology of the rupture zone was homogeneous, i.e., there were no pronounced cavity zones.

In the transition zone after the acute notch, a morphology similar to that obtained in the rPP sample is observed, i.e., small micro cavities uniformly distributed throughout the transition zone were generated (image at 500X). As previously mentioned, rPET-O already has 2.4% TiO_2 in its microstructure; in the image at 3000 aments, these small particles can be appreciated homogeneously dispersed in the sample and the coalescence of the small holes with the charge. The high density of voids in the mentioned area suggests that the inorganic charge would be acting as low adhesion stress concentrators.

Although a laminar morphology does not fully develop in the highly deformed area of the central part of the sample, at 500 magnification small superimposed layers of deformed material can be distinguished along the high flow area. At 3000 magnifications, the existence of these layers is more detailed, as well as the homogeneous distribution of TiO_2

rPP

Zoom	Centre	Transition
50x	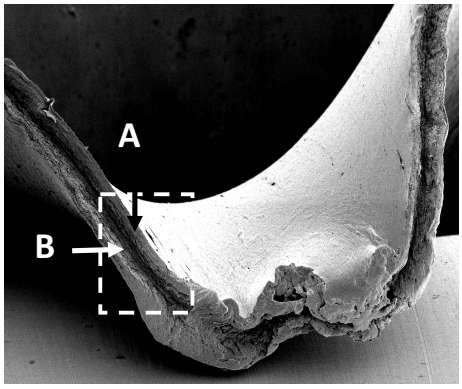	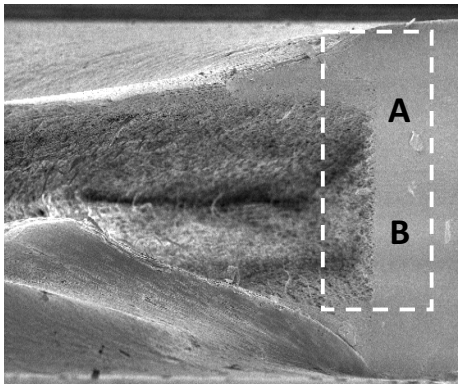
1500x	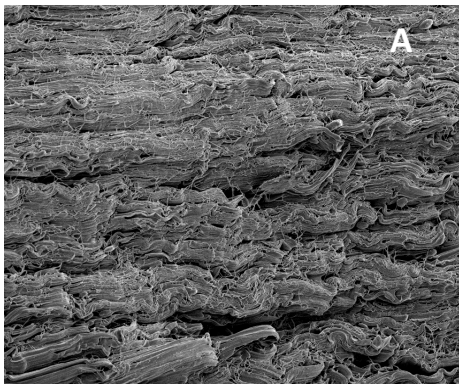	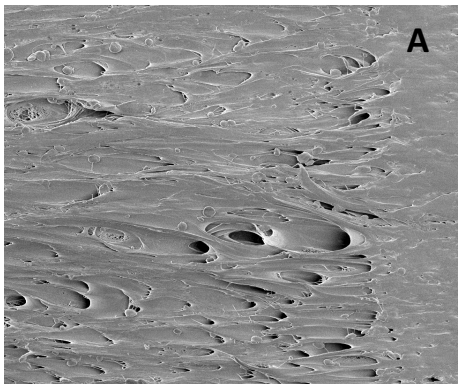
1500x	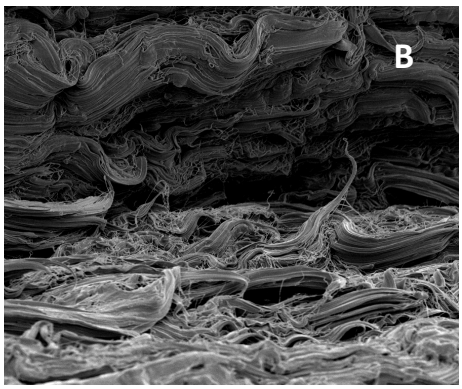	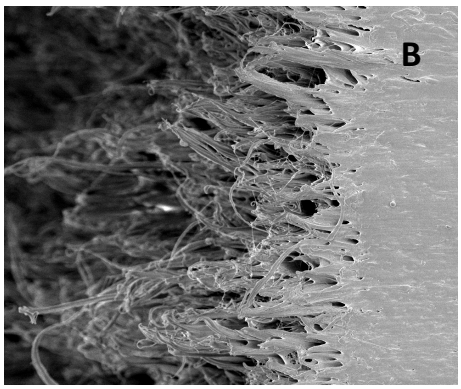

Figure 6.26: Images taken by scanning electron microscopic for rPP

rPET-O

Zoom	Centre	Transition
50x	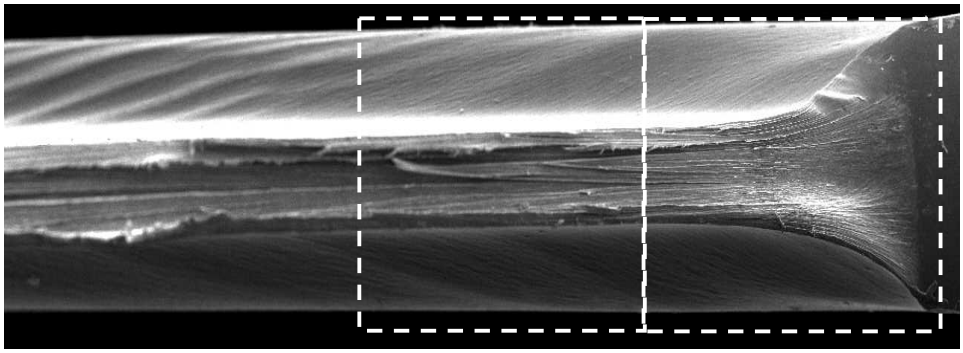	
150x	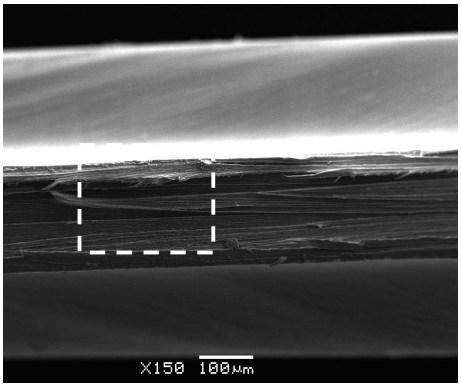	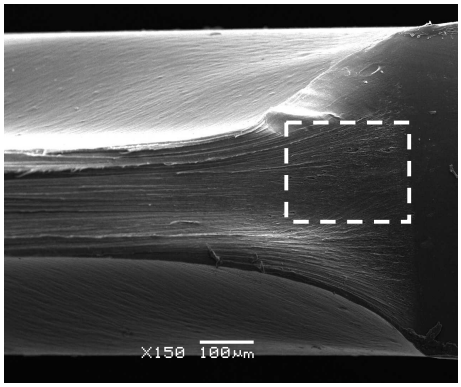
500x	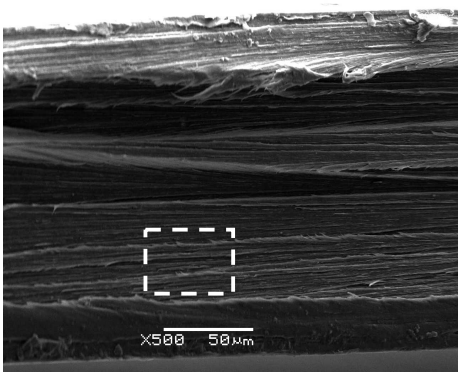	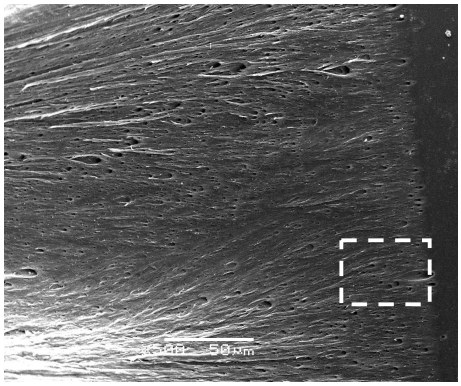

3000x

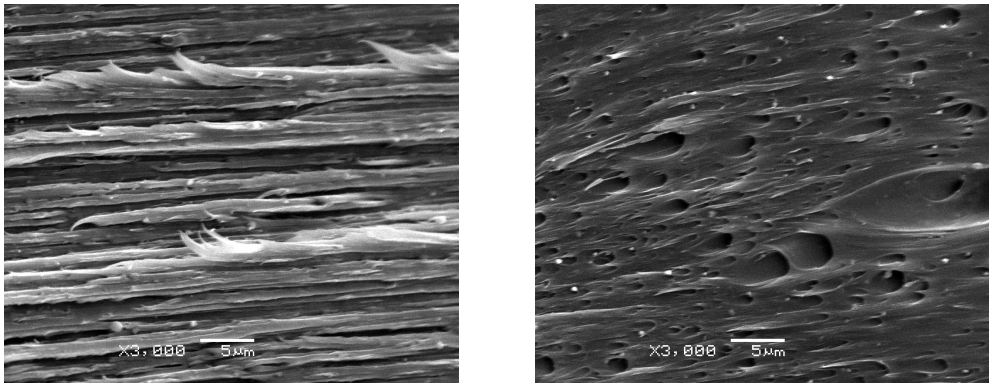

Figure 6.27: : Images taken by scanning electron microscopic for rPET-O

Regarding the compouds, figure 6.28 shows the general view of the samples analysed for each compound in order to determine three important aspects: the definition of the transition zone at the beginning of the notch cutting, the central and maximum deformation zone once the sample has completely broken and the numerical value of the length of h/2.

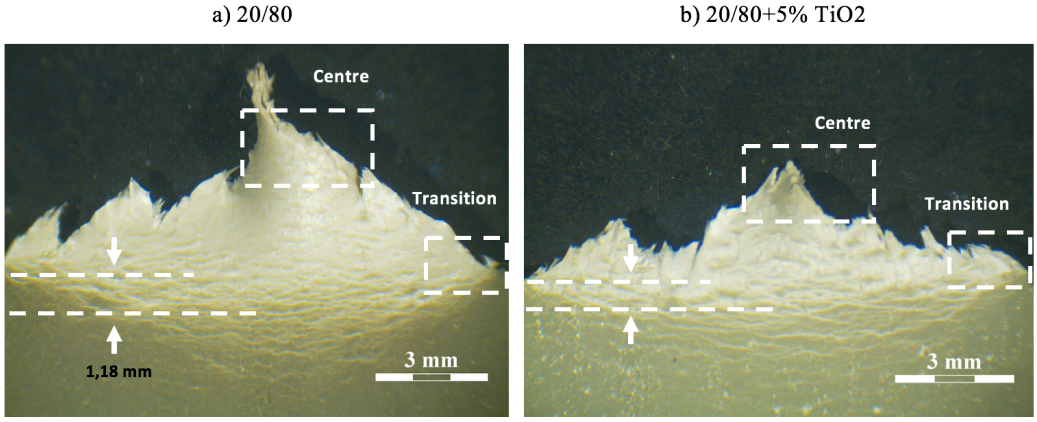

Figure 6.28: General view of the analyzed sample

The geometry of the plastically deformed zone in the sample (a) is visually larger than the sample (b), similarly, suggests a moderately homogeneous rupture since the rhomboid shape in this area of the sample (a) is more pronounced than in the sample (b).

It is important to highlight the size of h/2, where the mixture without addition of TiO_2 gave a value of 1,18 mm compared to the value of 0,79 mm of the sample with 5% of TiO_2 added in the microstructure. A physical explanation indicates the limited adhesion mechanism that exists between materials of a dissimilar nature, since there is no chemical bond between the polymer matrix and the ceramic reinforcement. The latter acts as a special tension concentrator in the Polymer-TiO2 interface, thus promoting premature tearing under monoaxial stress.

Figure 6.29 shows the images obtained by SEM divided into two areas of interest: the central and maximum deformation, and the lateral or transition area; all images were taken with two different magnifications: 50X to select the area of interest and 1500X for morphological analysis of the selected area. For the morphological analysis two sections were considered: the upper part (A) and the central part (B).

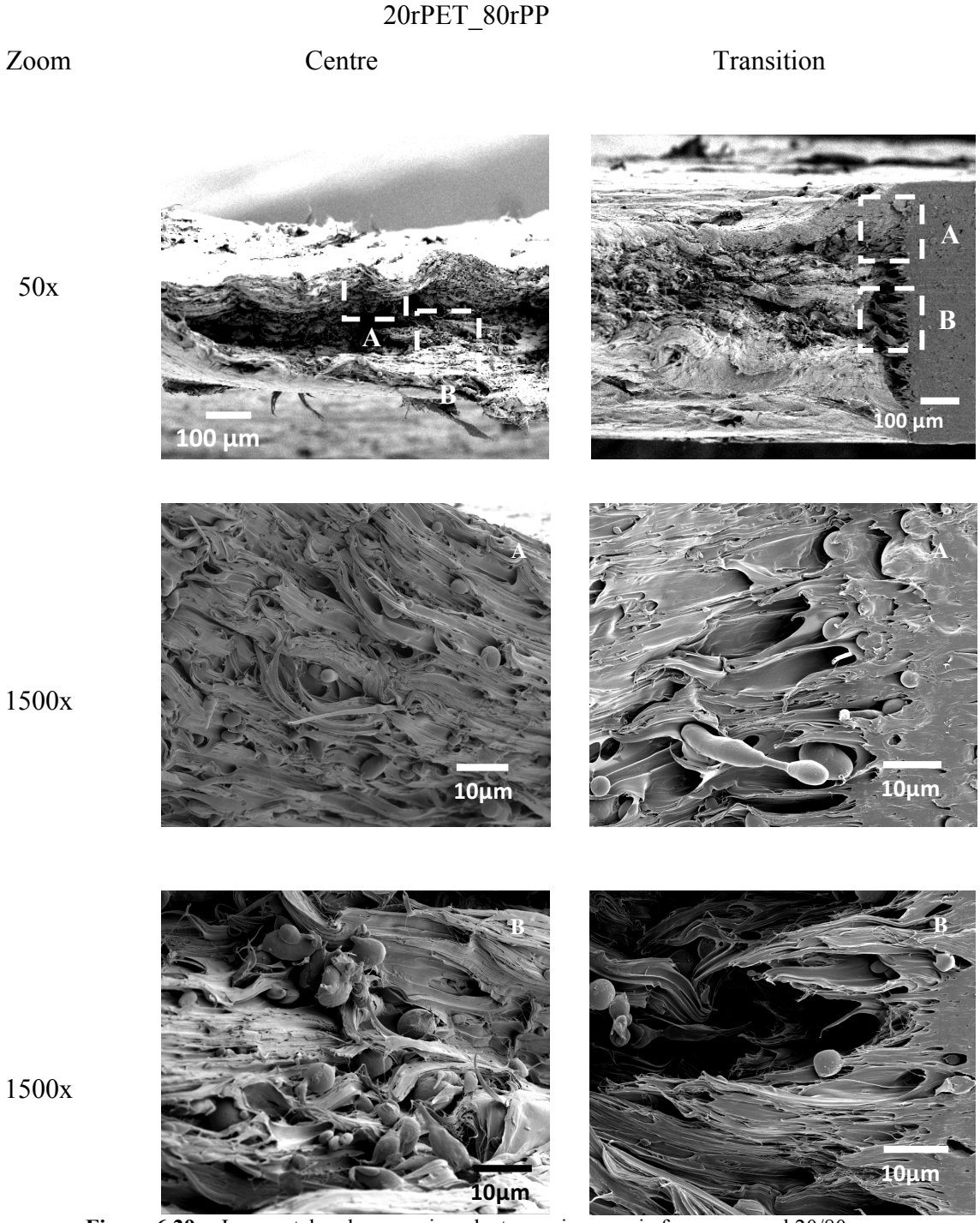

Figure 6.29: : Images taken by scanning electron microscopic for compound 20/80

As a result of the morphological analysis of the 20rPET/80rPP sample (Fig. 6.29), in the first approximation to X50 a sandwich structure is perfectly observed from the transition zone (at the beginning of the acute notch) to the central zone (maximum deformation). At the end of the transition zone (A) there is a small region where the material flow suggests a high level of plastic deformation followed, transversally to the flow, by a gradient in the internal sample tear (B). The same behaviour can be seen in the central area of the sample.

It is important to highlight the presence of small circular particles in zone A with diameters around 5 µm in the transition region and relatively smaller diameters (3 µm) in the central region and distributed along the rPP matrix; these correspond to the rPET fraction contained in the mixture and are the precursors of microcavities in regions A and B (x1500).

However, in zone A (transition and central) small elongated structures of the second phase (rPET microfibers) are observed, a phenomenon that could be explained in terms of cold elongation and the existence of mechanical anchors that the second phase undergoes. The heterogeneity of the microstructure is mainly due to the polarity of the polymers and the non-mixability between them, as well as to the absence of any type of compatible agent in the compound.

Examining the images at 1500 magnifications of zone B, it is possible to observe considerable differences in terms of cavities, microcavities and spherical particles. From the transition you can see a vacuum immediately after the notch, this is due to the internal plastic flow in the central area and the subsequent premature tearing from the surface to the inside. In the same observation, the minority phase follows the flow of the matrix so that the spherical presence is lower than that of zone A and the microfibrillated structure is superficially null, however, a possible rupture-discontinuity of an rPET microfiber can be appreciated. In the central region of Zone B, in addition to the plastically deformed matrix, there is a series of second phase beads ranging in size from 2 μm to 5 μm as a result of a heterogeneous distribution of rPET in rPP. As commented in the material description, the rPET fraction itself has 2.4% TiO_2 and can be appreciated as small particles on the surface of the rPET.

20/80 +5% TiO2

Zoom	Centre	Transition
50x	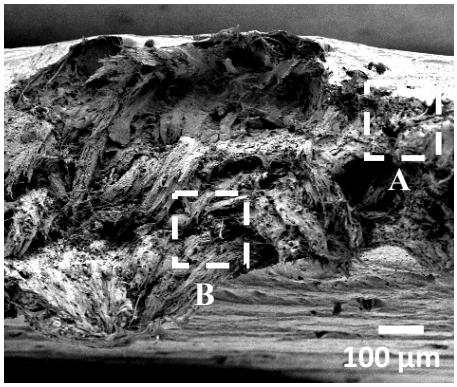	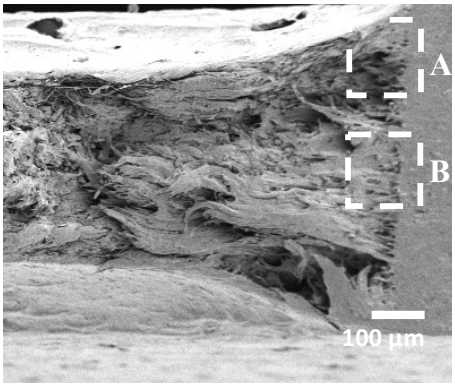
1500x	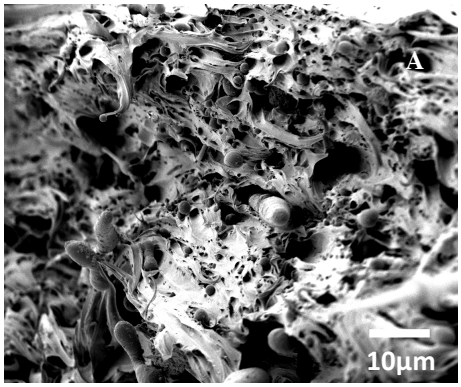	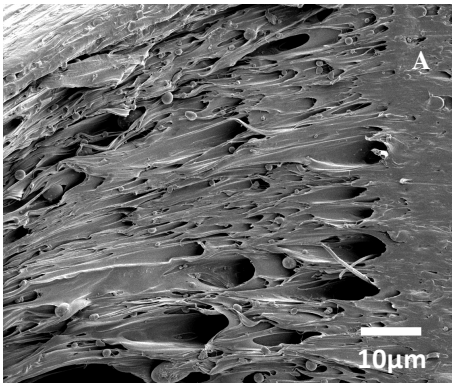

1500x

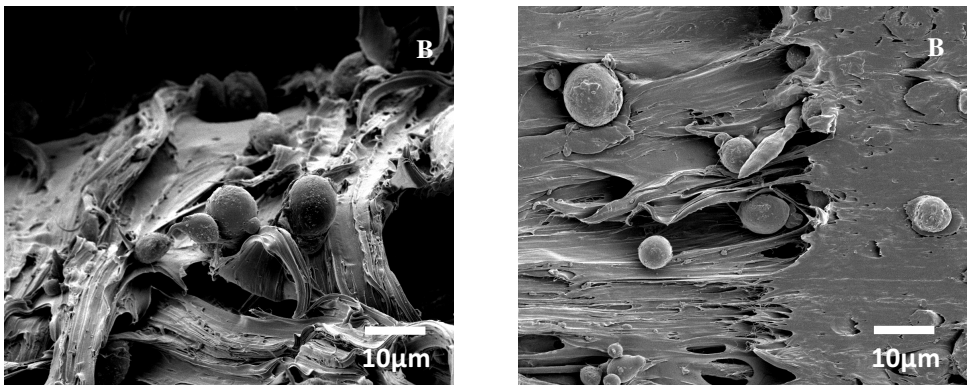

Figure 6.30: : Images taken by scanning electron microscopic for compound 20/80+5%TiO_2

For the sample 20rPET/80rPP+5%TiO2, morphological analysis was also carried out in the central and transition region of the sample, in each of which two parts (A and B) were analysed. Immediately after sharpening the notch, in the transition region (x50), a series of microcavities and voids can be observed along the cross-section. It is observed that the matrix does not have a uniform gradient of deformation, there is a continuous plastic deformation in zone A followed by a total surface laceration (space between zone A and zone B) and finally a new plastically deformed zone in zone B.

A similar event occurs in the central region (x50) where the morphology shows an unstable rupture of the workpiece with the presence of high plastic deformation zones and a high density of microcavity. Approaching 1500 magnifications in zone A of the transition region reflects a greater dispersion of spherical particles of rPET but with smaller sizes around 1-2 μm. An important fact to emphasize is the imprint that the larger particles have left on the surface, which suggests a low level of chemical interaction between the phases, limiting itself to a purely mechanical anchorage as there is no internal laceration of the larger cavities. In the central region of zone A a surface with special characteristics can be observed; the general appearance of the matrix shows that the plastic deformation achieved until unstable rupture is strongly influenced by the dispersion of the second phase and the low interaction between the phases. From this it can be observed a high porosity, typical of the detachment of the second phase.

Although small elongated particles such as microfibers are observed, they have an irregular geometry (globular type at the ends) and low continuity. This effect is caused by the addition of TiO_2, as the particle size is micrometric, so the effective contact surface is high, which interrupts the development of the deformation-induced crystallization phenomenon.

Similarly, in zone B of the transition region, perfectly distinct and larger rPET microspheres than zone A (5-8 μm) are observed. These also show a non-cohesive impression between the polymer phases, but with larger dimensions than those observed in zone A. This can be explained by the temperature gradient during film cooling, i.e. the activation of the diffusion and coalescence mechanisms of the second phase when the temperature is higher than its Tg at the centre of the film and its stability when the temperature is lower (surface).

The incorporation of 5% by weight of TiO_2 added to the 2.4% that rPET has in itself is observed on the surface of rPET with traces even in the matrix of the compound.

7. CONCLUSIONS

In this thesis work, the recycled opaque PET and two compounds were studied, one containing the same material with the addition of recycled Polypropylene and the other with the further addition of an inorganic charge, i.e. Titanium Dioxide. Therefore, the thermal, mechanical and fracture behaviour of the materials of interest was the subject of this study.
From the thermal point of view, the DSC was carried out, by means of which it was possible to identify the characteristic temperatures of the materials and the crystallinity of each material, and a comparison was also made between the materials obtained in the form of pellets and those subjected to further calendering treatment to obtain the laminas. It was noted that the recycled PP did not show any particular differences, while with regard to the recycled opaque PET it was quite visible the physical aging suffered due to the abrupt cooling and little controlled during the calendering process. As far as the compounds are concerned, the peaks present were those relative to all the phases present.
With reference to crystallinity, the value of rPET-O varies when the rPP matrix is added, reducing its crystallinity by 13,5% and by 10,8% when 5% of TiO_2 is added. Similarly, with rPP, its initial crystallinity of 36.3% is reduced by 18.5% when adding the second phase of rPET-O and by 21,6% when adding 5% of the inorganic load. Based on these results, it can be said that a possible preferential position of TiO_2 is found in the rPET-O matrix since the crystallinity increases when the charge is added, but not in the rPP where the crystallinity decreases even more with the presence of TiO_2.
From the point of view of mechanical behavior and fracture the analyses performed were the tensile test, the evaluation of the Crack Tip Opening Displacement (CTOD) and the Essential Fracture Work (EWF). The tensile test showed that recycled opaque PET has the highest values of modulus of elasticity and yield strength compared to other materials, to the detriment of elongation at break. This is consistent with the structure of PET itself, given the presence of aromatic rings in the chain. This result is also in line with what has been noticed in the compounds, in fact with the addition of 20% of rPET-O to the rPP matrix there has been an increase in the rigidity of the system and a decrease in the deformation at break, then even more accentuated with the further addition of TiO_2. In this case, the stiffness and yield strength increase slightly, but the yield and rupture deformation increase to a greater extent.
The evaluation of the CTOD continued and it was found that the highest values of c between the two raw materials are shown by rPP, this value is in fact 47% higher than that of rPET-O in line with what was found with the study of traction given the intrinsic characteristics of polyester. A decrease in the CTOD occurred, albeit slightly less marked, with the realization of the compound. As far as the compound with the addition of TiO2 is concerned, it is noted that at the filler-polymer interface, the inorganic charge acts as a stress concentrator and acts as a block for the unstable propagation of the crack.
Finally, the essential work of fracture was evaluated, comparing the two compounds, it was noted that the size of the plastic deformation zone is smaller in the samples made from the compound's sheets with titanium dioxide, which translates into better deformability before reaching the fracture. It is important to note that the curves for the rPP/rPET-O/TiO_2 compound have found some instability and this may be due to several factors, such as: poor dispersion of the charge within the compound, the effects of stress concentration that this could produce, as well as the low level of interaction of the phases.

8. BIBLIOGRAPHY

[1] Plasticfinder.it

[2] Ehrig, R.J. Plastics Recycling, Products & Processes. 1992. New York: Oxford University Press,1992.

[3] Brydson, J.A. Plastics materials. British Library Cataloguing in Publication Data. Ty. Oxford: 1999.

[4] Overview on Mechanical Recycling by Chain Extension of POSTC-PET Bottles

*Doina Dimonie1, Radu Socoteanu2, Simona Pop1, Irina Fierascu1, Radu Fierascu1, Celina Petrea3, Catalin Zaharia3 and Marius Petrache1

[5] Sorema.it

[6] Comité Technique pour le Recyclage des Emballages Plastiques (COTREP). Impact du developpement des emballages en PET opaque sur le recyclage des emballages en PET Coloré. Dossiers COTREP, Diciembre 2015.

[7] Asociación Zero Waste France. PET OPAQUE Dossier ZEROWASTE, enero 2017.

[8] William D. Callister, Material Science and Engineering: An Introduction, 5ª ed., John Wiley & Sons Inc, 1999, ISBN 0-471-35243-8.

[9] KIDV. Factsheet | Opaque PET bottles and recycling. A: [en línia]. 2017, núm. October, p. 1-3. Disponible a: https://www.kidv.nl/7523/factsheet-opaque-english.pdf.]

[O. O. Santana; A. D. Loaeza; J. Cailloux; M. Sánchez-Soto; M. Ll. Maspoch; Fractura de láminas extruidas a partir de PET opaco reciclado. A: Anales de Mecánica de la Fractura 35. 2018, p. 195.]

[10] Unidad de Negocio Químico-Plástico. Polímeros Polietilentereftalato Polyethylene Terephthalate. A: [en línia]. 2008, p.9. Disponible a: http://www.laseda.es/data/publicaciones/2008/pet_dossier.pdf].

[11] O. O. Santana; A. D. Loaeza; J. Cailloux; M. Sánchez-Soto; M. Ll. Maspoch; Fractura de láminas extruidas a partir de PET opaco reciclado. A: Anales de Mecánica de la Fractura 35. 2018, p. 195.]

[12] Martinez, A.B. et al. The Essential Work of Fracture (EWF) method - Analyzing the Post-Yielding Fracture Mechanics of polymers. A: , Engineering Failure Analysis. Elsevier Ltd, 2009, Vol. 16, núm. 8, p. 2604-2617

[13] Cailloux, J. Modified Poly(lactic acid) sheets manufactured by One-Step Reactive Extrusion-Calendering : Thermal , Rheological , Mechanical and Fracture Behaviours. Universitat Politècnica de Catalunya. 2015, núm. December, p. 118

[14] Maspoch, M.L. et al. Aplicación de la mecánica de la fractura post-cedencia a polímeros. A: Revista Latinoamericana de Metalurgia y Materiales. 2010, núm. 30, July

[15] Li, Z.M. et al. Essential work of fracture parameters of in-situ microfibrillar poly(ethylene terephthalate)/polyethylene blend: Influences of blend composition. A: Macromolecular Materials and Engineering. 2004, Vol. 289, núm. 5, p. 426-433

[16] Hashemi, S. Fracture toughness evaluation of ductile polymeric films. A: Journal of Materials Science. 1997, Vol. 32, núm. 6, p. 1563-1573

[17] Clutton, E.Q. ESIS TC4 Experience with the essential work of fracture method. A: European Structure Integrity Society. Grangemouth, Scotland, UK: BP Amoco Chemicals, 2000, p. 187-199

ACKNOWLEDGEMENTS

Le prime persone che ci tengo a ringraziare sono quelle che mi hanno consentito di portare a termine questo lavoro di sperimentazione. In primis il mio relatore Alberto Frache e tutto il gruppo del “Centre Català del Plastic”, in particolare Maria Lluisa e Orlando che mi hanno fatto sentire a casa durante tutta la mia permanenza a Terrassa. Un ringraziamento speciale va a David, mi amigo chicano, muchas gracias por toda su paciencia, por todo lo que me enseñó, por las canciones y por todos los cafés italianos divididos, nunca lo olvidaré.
Il ringraziamento più importante va alla mia famiglia, mamma, papà e Martina, per tutti i sacrifici e gli sforzi fatti per sostenermi sempre e per esser riusciti, con la loro presenza, ad accorciare la distanza che ci separa.
A Federica, Martina e Francesco i miei migliori amici da sempre, il per sempre in cui credo.
A Marco, punto di riferimento e sostegno con amore e pazienza.
Alla mia coinquilina, sorella, amica Alessandra.
Agli amici che ho conosciuto a Torino, senza i quali la mia prima esperienza lontana da casa non sarebbe stata la stessa, in particolare ad Alberta, che non mi stancherò mai di ascoltare.
A tutti i miei amici, Sbraps, Germana, Sara, Annachiara sperando un giorno di poter vivere un po' più vicini.
Infine ci tengo a ringraziare la mia terra, la Sicilia, spero che un giorno non sarai più costretta a vedere tutti i tuoi figli andare via, spero che un giorno ci vedrai ritornare.